AFIT/GAE/ENY/93D-17

FATIGUE BEHAVIOR OF A CROSS-PLY CERAMIC MATRIX COMPOSITE UNDER STRAIN CONTROLLED TENSION-TENSION AND TENSION-COMPRESSION LOADING

THESIS

James J. Gudaitis
Captain, USAF
AFIT/GAE/ENY/93D-17

AFIT/GAE/ENY/93D-17

FATIGUE BEHAVIOR OF A CROSS-PLY CERAMIC MATRIX COMPOSITE UNDER STRAIN CONTROLLED TENSION-TENSION AND TENSION-COMPRESSION LOADING

THESIS

Presented to the Faculty of the Graduate School of
Engineering of the Air Force Institute of Technology
Air University
In Partial Fulfillment of the
Requirements for the Degree of
Master of Science in Aeronautical Engineering

James J. Gudaitis
Captain, USAF

December 1993

Approved for public release; distribution unlimited

Preface

The primary purpose of this study was to investigate the fatigue behavior and failure mechanisms for a Nicalon/CAS ceramic matrix composite material under strain controlled tension-tension and tension-compression loading. An initial static tension test gave a baseline for the following tests. These tests then determined the fatigue and failure characteristics for tension-tension and tension-compression loaded Nicalon/CAS specimens.

This study could not have been successfully completed without the help of a great many people. On the top of the list would be my advisor Dr. Shankar Mall, whose advice and guidance kept me going and pointed in the right direction. Thanks also go out to my committee members, Dr. Peter Torvik and Capt. Robert Canfield, whose comments were very helpful, and to Dr. Walter Jones of AFOSR/NA for sponsoring this research.

The strain control computer program was written by Capt. Brian Sanders, and without it this study would not have been attempted. This test was a follow-on to Capt. Frank Opalski's load controlled test, and without access to his data and his help with the "little things", things would have gone slowly.

And finally, thanks to all the AFIT lab personnel for keeping the supplies flowing and equipment working, and to Mark Derriso (my workout buddy) who finally convinced me that there was no such thing as the "perfect test".

Table of Contents

List of Figures and Tables

Table

Abstract

The purpose of this study was to investigate the fatigue response of a cross-ply $[0/90]_{2s}$ Nicalon/Calcium-Aluminosilicate (Nicalon/CAS) ceramic matrix composite at room temperature under strain controlled tension-tension and tension-compression fatigue loading. The primary objectives were to determine strain fatigue limits (fatigue life of at least 1,000,000 cycles) for both loading cases and to complete a fatigue life diagram (i.e. strain range versus fatigue life, $\Delta\varepsilon$-N) for all tests. Failure mechanisms were also studied.

The average initial modulus value for this lay-up was 120 GPa. The ultimate tensile strain was 0.00988 mm/mm (285 MPa). Tension-tension tests were accomplished with a strain ratio R ($R=\varepsilon_{min}/\varepsilon_{max}$) of 0.1. Eight tests were conducted with maximum strains that ranged from 0.00300 mm/mm to 0.00722 mm/mm. The strain range, $\Delta\varepsilon$ was used to correlate the fatigue lives from these tests. The tension-tension fatigue limit was found to be $\Delta\varepsilon$=0.00270 mm/mm. The fatigue life diagram on a semi-log relationship between $\Delta\varepsilon$ and N was a straight line. There was no evidence of random fiber failure.

The tension-compression tests were conducted at a strain ratio R of -1.0. Five tests were performed at maximum strains that ranged from 0.00135 mm/mm to 0.00325 mm/mm. The fatigue limit for this set of tests was found to be the same as that fatigue limit for the tension-tension tests, $\Delta\varepsilon$=0.00270 mm/mm. Longitudinal cracks formed in all the specimens, and were the

major cause of failure. The fatigue life diagram for these tests coincided with the tension-tension tests until at the higher strains where the failure mode changed from tensile failure to compressive failure, and caused the specimens to fail at a much shorter life.

FATIGUE BEHAVIOR OF A CROSS-PLY CERAMIC MATRIX COMPOSITE UNDER STRAIN CONTROLLED TENSION-TENSION AND TENSION-COMPRESSION LOADING

I. Introduction

A. Background

When most people today think about ceramics, they would probably think about the common everyday household items made of ceramics such as ashtrays or holiday table decorations. These items are made to take advantage of of the ceramics high thermal capabilities, and are well suited to functions such as holding burning cigarettes or being covered with high temperature miniature lights. One serious drawback that items such as these have though, is their brittleness and low fracture toughness. It would surely be only a matter of time before this drawback would be overcome and the high temperature capabilities of this material exploited.

To increase the ceramic's strength and fracture toughness, high-strength reinforcing fibers made of materials such as carbon or silicon carbide can be added to the ceramic material. Additional increases in strength versus weight can be obtained by optimally orienting the direction of fibers in the ceramic, and by putting layers of this mixture together in

different ways. This mixture of fibers and ceramic gives us the ceramic matrix composite (CMC).

CMC's are currently being investigated for many uses in the industries where high strength to weight ratios and high temperature capability is needed to enhance the performance and life of the object. Thus the military and defense related industries are actively involved in the testing of CMC's. Parts of aircraft surfaces have utilized composite materials for many years, and now possible applications for CMCs in the space shuttle and National Aerospace Plane are being studied. Also, many components of jet engines, such as the fan blades and nozzles, could make use of the high temperature operating capabilities of CMCs.

A high performance jet engine doesn't just sit on the test pad. It is put into a high performance aircraft such as the F-15E and then expected to help the crew to out-perform any other aircraft in the world. A typical combat profile might consist of an afterburner takeoff followed by a climb up to an air refueling tanker, then a high altitude cruise for a few hundred miles until a combat descent to 200 feet is done. A low altitude 600 mph dash to the target could be followed by air-to-air combat on the way out of enemy territory, and then a climb back to high altitude for the flight back to home base. This type of mission may be flown two times a day, for many days in a row during wartime, thus reliability of all aircraft components is required. To be able to predict this

reliability, the fatigue properties of the materials that make up the aircraft must be known.

During the flight profiles all types of loadings will be imposed on the aircraft components. There will be not only tension and compression loads, but different combinations of the two. Also, high temperatures will contribute significantly to the loadings and strains on these components. To understand how the components will react to these loads and strains, studies need to be conducted on the composites using various types of testing methods.

Previous fatigue testing on CMCs have focused primarily on load controlled testing and will be discussed in Chapter II. This leaves the need for more studies using strain controlled methods with both tension-tension, and tension-compression strains.

B. Problem Statement/Scope

The purpose of this study was to investigate the effects of strain controlled fatigue loading on a silicon fiber (Nicalon) reinforced calcium-aluminosilicate (CAS) ceramic matrix composite at room temperature. Also, some effects of load controlled fatigue loading were investigated for the sake of completeness and for comparison between the two fatigue modes.

C. Approach

A Nicalon/CAS ceramic matrix composite plate with a cross-ply lay-up, manufactured by Owens-Corning was cut into test specimens each 7.62 cm long by 6.35 mm wide. Specimens were tested on a servohydraulic test machine using both the strain controlled and load controlled modes with different strain and load ratios. A static test was also performed to investigate the baseline behavior. A fatigue limit was established under both tension-tension and tension-compression conditions. Also, S-N curves were developed for both tension-tension and tension-compression cases under strain controlled and load controlled modes. A compression-compression test was done at the established fatigue limit to investigate the high compression effects.

Stress and strain data were recorded for each fatigue test at various cycle intervals. The composite's behavior and damage progression was recorded by five primary methods: stress-strain curves, elastic modulus, hysteretic energy densities, transverse strain, and acetate replicas.

The loading portion of the stress-strain curves was used to calculate the elastic modulus during certain cycles of the fatigue life. The normalized modulus was plotted as a function of the number of cycles to show how damage was progressing in the specimen. The stress-strain curves were also used to calculate the energy dissipated during a fatigue cycle using the area under these curves. Energy versus cycle

number was plotted to see how the energy state of a specimen changed with the damage occurring during cycling.

Transverse strain data was also taken to investigate how the transverse strain changes as damage in the specimen progresses.

At predetermined cycle intervals, the fatigue tests were stopped so that acetate replicas could be taken. From these replicas, crack development under the various loadings could be studied and correlations between crack density, maximum strain, and maximum stress obtained.

All the above methods were used to gather information on how the damage mechanisms contributed to the eventual failure of the specimens, and to determine the type of failure that actually occurred. Some of these results were then compared with the load controlled testing data that was obtained by Opalski [1] and from the load controlled tests done during this study.

II. Background

A. Experimental Background

Although interest in ceramic matrix composites is relatively new, many recent studies have recently been done to characterized this class of composite materials. The sequence of studies usually starts with the analysis of the composite's individual component's chemical composition and properties, followed by the determination of the lamina properties. After a certain layup is prepared, static and then fatigue tests are done to determine the strength and life of the composite. Then analytical models are applied to the composite to see if predictions can be made about its performance. Many of the CMC studies that are currently being investigated fall somewhere between the fatigue and analytical stages. Almost all of these tests have been done under load control, and thus there is a need for some strain controlled testing to be done.

Rousseau [2] described crack progression in a Nicalon/CAS cross-ply specimen in stages. First, the 90° plies lost their load capacity from the development of transverse cracks. Matrix cracking then began in the 0° plies followed by fiber breakage and then failure. Similiarly, Zawada, Butkus, and Hartman [3] tested SiC/1723 and identified two distinct proportional limits corresponding to the 90° plies cracking, and to the 0° ply matrix cracking.

Mall, Finn, and Kim [4] also observed the matrix transverse cracking in both the 0° and 90° layups of a Nicalon/CAS specimen. During crossply testing of a Nicalon/CAS layup Mall and Kim [5] duplicated this transverse cracking sequence.

Reifsnider and Stinchcomb [6] proposed a residual fatigue life estimation method for polymeric based composites called the "Critical Element Approach". This method suggested that the life of the specimen depended upon the critical plies of the material which usually correspond to the on-axis plies. When these plies failed the material would fail.

During fatigue tension-tension testing, Rousseau observed damage similiar to that in static tension tests in Nicalon/CAS, and saw that the majority of the damage occurred during the first cycle. He believed that this large modulus stiffness loss in the first cycle was not really a result of cycling.

Karandikar and Chou [7] tested cross-ply layups of Nicalon/CAS under tension-tension and static fatigue loadings. They determined that the crack growth was environmentally driven and dependent on both the maximum load and time, and that a matrix crack growth limit strain exists. This limit corresponded to matrix crack initiation strain.

For tension-compression testing, Rotem and Nelson [8] tested a cross-ply and unidirectional graphite/epoxy composite. They saw that both layups failed in compression,

and that this was the result of splitting fiber bundles, ply delamination, and then buckling. Opalski [1] did tension-compression tests on cross-ply Nicalon/CAS and all of these specimens failed in compression due to ply buckling.

Rotem [9] proposed a "Fatigue Failure Envelope" for a carbon reinforced epoxy. Figure 1 shows an example of this envelope. A specimen stress ratio that is on the right side of line B-D should fail in tension, while those on the left side should fail in compression. His envelope was constructed using applied stress-cycles to failure curves of both tension-tension and tension-compression tests. This envelope was investigated to see if it could be applied to Nicalon/CAS.

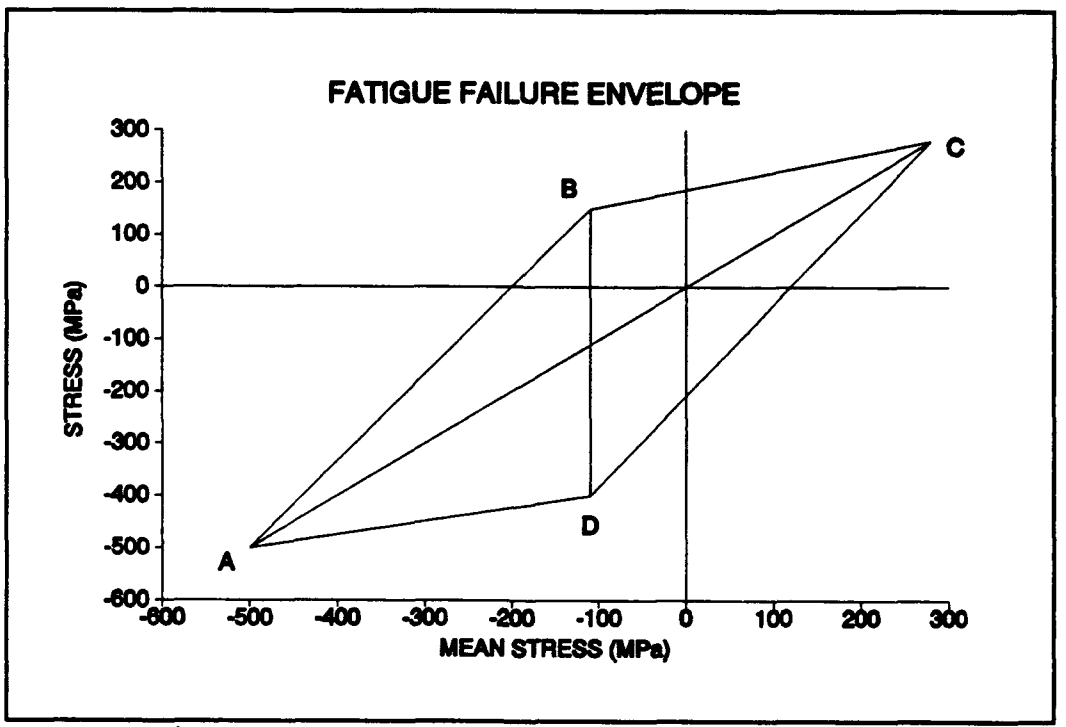

Figure 1. Rotem's Fatigue Life Envelope

Talreja [10] introduced a fatigue life diagram to analyze fatigue of polymer matrix composites. Figure 2 shows a typical diagram with the three distinct failure regions proposed along with the associated scatter bands labeled. He attempted to apply this diagram to unidirectional ceramic matrix composites. The fatigue life data from this study was plotted in a fatigue life diagram to see if the failure modes fell into distinct regions.

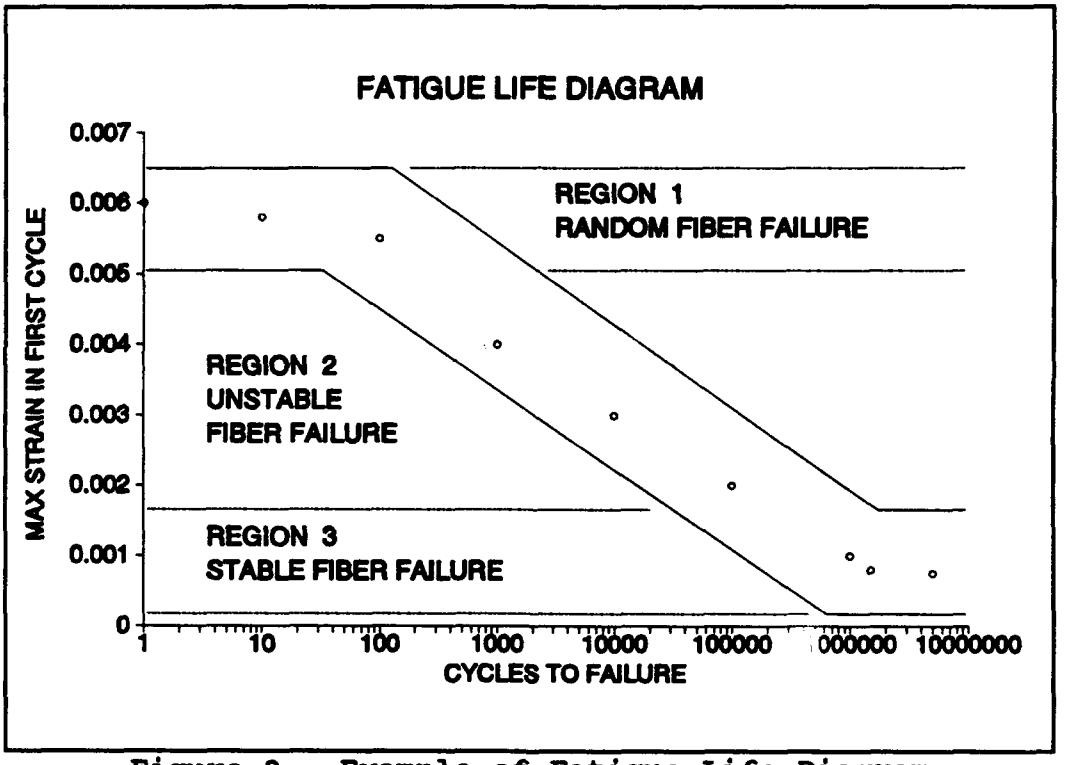

Figure 2. Example of Fatigue Life Diagram

As mentioned earlier, there is limited published information on strain controlled testing. Zawada and Butkus [3] showed for Nicalon/1723 that the fatigue life was related to the nonlinear stress-strain behavior of the 0° plies, and

that the fatigue strain limit was 0.3 percent under load controlled testing. Zawada and Pernot [11] did cross-ply tension tests on SiC/BMAS and showed that there were time dependent effects on the specimen when using different loading or strain rates.

B. Models and predictions

Since no available analytical models available accurately predict the fatigue life of a ceramic matrix composite, the Classical Laminated Plate Theory (CLPT) is usually used to estimate various laminate properties and failure stresses and strains.

From the "critical element approach", the 0° plies are the critical elements for the $[0/90]_{2s}$ Nicalon/CAS specimens tested. Since the 90° plies are not critical to the specimen's failure, they can be eliminated from the CLPT equations after the first cycle by using the Total Discount Method of CLPT. The unidirectional properties of a Nicalon/CAS composite were calculated by Mall, Fink, and Kim [4] and are shown in table 1.

Table 1

Longitudinal Modulus	E_1	139 GPa
Transverse Modulus	E_2	93 GPa
In-Plane Shear Modulus	G_{12}	42 GPa
Major Poisson's Ratio	ν_{12}	0.25

For an orthotropic material under plane stress the stress-strain relation for the principal material directions is given

by:

$$\{\sigma\} = [Q]\{\epsilon\} \tag{1}$$

The components of the stiffness matrix [Q] are expressed in terms of the engineering constants:

$$Q_{11} = \frac{E_1}{(1-\nu_{12}\nu_{21})} \tag{2}$$

$$Q_{22} = \frac{E_2}{(1-\nu_{12}\nu_{21})} \tag{3}$$

$$Q_{12} = Q_{21} = \frac{\nu_{12}E_2}{(1-\nu_{12}\nu_{21})} = \frac{\nu_{21}E_1}{(1-\nu_{12}\nu_{21})} \tag{4}$$

$$Q_{16} = Q_{26} = Q_{61} = Q_{62} = 0 \tag{5}$$

$$Q_{66} = G_{12} \tag{6}$$

Substituting in the material properties, the [Q] matrix is

$$Q = \begin{vmatrix} 145.07 & 24.26 & 0 \\ 24.26 & 97.06 & 0 \\ 0 & 0 & 42 \end{vmatrix} GPa \tag{7}$$

For any other coordinate system the stress-strain relation is

$$\{\sigma\} = [\bar{Q}]\{\epsilon\} \tag{8}$$

To transform from the [Q] to the [Q] matrix the transformation matrix [T] is used

$$[\bar{Q}] = [T]^{-1}[Q][T]^{-1} \tag{9}$$

With the [T] matrix being

$$[T] = \begin{vmatrix} \cos^2\theta & \sin^2\theta & -2\sin\theta\cos\theta \\ \sin^2\theta & \cos^2\theta & 2\sin\theta\cos\theta \\ \sin\theta\cos\theta & -\sin\theta\cos\theta & \cos^2\theta - \sin^2\theta \end{vmatrix} \tag{10}$$

For the $[0/90]_{2s}$ composite there will be two $[\bar{Q}]$ matrices that are obtained by substituting in 0° and 90° for θ above

$$\bar{Q}_{[0]} = \begin{vmatrix} 145.07 & 24.26 & 0 \\ 24.26 & 97.06 & 0 \\ 0 & 0 & 42 \end{vmatrix} GPa \tag{11}$$

$$\bar{Q}_{[90]} = \begin{vmatrix} 97.06 & 24.26 & 0 \\ 24.26 & 145.07 & 0 \\ 0 & 0 & 42 \end{vmatrix} GPa \tag{12}$$

An extensional matrix [A] is needed and is defined as the sum of the $[\bar{Q}]$ matrices multiplied by each individual ply thickness, and in equation form given by

$$A_{ij}=\sum \bar{Q}_{ij}(h_k-h_{k-1}) \tag{13}$$

The thickness of each ply (h_k-h_{k-1}) is calculated by dividing the number of plies into the total plate thickness. With the thicknesses and $[\bar{Q}]$ matrices included in the summation, [A] is

$$A_{ij}=\begin{vmatrix} 353.5 & 70.8 & 0 \\ 70.8 & 353.5 & 0 \\ 0 & 0 & 122.6 \end{vmatrix} MPa \tag{14}$$

For a symmetrical laminate with the external forces [N] being applied, the mid-plane strains [ϵ°] are related to the forces by the [A] matrix

$$\begin{vmatrix} N_x \\ N_y \\ N_{xy} \end{vmatrix} = \begin{vmatrix} A_{11} & A_{12} & A_{16} \\ A_{12} & A_{22} & A_{26} \\ A_{16} & A_{26} & A_{66} \end{vmatrix} \begin{vmatrix} \epsilon^0{}_x \\ \epsilon^0{}_y \\ \gamma^0{}_{xy} \end{vmatrix} \tag{15}$$

Under x-direction loading only, the standard elastic stress-strain relation applies

$$E_x=\frac{\sigma_x}{\epsilon^0{}_x} \tag{16}$$

After inverting the [A] matrix in equation (15), and setting N_y and N_{xy} to zero (0° loading only), the two laminate modulii are given by

$$E_x = E_y = \frac{A_{11}A_{22} - A_{12}^2}{tA_{22}} = 116\,GPa \qquad (17)$$

From the initial portion of the static tension test stress-strain curve, the measured modulus was 118 GPa, or within two percent of this predicted value.

Since the 90° plies will be weaker than the 0° plies and therefore fail first, the Total Ply Discount Method can be applied to find the modulus after 90° ply failure. This will mean that the 0° plies will be assumed to be carrying the entire load. To calculate the new [A] matrix, the [Q] matrix for the 90° plies is set to zero or fully "discounted". This gives a new [A] matrix of

$$A_{ij} = \begin{vmatrix} 211.8 & 35.4 & 0 \\ 35.4 & 141.7 & 0 \\ 0 & 0 & 61.3 \end{vmatrix} MPa \qquad (18)$$

The modulus in the loading direction then becomes 69.5 GPa or 60 percent of the initial value. The measured modulus on the fatigue tests fell to between 40-70 percent of the initial modulus after the first cycle, depending on the maximum strain.

III. Experimental Procedure

A. Test Station

The test stand consisted of five equipment items: a test frame, a control console, a gripping system, an extensometer, and a personal computer. The test frame was an MTS model with a 22.2 KN MTS Servoram Actuator. The control console consisted of an MTS 458.20 Microconsole, an MTS 458.91 Microprofiler, an MTS 464.80 Data Display unit, a Measurements Group 2310 Signal Conditioning Amplifier, and an oscilloscope. The gripping system consisted of a set of grip fixtures that were closed by pistons actuated by pressurized air. The extensometer was an MTS brand with a 7.72 mm gage length. The personal computer was an IBM PC AT with a 286 chip that housed the testing software and stored the data collected. Figure 3 shows the test stand area.

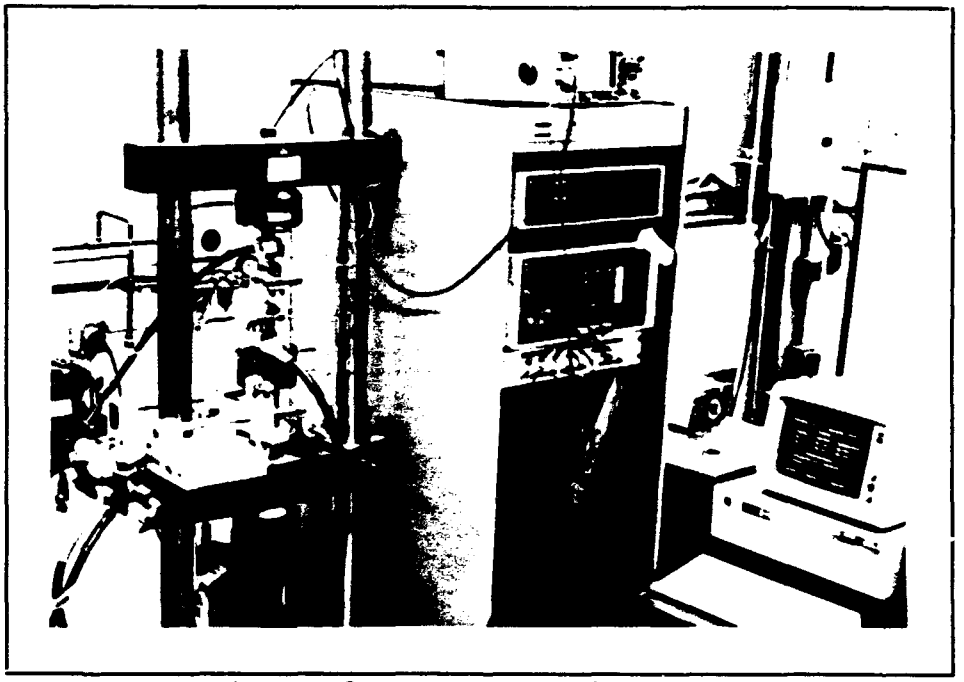

Figure 3. Test Station Setup

B. Test Station Alignment

Before any tests were accomplished, the gripping fixtures had to be properly aligned to ensure that only pure tension or compression loads would be applied to the test specimens. This is especially important with small specimens of ceramic matrix composites. A misalignment could introduce some bending and non-symmetrical loads into the tests and thus affect the resulting fatigue life of the specimen, and ultimately lead to premature failure. Air Force Institute of Technology (AFIT) lab technicians had previously aligned the grips prior to the first test using a Woods Metal Pot. A detailed explanation of this procedure was given by Tracey [14] and Opalski [1].

Once the grips were aligned, an alignment test was conducted in accordance with ASTM Procedure E1012-89 to verify the alignment. To do this, a polished, stainless steel square specimen 10 cm long with 6.35 mm wide sides was used. A strain gage was attached to the center of each side to measure the longitudinal strain. These four gages were then connected to a Measurements Group SB-10 Switch and Balance Unit that was connected to a BLH Model 1200B Digital Strain indicator. This specimen was then inserted into the grips and tension loaded in 100 Newton increments while the strains for each of the four sides were manually recorded. This strain data was reduced using the bending equations as given by Opalski [1].

The percent bending was then plotted versus the applied load to see if the grips were adequately aligned.

Several alignment tests were run. The specimen was then rotated 90° and reinserted into the grips. This ensured that any gage or measurement discrepencies could be noted and fixed. The specimen had to be carefully placed into the fixture to prevent bending due to gripping the specimen in a slightly less then vertical position. For the loads that were used for testing, the percent bending was below three percent, thus showing that the grips were adequately aligned.

C. Specimen Background and Preparation

The material tested was a silicon fiber (Nicalon) reinforced calcium-aluminosilicate ceramic matrix composite in a $[0/90]_{2s}$ lay-up. This type of composite was made in a two-stage process. The first stage involves passing a fiber tow through a slurry tank and then winding it on a drum to dry. In the second stage, the tows are cut, stacked, and then consolidated by being hot-pressed at temperatures above 1200°C.

Nicalon is an amorphous/crystalline fiber usually made of silicon carbide that is manufactured by the Nippon Carbon Company. Its diameter is about 15 μm, and is commonly available in 1800 denier tow. This composite was made up with about forty percent fiber volume. The composite matrix is a calcium-aluminosilicate crystalline glass-ceramic, and is manufactured by Corning Glass.

The Nicalon/CAS composite used for this test was the second half of a 15.25 cm square plate approximately 3 mm thick that was left over from Opalski's [1] testing. This plate was manufactured in October 1990. Material for testing was maximized by cutting each specimen no bigger than 7.62 cm long and 6.35 mm wide.

The 15.25 cm by 7.62 cm plate was cut in half using a Buehler Isomet low Speed Saw with a 0.381 mm thick, 12.7 cm diameter diamond wafering blade. The two 7.62 cm square pieces were then each cut into 11 specimens giving a total of 22 specimens available for testing. Each of these specimens were measured for uniformity and checked for any noticeble damage. The best ones were used for actual testing. Figure 4 shows where the specimens were cut from the plate.

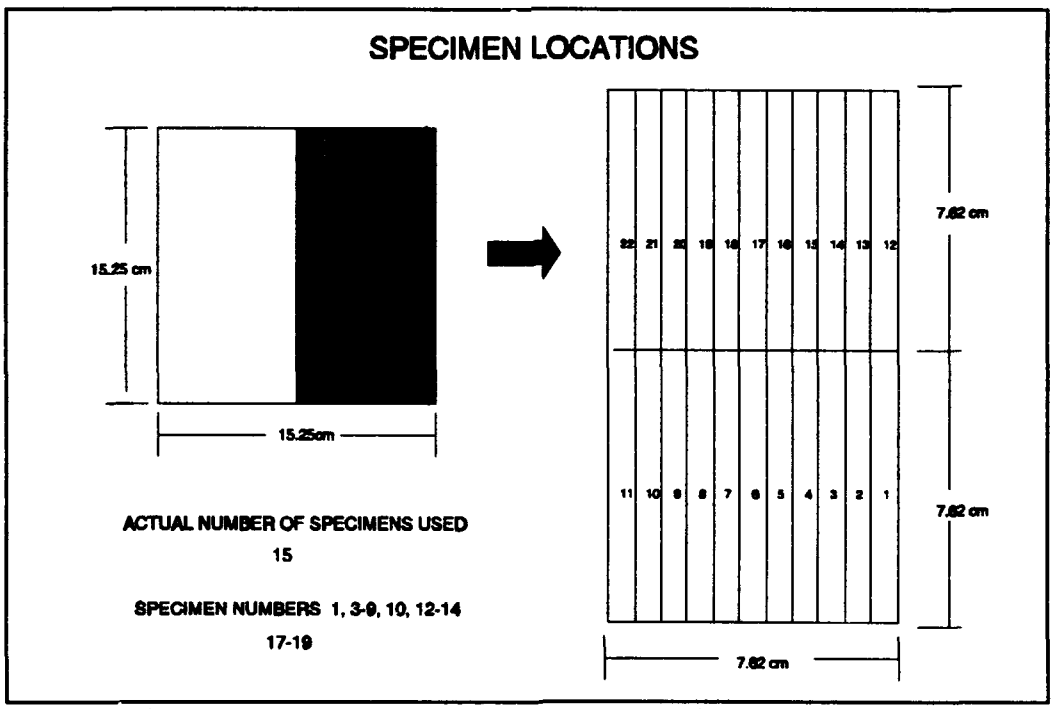

Figure 4. Test Specimen Locations on Plate

The first step in getting the specimens ready for testing was to polish the edges so that replicas could be taken. A Buehler Polimet I Polisher with a 20.3 cm wheel was used to do the polishing. All polishing was done at 200-300 RPM. Six stages were involved: three using a polishing disc and three using a polishing cloth. First, a Fine-Grind polishing disc was used for 20-30 minutes. This was then followed by 30 minutes of polishing with a Rough-Polish disc, and another 30 minutes on a Medium-Polish disc. The last three stages involved polishing on a nylon cloth sprayed first with a six-micron diamond suspension fluid, followed by three-micron diamond suspension fluid and then finally with one-micron diamond suspension fluid. These three stages each were done for one to two hours. Between each stage of polishing the specimens were inspected under a microscope to determine if more polishing was required. After complete polishing, the fibers and matrix in each ply could be clearly seen.

Following polishing, fiberglass tabs were attached to the specimens to prevent the test station grips from damaging or crushing the specimens. The tabs were each 1.9 cm long, 1.52 mm thick, and cut to the same width as the individual specimens. A 30 degree bevel was cut on one end of each tab to minimize the stress concentration factor in the grip. Four tabs per each specimen were then glued onto the specimens using a 50/50 mixture of a V-40 curing agent and an epoxy

resin. The tabs were held in place while curing in a 70°C oven for 90 minutes with binder clips. After removal from the oven the specimens were ready for strain gage installation.

The specimen surface was smoothed and cleaned prior to installing the strain gage. A Measurements Group 0.81 mm general purpose gage was then applied to the center of one side of the specimen. These gages were used to measure the transverse strain. Gage terminals were then glued to the specimens and lead wires soldered to the gage and terminals. The specimens were now ready for testing. Figure 5 shows a prepared specimen along with the specimen dimensions.

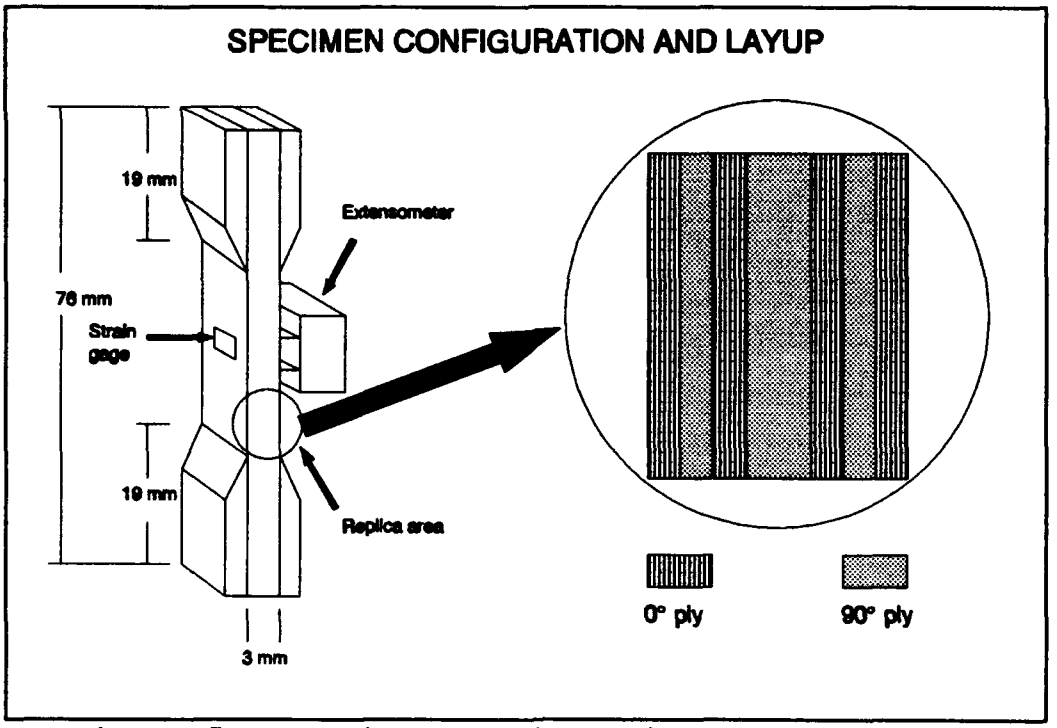

Figure 5. Specimen Configuration and Dimensions

D. Experimental Procedure

Before the specimen was installed for testing, the appropriate loading card was inserted into the microconsole of the test machine so that the maximum load necessary for each test would be provided for by the card. Specimens with the tabs and strain gage attached were now ready to be installed in the test station grips. Hydraulic pressure to raise and lower the grips was actuated via the MTS Microconsole. The microconsole provided for three types of test control: displacement, load and strain. The grips were raised and lowered for specimen installation using displacement control. Air pressure to the grips was then turned on and the grip pressure adjusted to between 17.2-20.7 MPa.

For installation, grip inserts were placed into the grips, with a minimal clearance between the tab and the insert, before the grip was closed. This provided a ridged gripping surface, and helped to ensure that the specimen would not slip out of the grips. The specimen was first placed into the bottom grip and then aligned with an alignment tool before grip pressure was actuated. After the bottom was secured, the microconsole controller was switched to load control before the top of the specimen was gripped. This ensured that no load would be on the specimen during the applying of the top grip pressure. The alignment was again checked, and if necessary, realigned. Figure 6 shows a specimen aligned in the grip fixture and a table of all the tested specimen's dimensions.

SPEC #	THICK (mm)	WIDTH (mm)	AREA (mm^2)
1	2.97	5.79	17.20
3	2.97	5.74	17.05
4	2.92	5.74	16.76
5	2.95	6.17	18.20
6	2.95	5.69	16.79
7	2.95	5.74	16.93
8	2.97	5.89	17.49
9	2.95	5.56	16.40
10	2.95	5.46	16.11
12	2.97	5.46	16.22
13	2.97	5.28	15.68
14	2.97	5.74	17.05
17	2.95	5.84	17.23
18	2.95	5.86	17.29
19	2.95	5.82	17.17

Figure 6. Grip Fixture and Specimen Dimensions

Next a clip-on extensometer was attached to the specimen face opposite the strain gage. Springs were used to secure the extensometer, and then rubber bands were fastened over the springs to ensure that the extensometer would not slip. The extensometer was zeroed on the microconsole so that zero strain was read for zero load.

Prior to connection to the strain gage, the amplifier was calibrated using a strain gage calibrator. The full scale strain to be used was as close to the expected strain as possible to increase the accuracy of the readings obtained. The strain gage was then connected to the amplifier and zeroed prior to testing.

The static tension test was completed using a C program called "STATIC.EXE". The microconsole strain controller was used to strain the specimens at a strain rate of 0.0004 (mm/mm)/sec. Stress and strain data was then stored in an ASCII file for later reduction.

The fatigue tests were accomplished using a strain control C program called "STRNTEST.EXE" written by Capt Brian Sanders, an AFIT PhD student. This was a menu driven program that required operator inputs of information such as the maximum strain, the strain ratio, the strain rate, and specimen dimensions. All strain controlled fatigue tests were run at a strain rate of 0.015 (mm/mm)/sec, yielding a cyclic frequency for most of the tests between 2-3 Hz. Load controlled fatigue tests were run at 10 Hz. Fatigue tests were run until the specimen failed or until one million cycles was reached.

Replicas were taken on all the fatigue tests after cycles 1, 10, 100, 1000, 10000, 100000, and 1000000. A tensile load of approximately 30 percent of the maximum was applied to the specimen during the replica procedure to ensure that the cracks would show during replication. For compression tests a compressive load of 30 percent was applied. To take a replica, the specimen's edge was coated with acetone, and then a piece of acetate wrapped around an eraser was firmly pressed against the edge for 30-40 seconds. The eraser pressure ensured that even pressure was applied to

the entire edge, and that any excess fluid or air bubbles were forced out.

The replicas were then viewed under a microscope, and if found acceptable, placed in a 70°C oven for 30 minutes to prevent curling. These replicas were used to determine the specimen's damage progression, and crack densities by counting the ply cracks along the replica length. Some of the replicas were photographed to further document this damage. Figure 5 shows the specimen's ply lay-up and area that had replicas and photographs taken. Photographs were also taken of some of the fracture surfaces.

From the stress-strain curves, the elastic modulus for all tests was measured from the initial tensile portion of the loading cycle. The hysteretic energy for each test was found by measuring the area under the stress-strain curves during various cycles.

IV. Results and Discussion

The primary purpose of this study was to investigate the effects of strain controlled fatigue loading on a Nicalon/CAS cross-ply composite under both tension-tension and tension-compression loading. To do this, 15 strain controlled tests and 2 load controlled tests were accomplished. The load controlled tests were done to supplement Opalski's data [1], and enable S-N curves to be produced from load controlled data and then compared with the strain controlled $\Delta\varepsilon$-N curves. Section A will cover the types of tests conducted and give a short summary of results for each test while Section B will analyze and compare these results.

Further, the modulus degradation is plotted in the form of a normalized modulus versus cycle relationship as one measure of identifying damage. The normalized modulus for any fatigue cycle, referred to in this study, is the modulus at the current cycle divided by the initial modulus, or E/E_1.

A. Results

Table 2 shows a summary of the strain controlled tests accomplished in this study. R is the ratio of the minimum strain to the maximum strain ($\varepsilon_{min}/\varepsilon_{max}$). ε_{min} is defined as the smallest positive strain for tension-tension tests or the largest negative strain for tension-compression or compression-compression tests. ε_{max} is defined as the largest positive strain for tension-tension tests or the smallest negative strain for tension-compression or compression-compression tests. It should also be noted that under strain

controlled fatigue testing which cycled from maximum tensile strain to minimum tensile strain, compressive loads are experienced by the specimens to obtain the minimum strain. This was due to fatigue damage induced during cycling.

TABLE 2

SPECIMEN #	TEST TYPE *	MAX STRAIN (mm/mm)	R	MAX STRESS (MPa)	CYCLES
8	S	0.00988	-	285.8	-
3	T-T	0.00300	0.1	140.0	1,000,000**
9	T-T	0.00350	0.1	152.8	190,013
6	T-T	0.00375	0.1	163.7	402,162
5	T-T	0.00425	0.1	158.2	380,808
13	T-T	0.00500	0.1	176.6	19,495
4	T-T	0.00550	0.1	184.1	16,377
18	T-T	0.00650	0.1	211.8	7,714
19	T-T	0.00722	0.1	224.3	2,663
10	T-C	0.00135	-1.0	93.3	1,000,000**
7	T-C	0.00175	-1.0	109.7	310,254
14	T-C	0.00236	-1.0	140.4	50,531
1	T-C	0.00293	-1.0	145.2	510
17	T-C	0.00325	-1.0	159.6	60
12	C-C	-0.0003	10.0	-	164
* S:Static T-T:Tension-Tension T-C:Tension-Compression					
C-C:Compression-Compression, ** No failure, test stopped					

A static tension test was conducted to establish a baseline at a strain rate of 0.0004 (mm/mm)/sec. This is a rate similiar to the 10 MPa/sec used by Opalski under load control [1]. Figures 7 and 8 show the stress-longitudinal strain and stress-transverse strain curves obtained from this test.

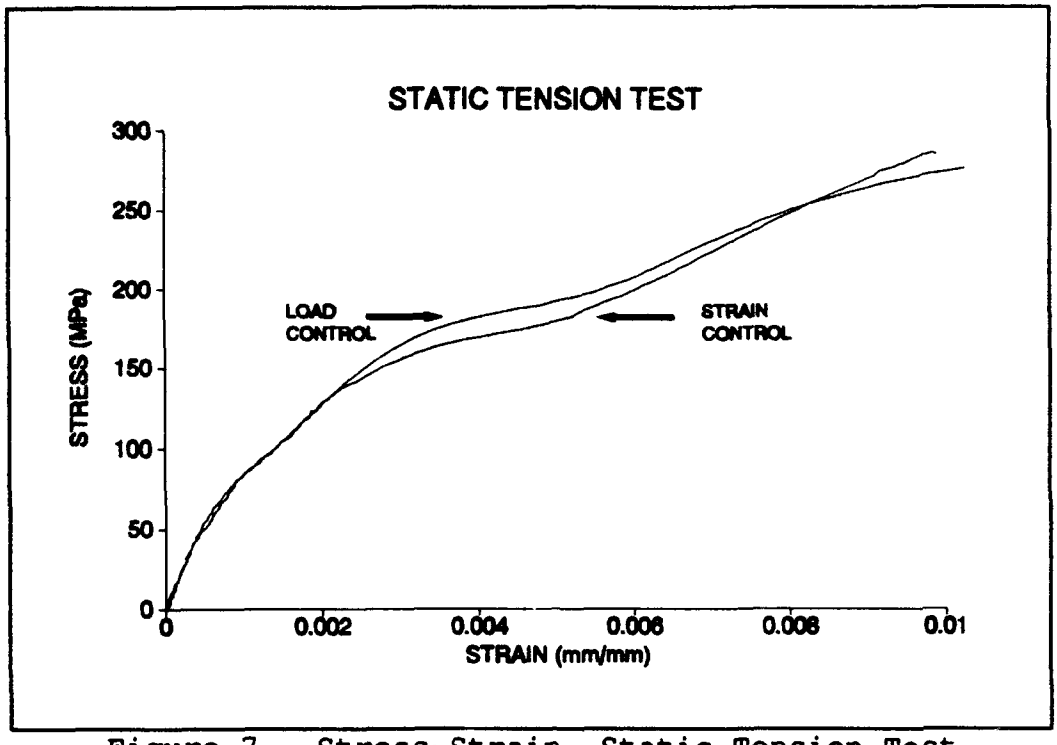

Figure 7. Stress-Strain, Static Tension Test

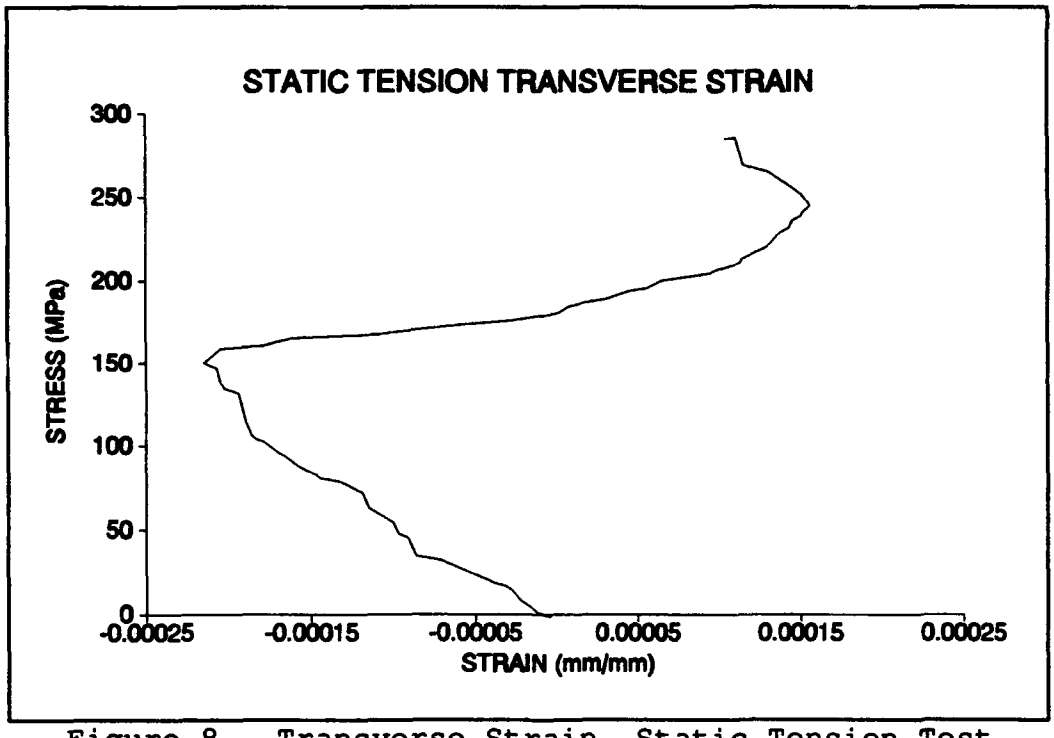

Figure 8. Transverse Strain, Static Tension Test

The load and strain controlled stress-strain curves are very similiar. Both curves have the same "bends", and both curves have similiar ultimate stresses and strains. The major difference between the two curves is that the strain controlled curve is slightly below the load controlled curve between strain values of 0.002-0.008 mm/mm. This is probably due to more relaxation occuring during the strain controlled test. This relaxation was also noticed on almost all of the other strain controlled tests. No replicas were taken during this test. Opalski [1] documented well the crack progression during a load controlled static tension test.

On the stress-transverse strain curve, "bends" in the curve occur at around 50 MPa as the transverse cracks in the 90° plies start to form, and again at 100 MPa as the matrix cracks in the 0° plies begin forming. At 150 MPa a large amount of relaxation occurs as the cracks bifurcate and spread across the entire specimen.

A series of eight tension-tension tests were then conducted to establish a fatigue limit, to establish a $\Delta\varepsilon$-N curve, and to study the damage and failure mechanisms. Based on the static tension test curve, the first test was conducted at a maximum strain of 0.00300 mm/mm, this strain is right at the second "bend" in the curve. This test achieved cycle runout (did not fail over 1,000,000 cycles). Figures 9-12 show the stress-strain, stress-transverse strain, modulus degradation and crack density curves for this test.

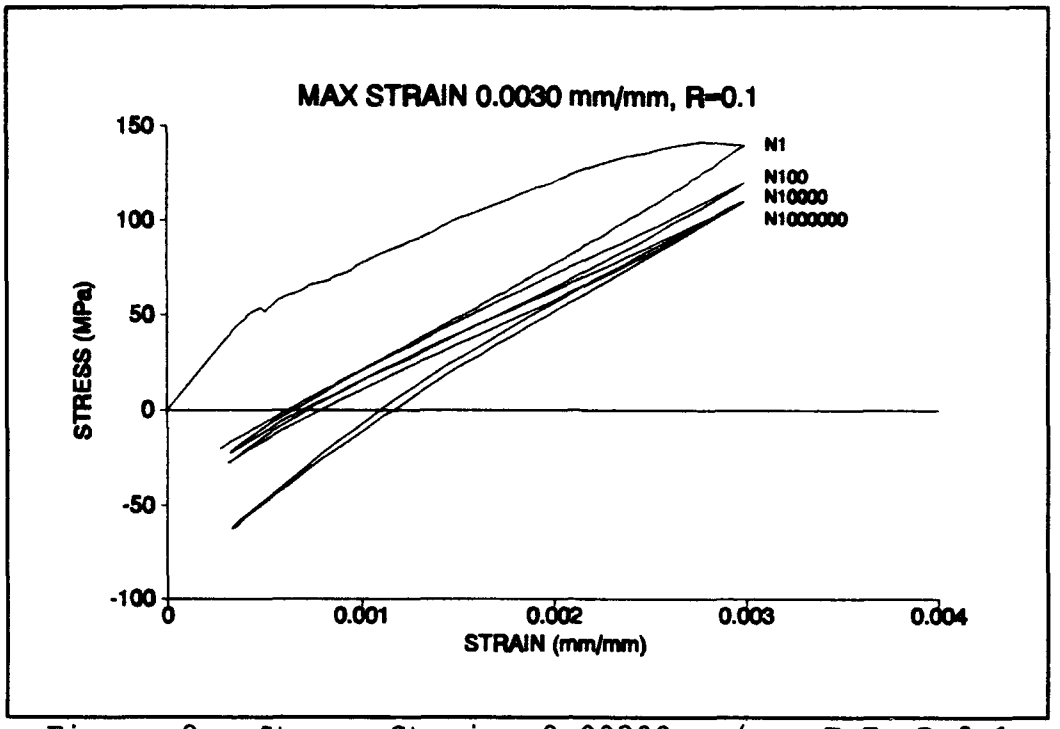

Figure 9. Stress-Strain, 0.00300 mm/mm, T-T, R=0.1

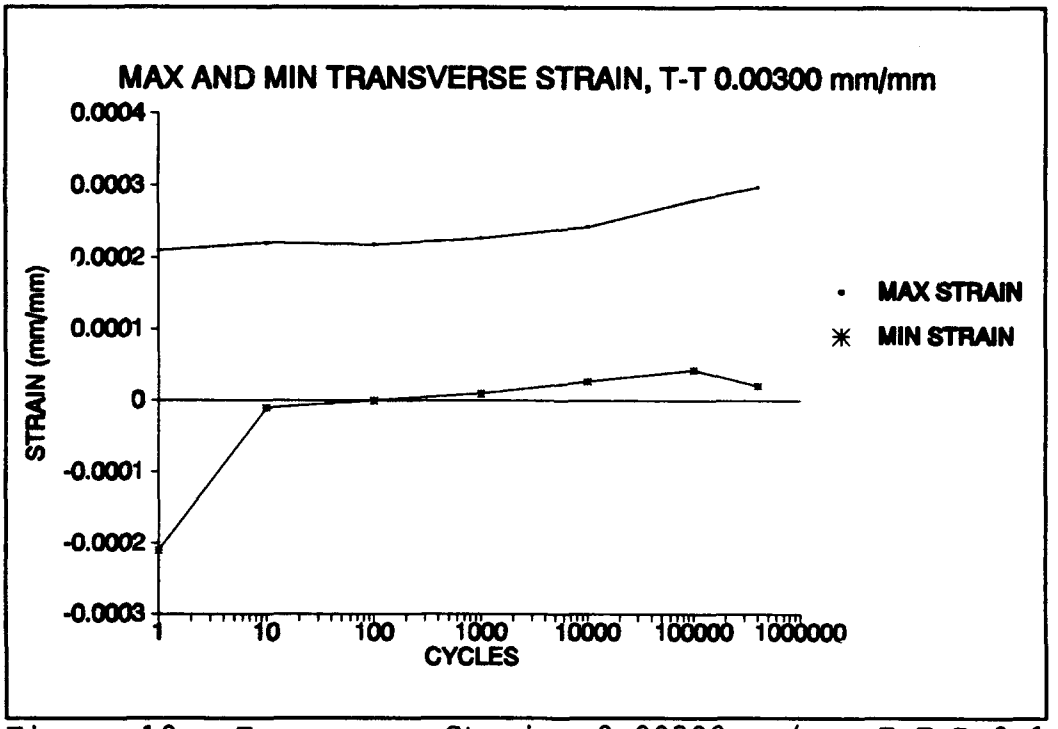

Figure 10. Transverse Strain, 0.00300 mm/mm, T-T,R=0.1

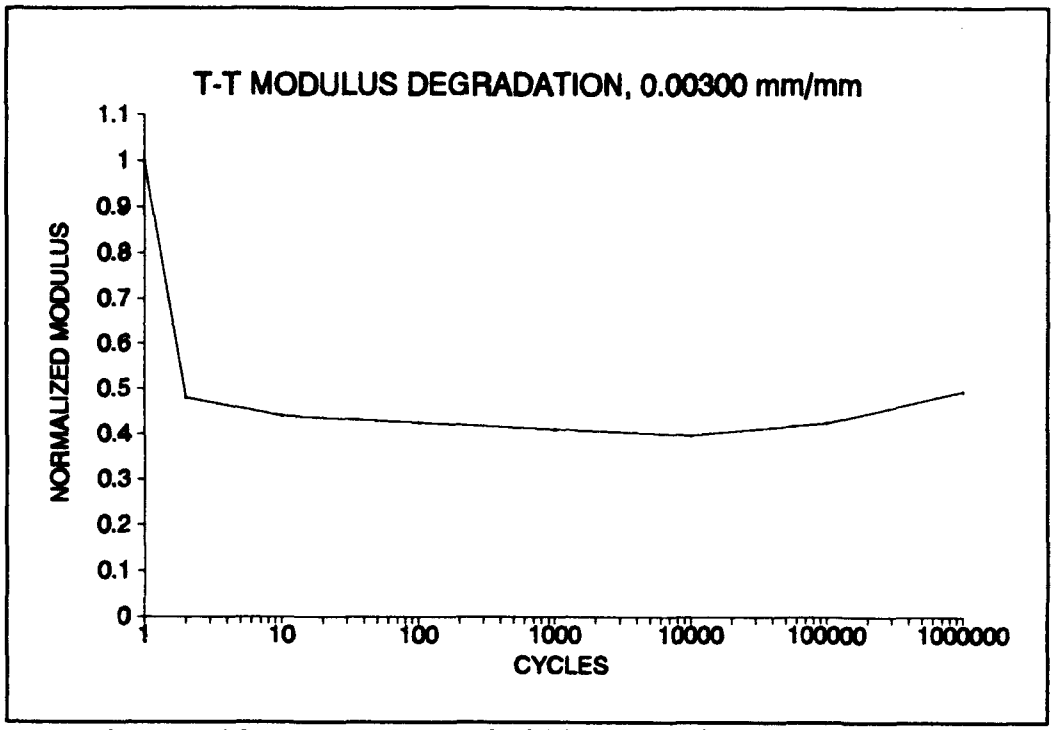

Figure 11. Modulus, 0.000300 mm/mm, T-T, R=0.1

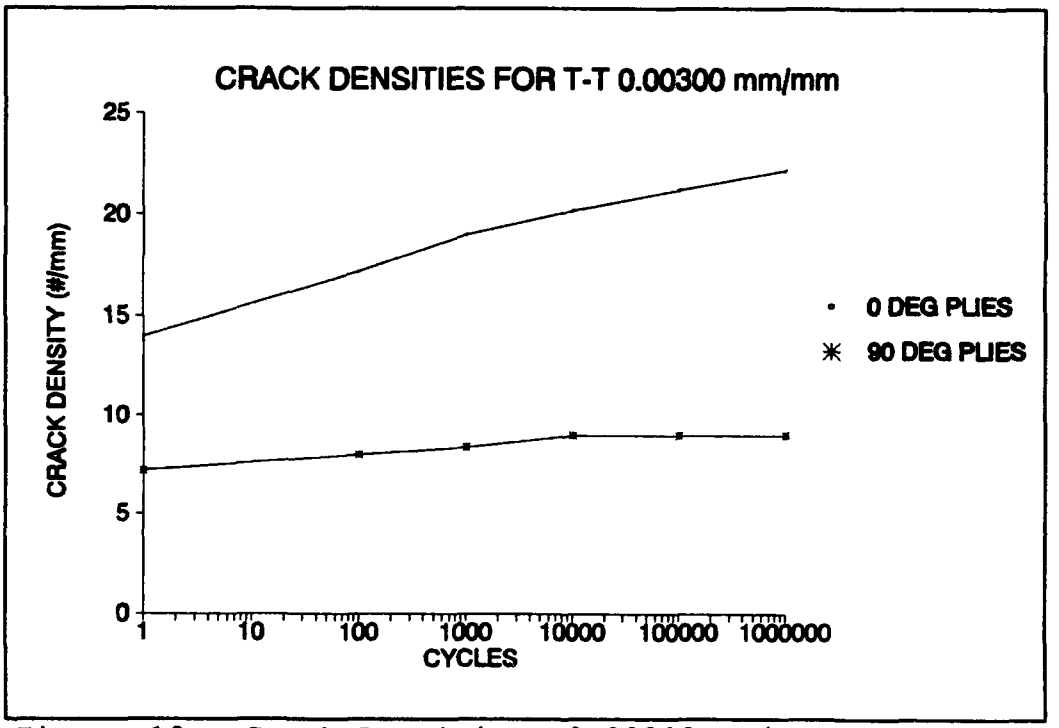

Figure 12. Crack Densities, 0.00300 mm/mm, T-T, R=0.1

Figure 13 shows the transverse cracks in a 90° ply and the matrix cracks in a 0° ply after the first cycle.

Figure 13. Cycle 1, 0.00300 mm/mm, T-T, R=0.1, 500X

Seven more tension-tension tests were conducted with maximum strains ranging from 0.00350 mm/mm to 0.00722 mm/mm. Stress-strain curves for these tests are presented in the Appendix, and all the data for the tension-tension tests are shown together in the discussion section of this chapter. All of these specimens failed before reaching 1,000,000 cycles. Therefore, the maximum strain for which this Nicalon/CAS cross-ply composite could reach 1,000,000 cycles in a tension-tension loading was determined to be 0.00300 mm/mm.

The next step was to study the effects of tension-compression loading on the composite. To compare tension-

tension and tension-compression results, the strain range $\Delta\varepsilon=\varepsilon_{max}-\varepsilon_{min}$ could be used. For a tension-tension maximum strain of 0.00300 mm/mm and R=0.1, the $\Delta\varepsilon$ would be 0.00270 mm/mm (0.00300-0.00030 mm/mm). For a tension-compression test with R=-1.0, a $\Delta\varepsilon$ of 0.00270 mm/mm would give maximum and minimum strains as +/-0.00135 mm/mm, respectively.

Since $\Delta\varepsilon$ of 0.00270 mm/mm achieved 1,000,000 cycles for the tension-tension tests, this value of $\Delta\varepsilon$ was used in the first tension-compression test. This first tension-compression test also reached 1,000,000 cycles without failure. Figures 14-17 show the stress-strain, stress-transverse strain, normalized modulus and crack density curves, respectively. Figure 18 shows a longitudinal crack that developed in a 90° ply between 500,000 and 1,000,000 cycles. Longitudinal cracks like this would have grown significantly if cycling continued and ultimately could lead to specimen failure.

Four more tension-compression tests were run at strain ranges that ranged from 0.00350-0.00650 mm/mm. All of these specimens failed before reaching 1,000,000 cycles. Longitudinal cracks were present in all of these specimens before failure. All of these results are compared together in the discussion section of this chapter.

From these tension-compression tests, the maximum, strain range $\Delta\varepsilon$ for which 1,000,000 cycles would be reached was determined to be 0.00270 mm/mm. This is the same $\Delta\varepsilon$ that reached 1,000,000 cycles for the tension-tension tests.

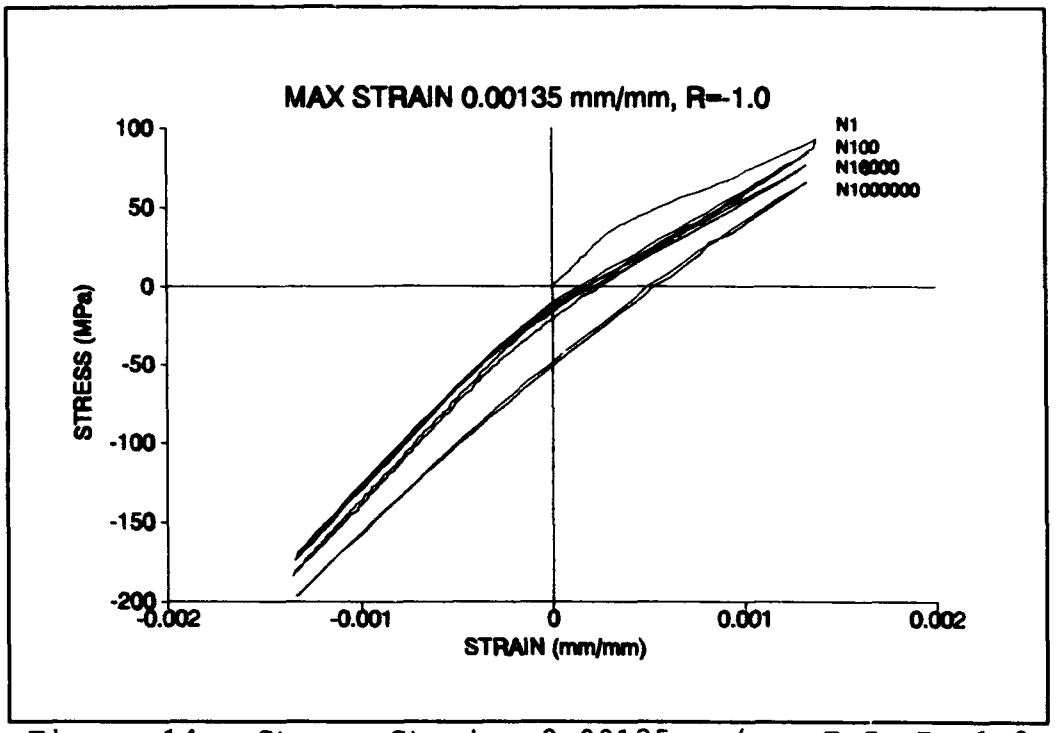

Figure 14. Stress-Strain, 0.00135 mm/mm, T-C, R=-1.0

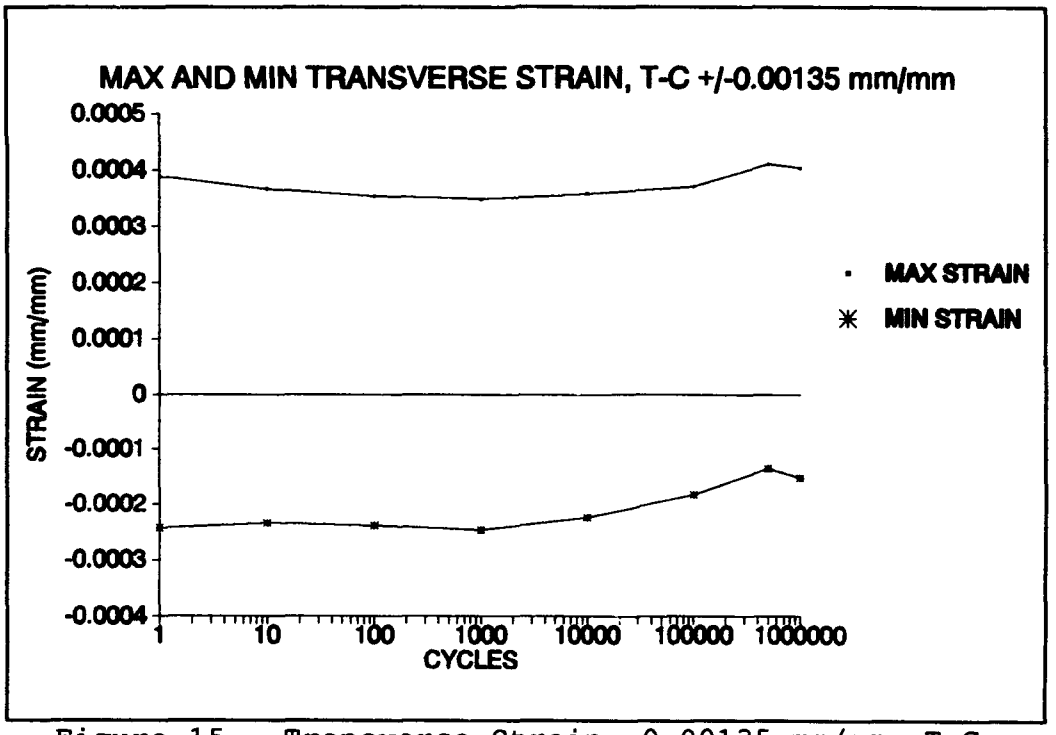

Figure 15. Transverse Strain, 0.00135 mm/mm, T-C, R=-1.0

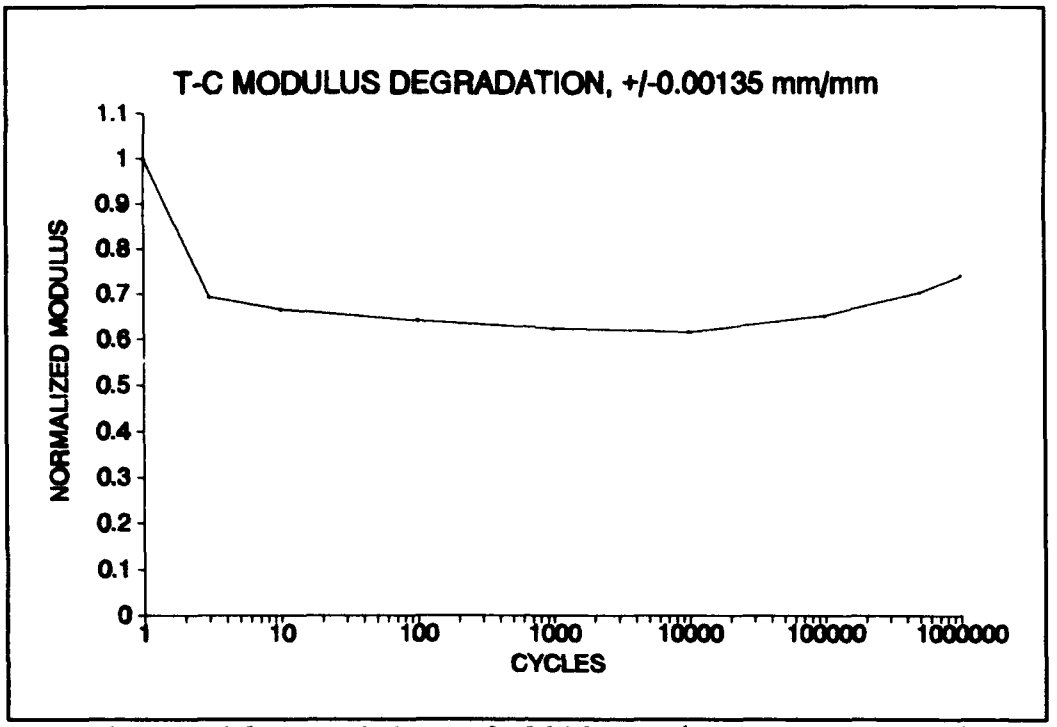

Figure 16. Modulus, 0.00135 mm/mm, T-C, R=-1.0

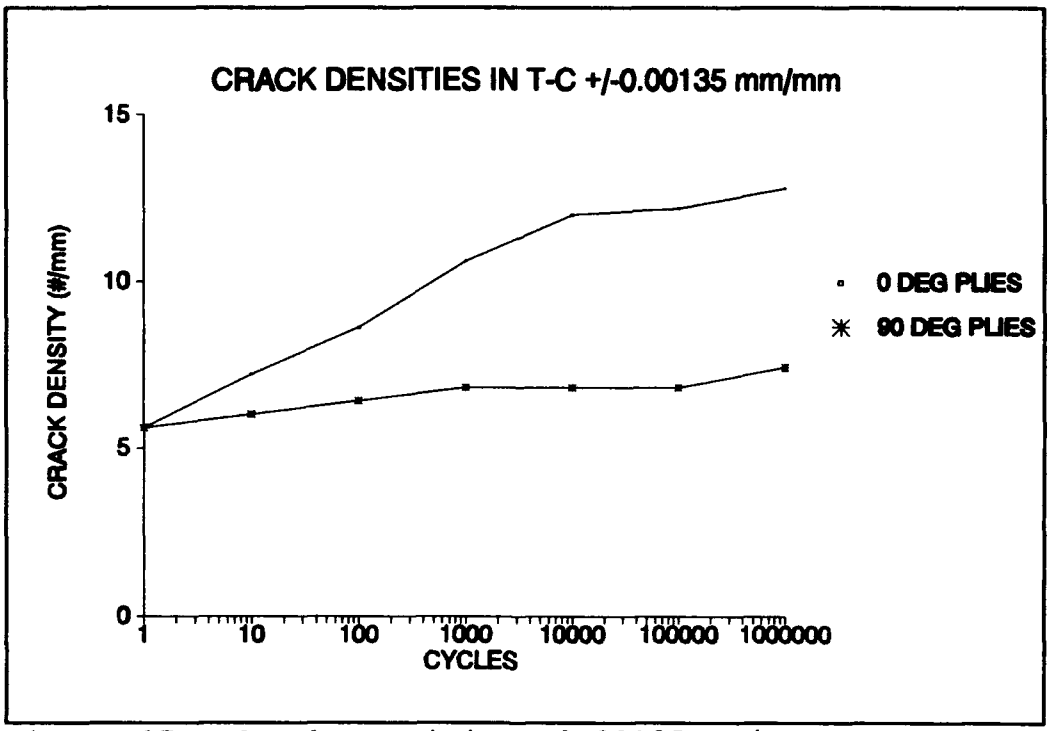

Figure 17. Crack Densities, 0.00135 mm/mm, T-C, R=-1.0

Figure 18. Cycle 1,000,000, 0.00135 mm/mm, T-C, R=-1.0, 500X

The final step in the strain controlled study was to conduct a compression-compression test for a $\Delta\varepsilon$ of 0.00270 mm/mm. This gave a maximum strain of -0.00030 mm/mm and a minimum strain of -0.00300 mm/mm for R=10. Figures 19-21 show the stress-strain, stress-transverse strain and normalized modulus curves, respectively. This specimen lasted for only 164 cycles. The minimum stress on the first cycle was -404 MPa. On Opalski's [1] static compression test the minimum stress at specimen failure was 504 MPa. During the cycle just before failure for this test, the minimum stress had decreased to -450 MPa, so this test was at a strain that put it very close to the top of the static compression curve.

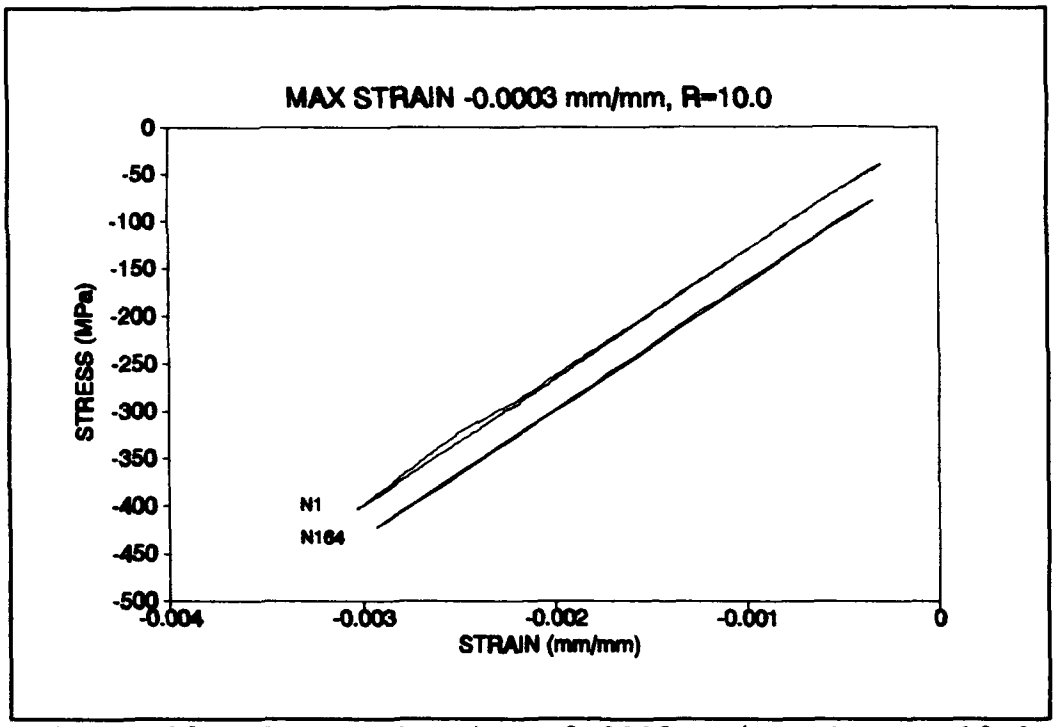

Figure 19. Stress-Strain, -0.0003 mm/mm, C-C, R=10.0

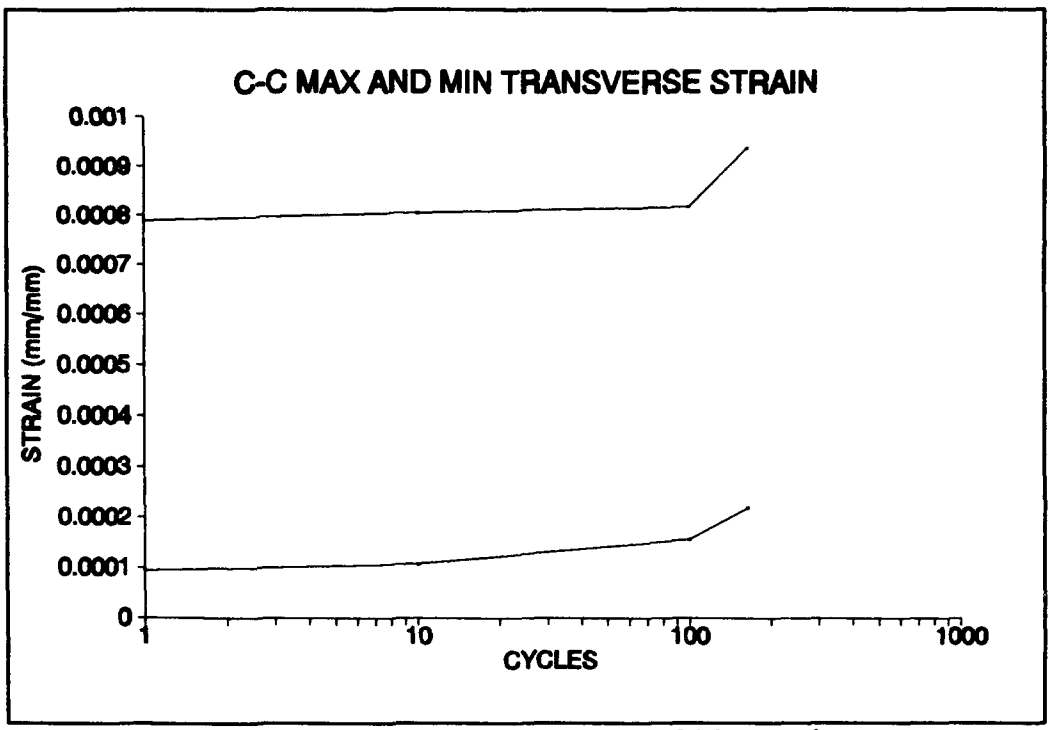

Figure 20. Transverse Strain, -0.00030 mm/mm, C-C,R=10

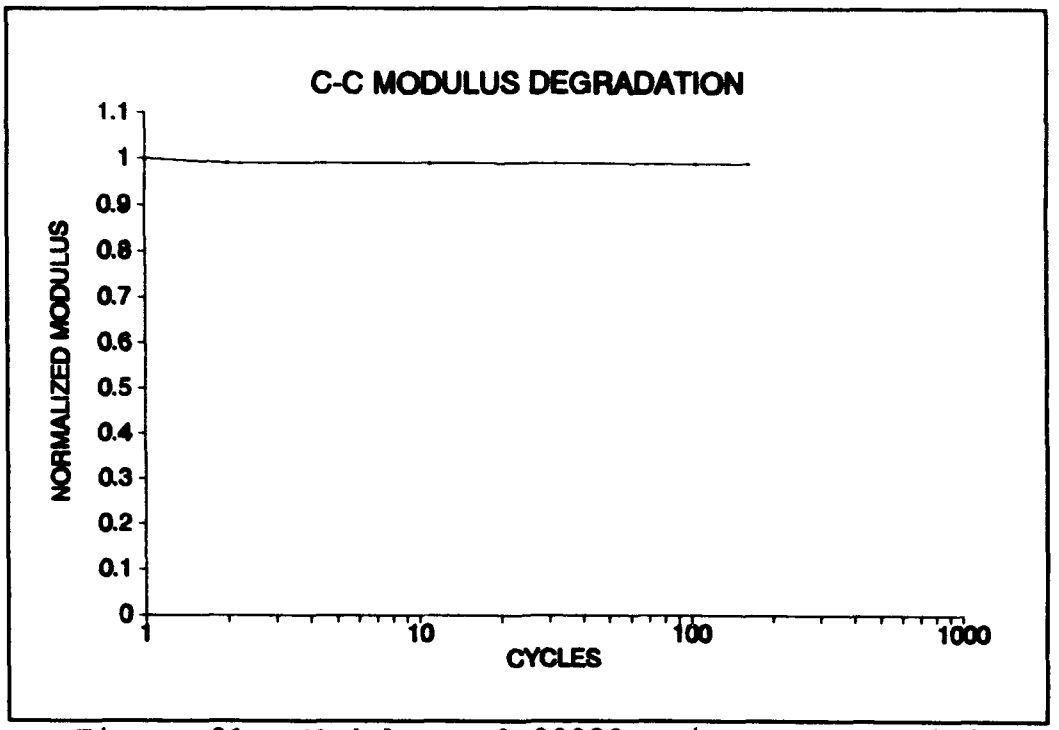

Figure 21. Modulus, -0.00030 mm/mm, C-C, R=10.0

The modulus remained within 95 percent of its initial value right up until failure. Cracks did not start to form until after 100 cycles. Figure 22 shows both longitudinal and transverse cracks that formed after 100 cycles. This replica was taken after the specimen failed. Figure 23 shows both sides of the compressive failure fracture surface.

To finish up the tests conducted during this study, two load controlled tension-compression tests were run to supplement Opalski's data [1]. The first test was done at a maximum stress of 160 MPa and R=-1.0. This specimen failed after 20,424 cycles. The second test was done at a maximum stress of 180 MPa and R=-1.0. This specimen failed after 505 cycles.

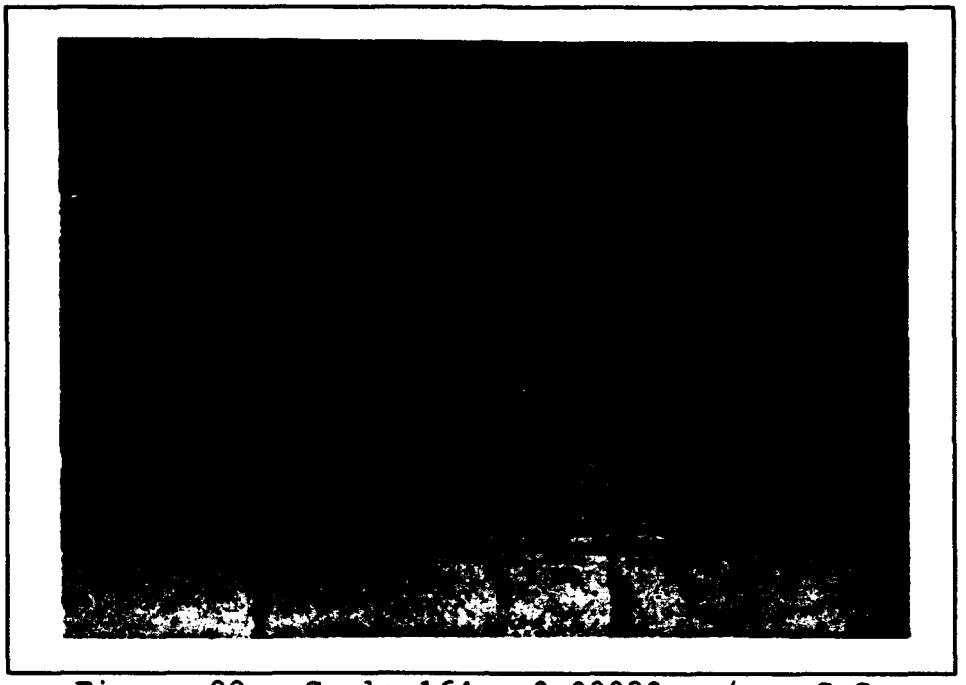

Figure 22. Cycle 164, -0.00030 mm/mm, C-C, R=10.0, 100X

Figure 23. Fracture Surface, -0.0003 mm/mm, C-C, R=10.0, 50X

B. Discussion

In this section the consolidated test results are presented and failure mechanisms discussed for both the tension-tension and tension-compression tests. Models and predictions for failure mechanisms and fatigue life are also discussed.

Figures 24 and 25 show the variation of maximum and minimum stresses for the eight tension-tension tests as a function of number of cycles. As a reminder, the only test that reached 1,000,000 cycles was the 0.00300 mm/mm maximum strain. As expected, the stresses generally decrease with the increase in cycles. This is due to the fact that as the specimen weakens with cycling, the stress necessary to maintain a constant strain will decrease. To maintain the minimum strain the opposite is true, the compressive stress must become larger (more negative) to "push" the specimen back together after the tensile damage has occurred. This is analogous to the strain increasing with the number of cycles for a load controlled test. In general, the stress decreased more rapidly in the cycles just prior to failure, which would be expected as the specimen weakens.

Opalski [1] found the fatigue limit for this Nicalon/CAS lay-up to be 140 MPa under load controlled tests. For these strain controlled tests performed, the only specimen that did not fail (0.00300 mm/mm maximum strain), had a maximum first cycle stress of 140 MPa. All the other tension-tension tests had first cycle maximum stresses above 150 MPa.

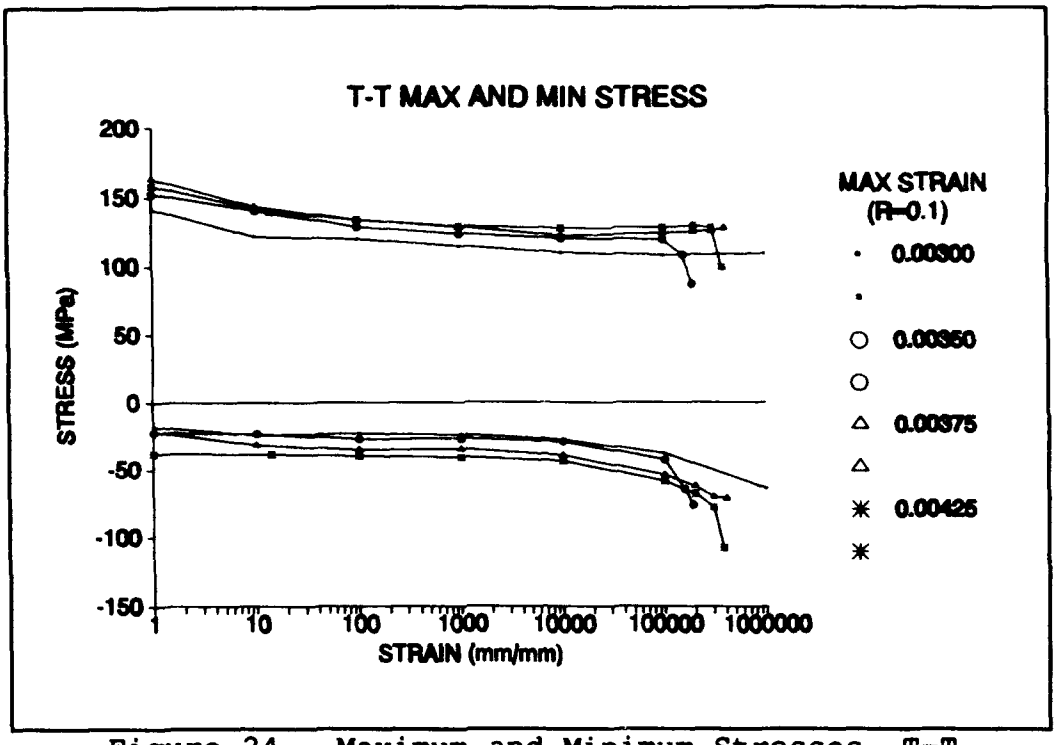

Figure 24. Maximum and Minimum Stresses, T-T

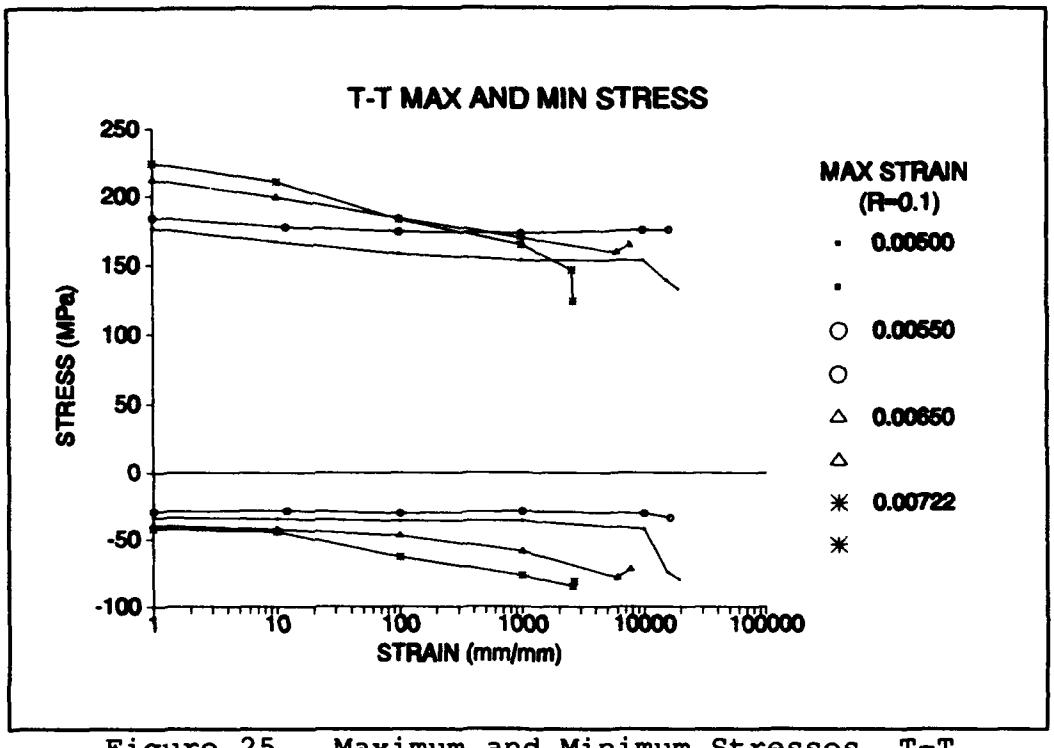

Figure 25. Maximum and Minimum Stresses, T-T

Figures 26 and 27 show the maximum and minimum transverse strain versus number of cycles for the tension-tension tests. Note that in Figure 26, the strain gages failed at 400,000 cycles and 400 cycles respectively for the tests conducted at 0.00300 mm/mm and 0.00425 mm/mm maximum strains.

The maximum transverse strain is reached during the maximum compressive stress of each cycle, and the minimum transverse strain is reached during the maximum tensile stress of each cycle. In all tests, the minimum transverse strain went to a positive value shortly after the first cycle. This was due to the large amount of permanant damage that occurred to the specimen during the first cycle. In general, both the maximum and minimum transverse strains increased as the number of cycles increased and damage progressed.

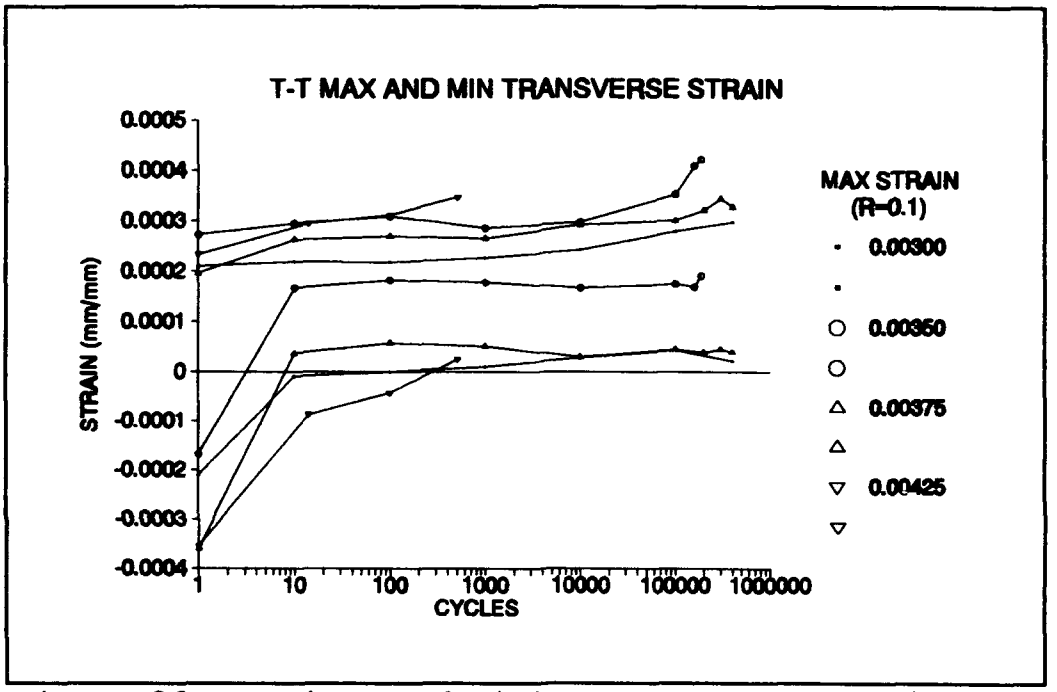

Figure 26. Maximum and Minimum Transverse Strain, T-T

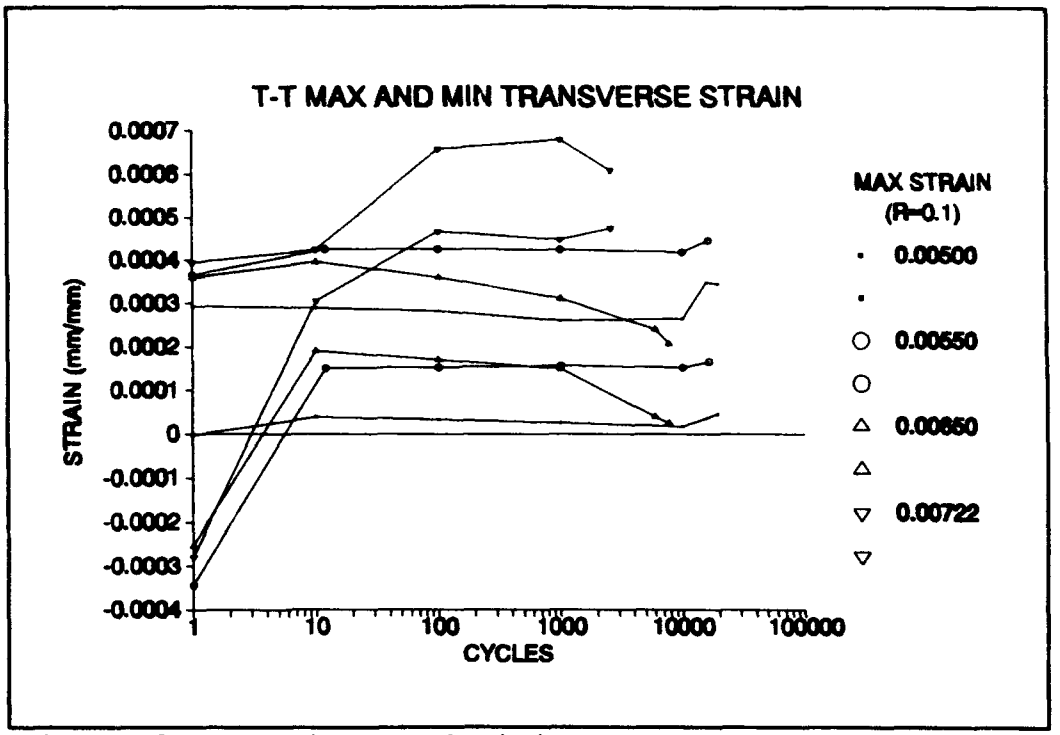

Figure 27. Maximum and Minimum Transverse Strain, T-T

Modulus degradation is sometimes used as a way to measure the damage progression in a specimen. Figure 28 shows the modulus degradation for the tension-tension tests. The modulus drops to between 40 and 50 percent of the initial modulus value after the first cycle. This large reduction is due to the failure of the 90° plies and load transfer to the matrix and fibers of the 0° plies during the first cycle. Each modulus decreased slowly and then stabilized around 40 percent. For the tests that went past 10,000 cycles, each modulus even started to increase back to around 50 percent. This phenomenon was seen in studies by Opalski [1] and Zawada [3]. Zawada theorized that debris from the progressing damage in a specimen starts to fill in the voids and prevents the complete closure of the cracks during unloading.

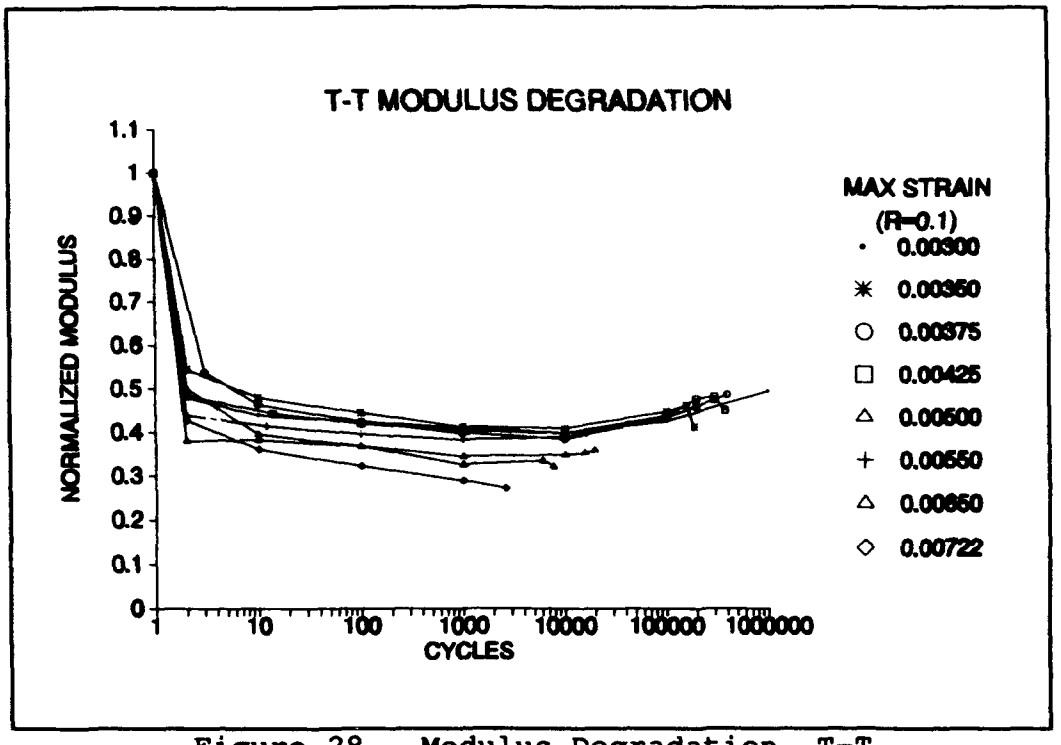

Figure 28. Modulus Degradation, T-T

Once a specimen's modulus degradation levels off or starts to increase again, it would be very difficult to predict when a specimen would fail. Another possible approach to predicting failure is the energy approach. This method was used by Opalski [1], and his energy program was used to calculate the energy for this series of tests. The program calculates the energy under the stress-strain curve for each cycle of the test. Figure 29 shows the energy versus number of cycles for the tension-tension tests.

The largest decrease in energy appears during the first cycle, confirming that the most damage to the specimen occurs during this cycle. The energy values then slowly decrease and level off or increase only minimally during the damage progression. Opalski saw much larger increases of energy

prior to the specimen failure as is seen from the energy curves of the strain controlled tests of this study shown in Figure 29. Thus, for these strain controlled tests, the energy method does not appear to provide a reliable way to predict failure. This needs further study to ascertain its usefullness.

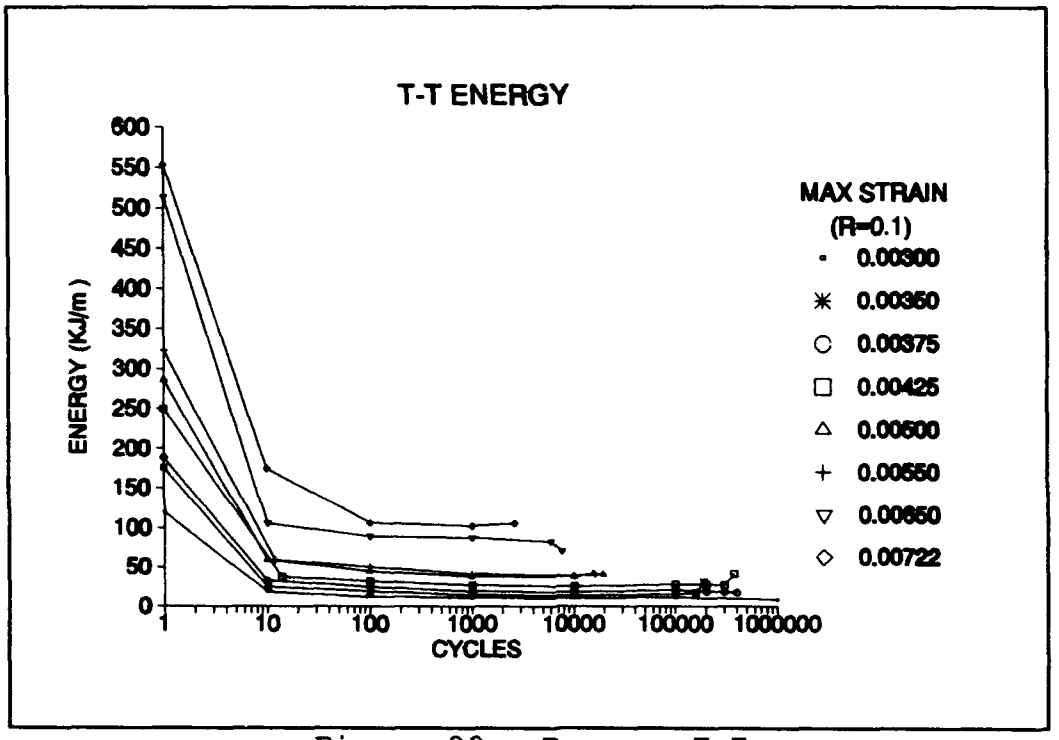

Figure 29. Energy, T-T

The final method used to study fatigue damage was that of crack density measurement. Figures 30 and 31 show the crack densities in the 0° and 90° plies respectively for the tension-tension tests. The crack densities in the 90° plies started out at between 7 and 10/mm after the first cycle and then were fairly constant at between 10 and 15/mm for the rest of the cycles. This shows that the 90° plies essentially "failed" during the first cycle and the strain is now mainly

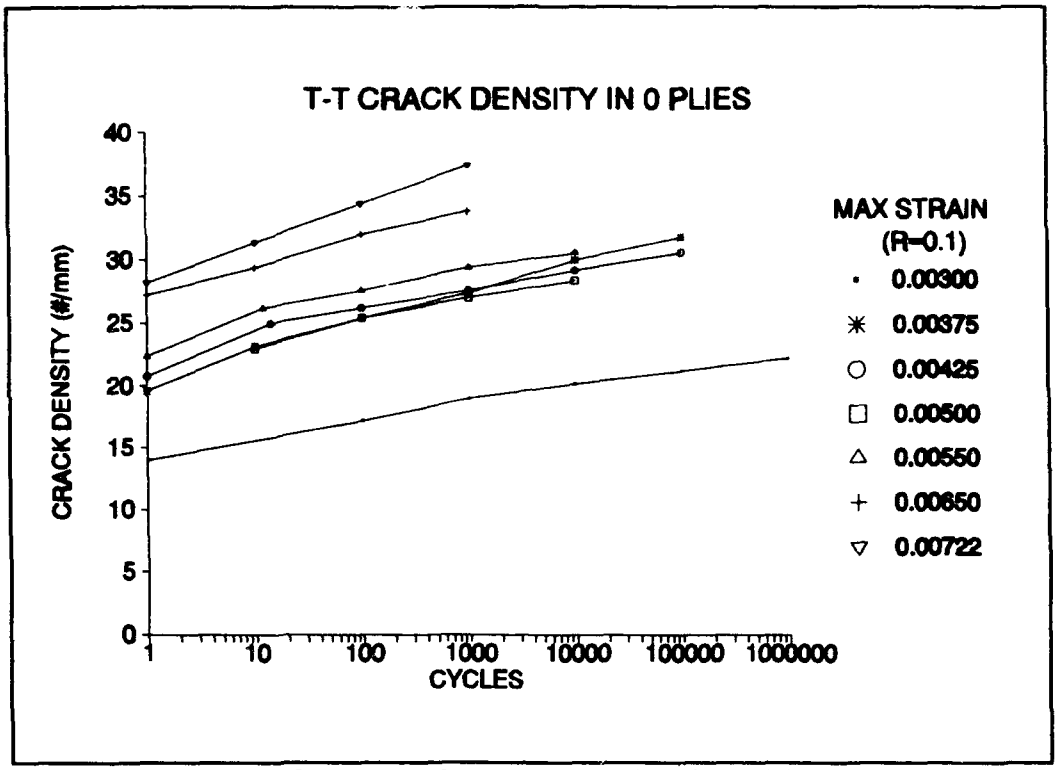

Figure 30. Crack Density in 0° Plies, T-T

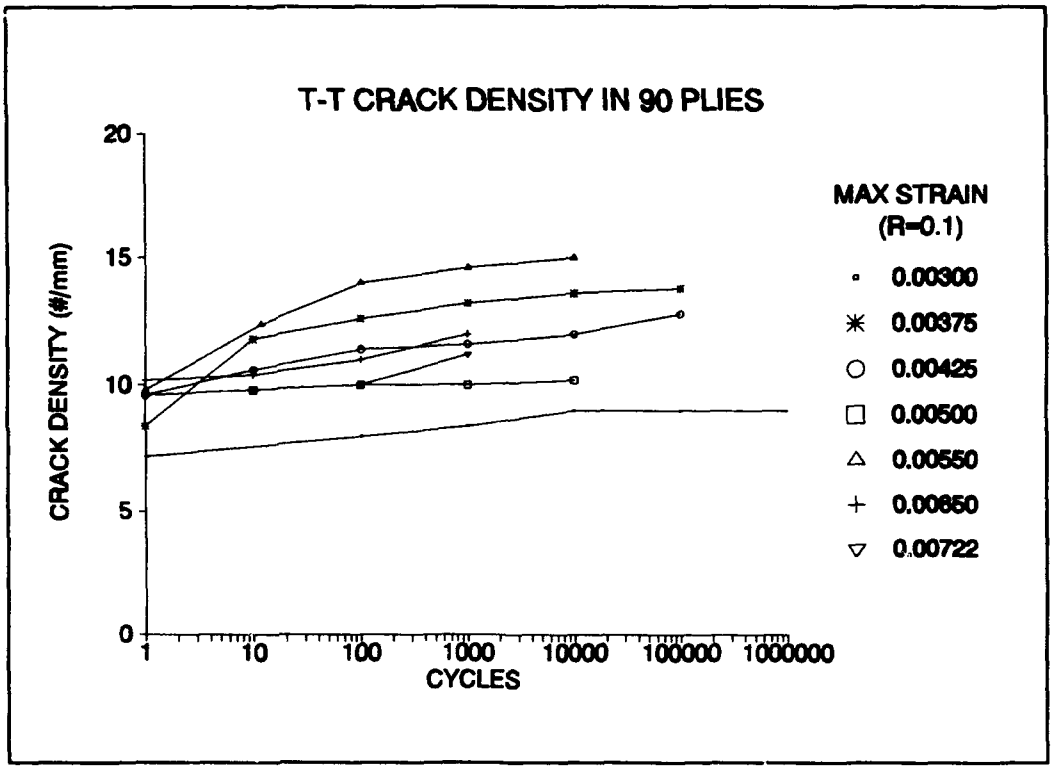

Figure 31. Crack Density in 90° Plies, T-T

affecting only the fibers and matrix of the 0° plies.

The crack densities in the 0° plies range from 14/mm for the 0.00300 mm/mm test to 28/mm for the 0.00722 mm/mm test after the first cycle. The density for the 0.00300 mm/mm test slowly increased to 22/mm at 1,000,000 cycles. All of the specimens that failed had crack densities of more than 28/mm prior to failure. This shows that the crack density in the 0° plies matrix steadily increased until the matrix became unable to support the strain and, thereafter, the strain is only affecting the 0° fibers. The fibers are now the only component of the specimen that is being fatigued and soon fail from the overloading.

Transverse cracks, after the first cycle, in the specimens tested at the maximum strains of 0.00300 mm/mm and 0.00722 mm/mm during the tension-tension tests can be seen in the replica photographs of Figures 32 and 33. The densities in the 90° plies are comparable, but the amount and length of cracks in the 0° plies are very different. The matrix cracks in the 0.00300 mm/mm specimen do not span across the entire matrix of the 0° plies as do the matrix cracks in the 0.00722 mm/mm specimen. There were also some small longitudinal cracks that developed in the 90° plies prior to specimen failure in the two highest strain tension-tension tests (0.00722 mm/mm and 0.00650 mm/mm). This was due to the high compressive loading that was needed to achieve the minimum strain on each cycle.

Figure 32. Cycle 1, 0.00300 mm/mm, T-T, R=0.1, 100X

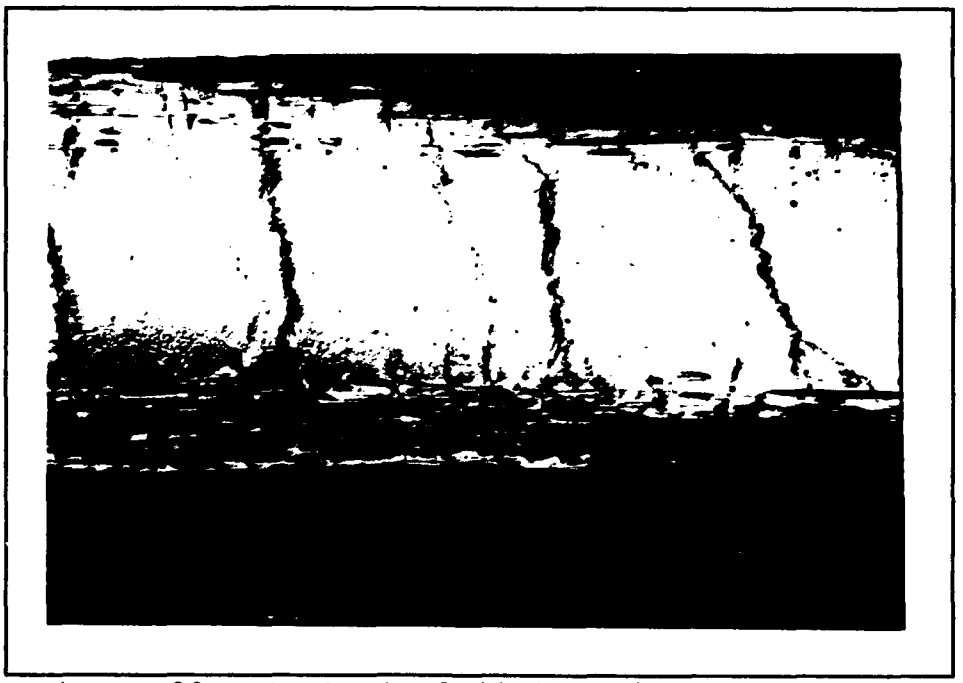

Figure 33. Cycle 1, 0.00722 mm/mm, T-T, R=0.1, 100X

Figure 34 shows a typical fracture surface for a tension-tension test specimen. All of the tension-tension test specimens failed in tension. The transvese cracks in the 90° plies and the matrix cracks in the 0° plies are clearly visible.

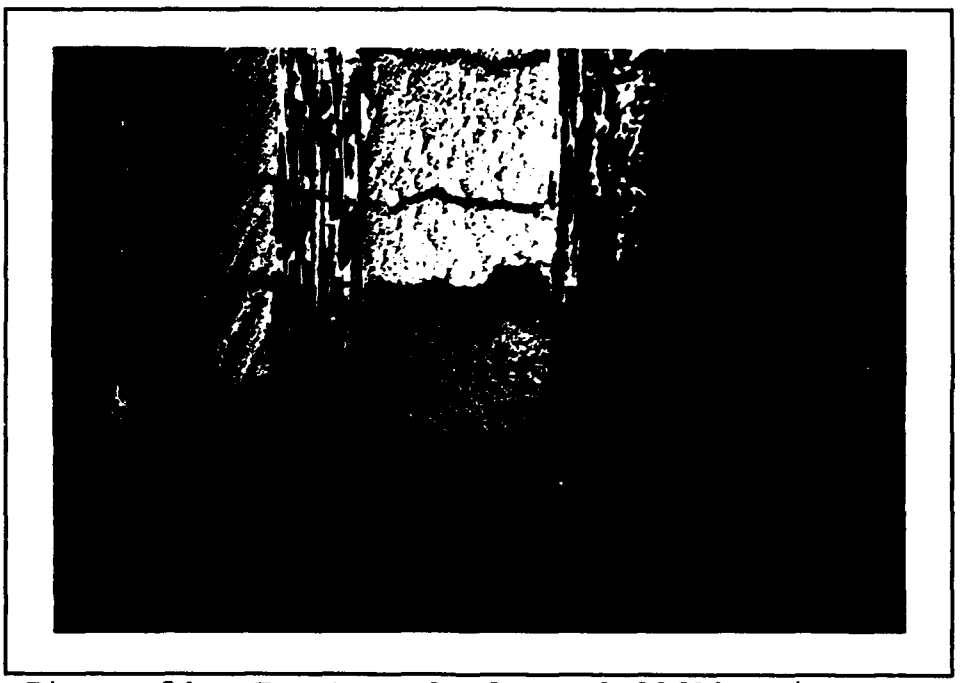

Figure 34. Fracture Surface, 0.00650 mm/mm, T-T, R=0.1, 80X

The tension-compression tests will be discussed next. Five tension-compression tests were completed. The maximum strains for these tests ranged from 0.00135 mm/mm to 0.00325 mm/mm, and the strain ratio R, was -1.0 for all tests. The 0.00135 mm/mm specimen was the only one to reach 1,000,000 cycles.

Figure 35 shows the maximum and minimum stresses for all tests. Almost all of the stresses decreased very slowly as cycling progressed. The minimum stresses for the 0.00175 mm/mm and 0.00236 mm/mm tests were the exceptions. Just before failure the minimum stress decreased significantly due to the effects of longitudinal cracks. The formation of these cracks will be discussed shortly.

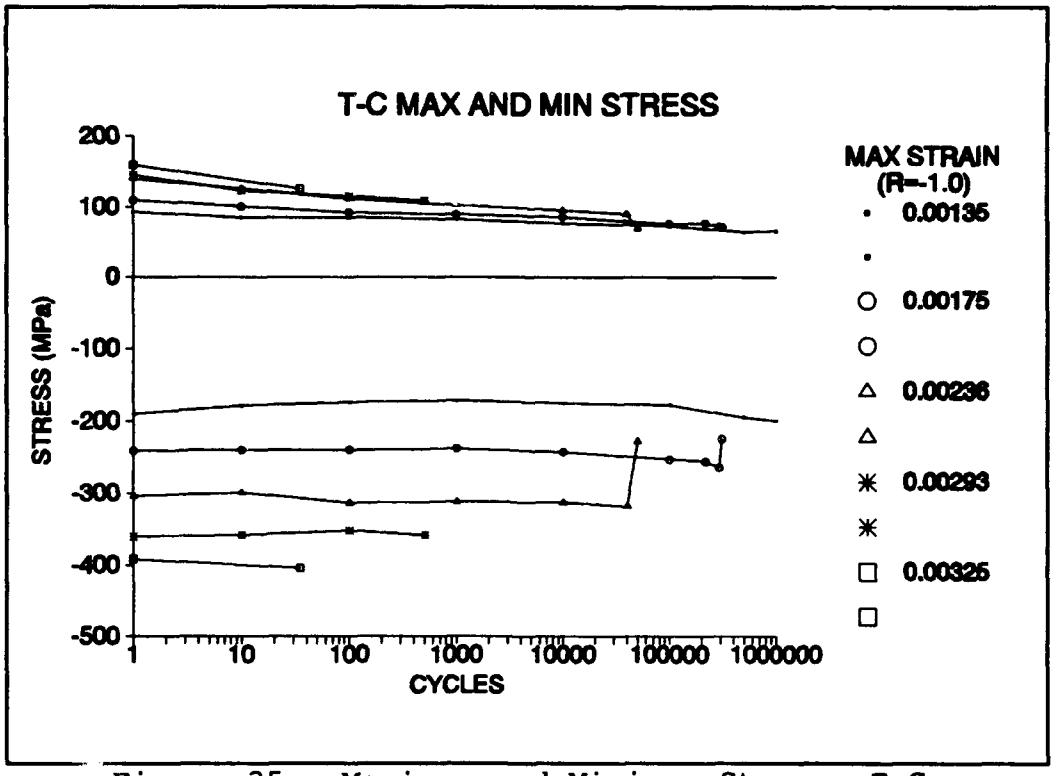

Figure 35. Maximum and Minimum Stress, T-C

The maximum and minimum transverse strains for all tests are presented in Figure 36. The strain resulting from the compressive portion of the cycle is seen to remain fairly constant, while the strain from the tensile portion of the cycle steadily increases to around 0 mm/mm as the damage progresses. The two exceptions to the fairly constant maximum strain are again the 0.00175 mm/mm and 0.00236 mm/mm specimens. These large decreases in the maximum strains which again resulted from the rapid development of longitudinal cracks prior to specimen failure. These cracks severely weaken the specimen and need a smaller compressive load to reach the minimum strain.

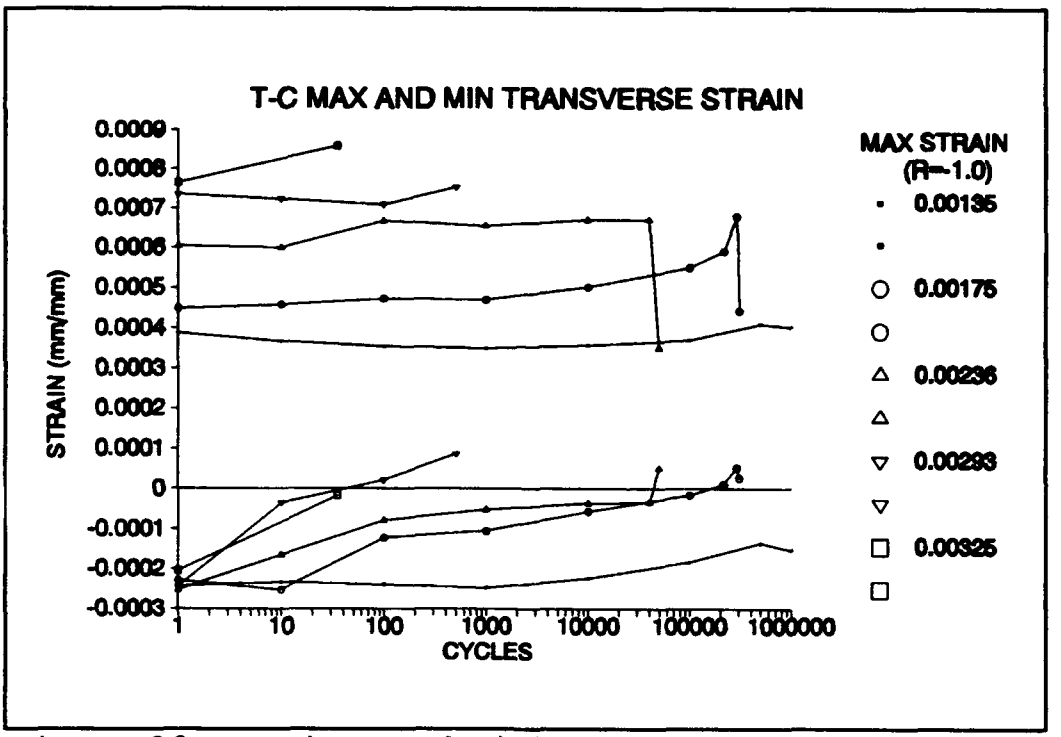

Figure 36. Maximum and Minimum Transverse Strain, T-C

Figure 37 shows modulus degradation curves from these tension-compression tests. Here, each modulus dropped to between 45-70 percent of its initial value after the first cycle. These curves are slightly higher than the tension-tension curves because of the smaller maximum strains. For the 0.00135 mm/mm specimen, the maximum strain was not sufficient to cause the 90° plies to completely fail, thus the modulus only dropped to 70 percent after the first cycle and was fairly steady after that. In general, these curves leveled off and then started to increase again for specimens that lasted more than 1000 cycles. The effects of longitudinal cracks on the modulus can be seen for the 0.00175 mm/mm and 0.00236 mm/mm specimens as the modulus decreases prior to specimen failure.

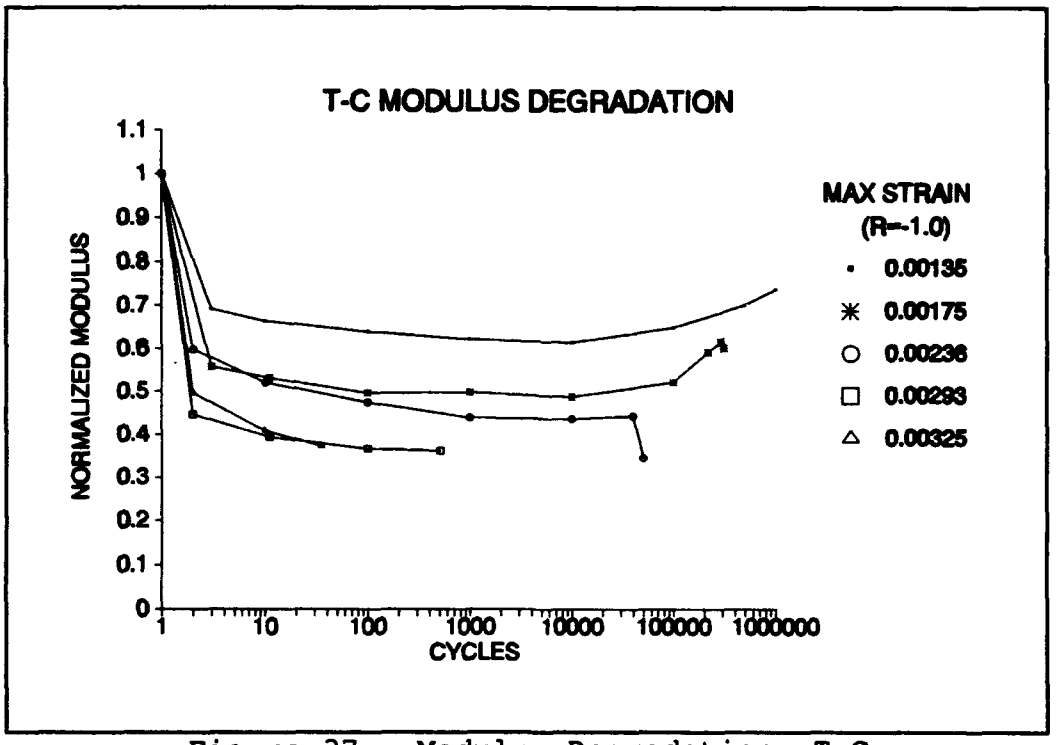

Figure 37. Modulus Degradation, T-C

Figure 38 shows the energy curves for the tension-compression tests. The tension-compression energy curves are similiar to those of the tension-tension tests discussed earlier. Like for the tension-tension tests, these curves also show only small increases in energy after 10,000 cycles. Thus, it seems again that as the damage progresses under strain controlled tests, only small increases in energy can be

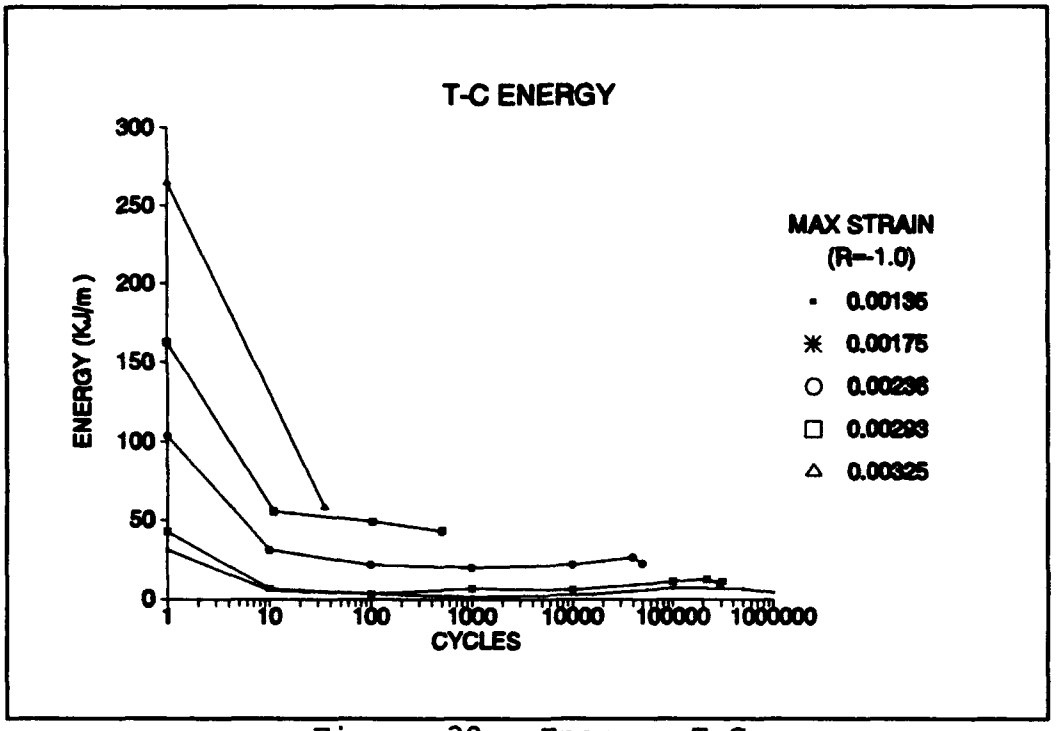

Figure 38. Energy, T-C

seen from the curves.

Figures 39 and 40 show the crack densities for all the tension-compression tests in both the 0° and 90° plies, respectively. These densities were measured from the replicas taken after certain cycles were reached.

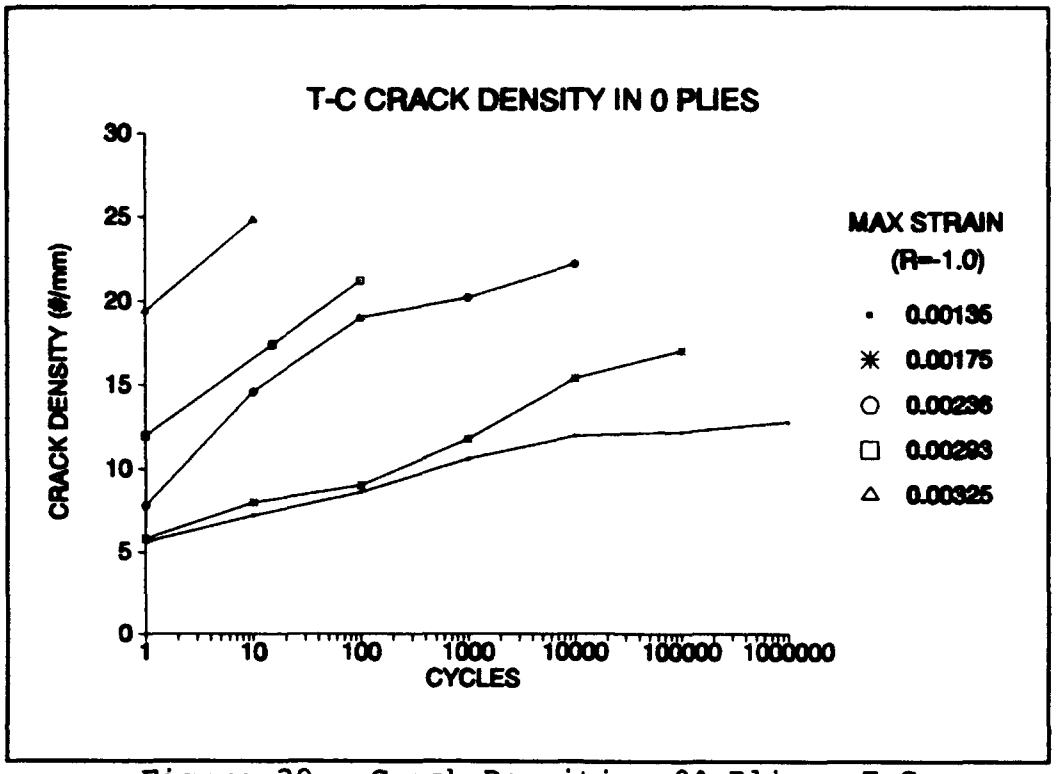

Figure 39. Crack Densities 0° Plies, T-C

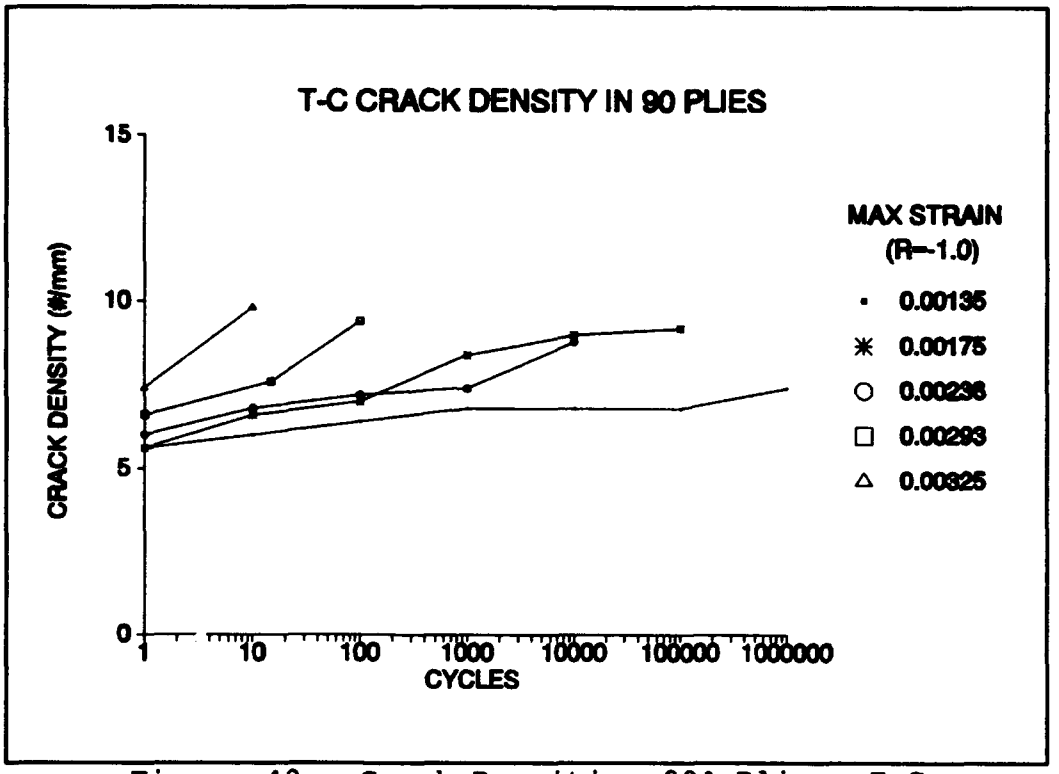

Figure 40. Crack Densities 90° Plies, T-C

The crack densities in the 90° plies range from 6/mm to 10/mm and increase gradually as cycling progresses. This is similiar to the crack progression in the tension-tension tests since most of the damage in the 90° plies is done during the first cycle and the rest of the cracks result from bifurcation and from some longitudinal cracks developing. The main difference between the tension-tension and tension-compression tests is in the densities of the 0° plies. The tension-compression crack densities in the 0° plies did not "saturate" the matrix, and leave the fibers to carry the majority of the load as was the case for the tension-tension tests. The failure mechanisms for all four of the tension-compression specimens that failed were very different from the failure mechanisms of the tension-tension specimens. These failure mechanisms will be discussed after presenting some replica photographs and fracture surfaces.

Figures 41 and 42 show a sequence of two replicas taken at cycles 100,000 and 310,000 respectively for the 0.00175 mm/mm tension-compression specimen. A few small longitudinal cracks were first seen in the 90° plies on the 100,000 cycle replica. These cracks then developed into the huge cracks that are seen in the 310,000 cycle replica. These types of cracks cause ply delamination and buckling of individual plies. The 0.00236 mm/mm specimen also had longitudinal crack development like this. Both of these specimens failed during the tensile portion of the load cycle.

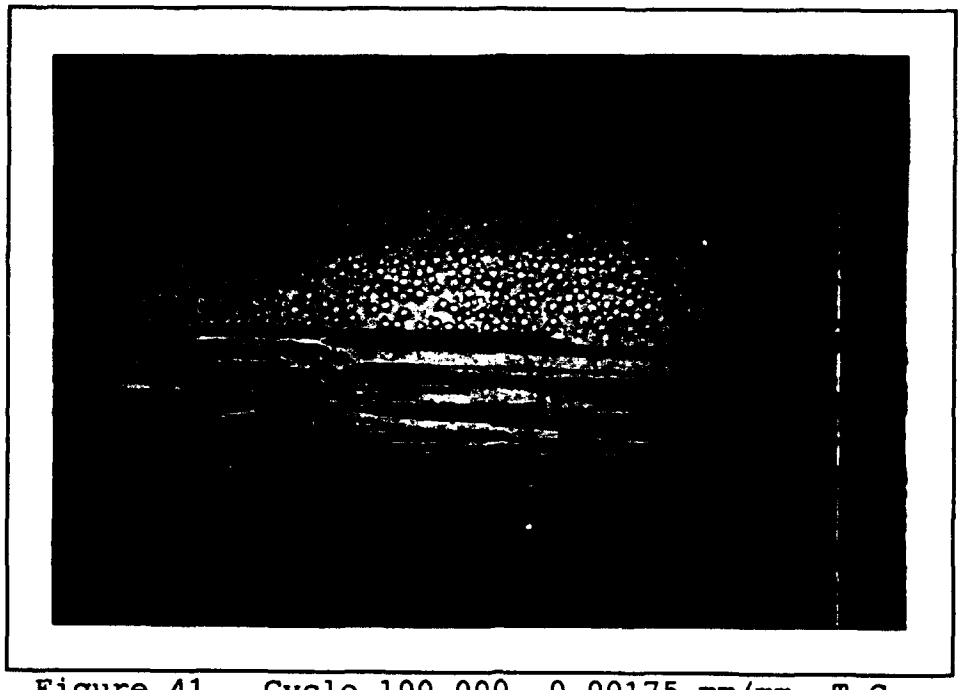

Figure 41. Cycle 100,000, 0.00175 mm/mm, T-C, R=-1.0, 500X

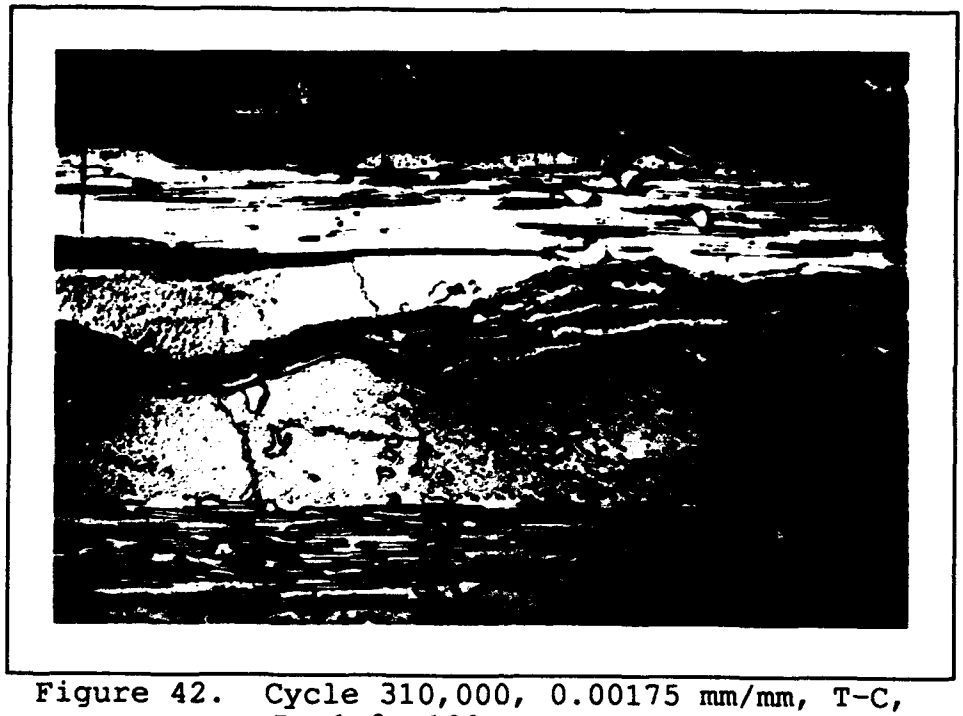

Figure 42. Cycle 310,000, 0.00175 mm/mm, T-C, R=-1.0, 100X

Specimens with maximum strains of 0.00293 mm/mm and 0.00325 mm/mm did not have any significant longitudinal crack development seen on the replicas taken, but evidence of these cracks contributing to the specimens failure can be seen on the fracture surfaces. Both of these specimens failed during the compressive portion of the loading cycle.

The fracture surfaces of the 0.00175 mm/mm specimen and 0.00325 mm/mm specimen are shown respectively in Figures 43 and 44. As a reminder, the first specimen failed in tension and the second specimen in compression. Evidence of longitudinal cracks and ply delamination is clearly seen in these photographs.

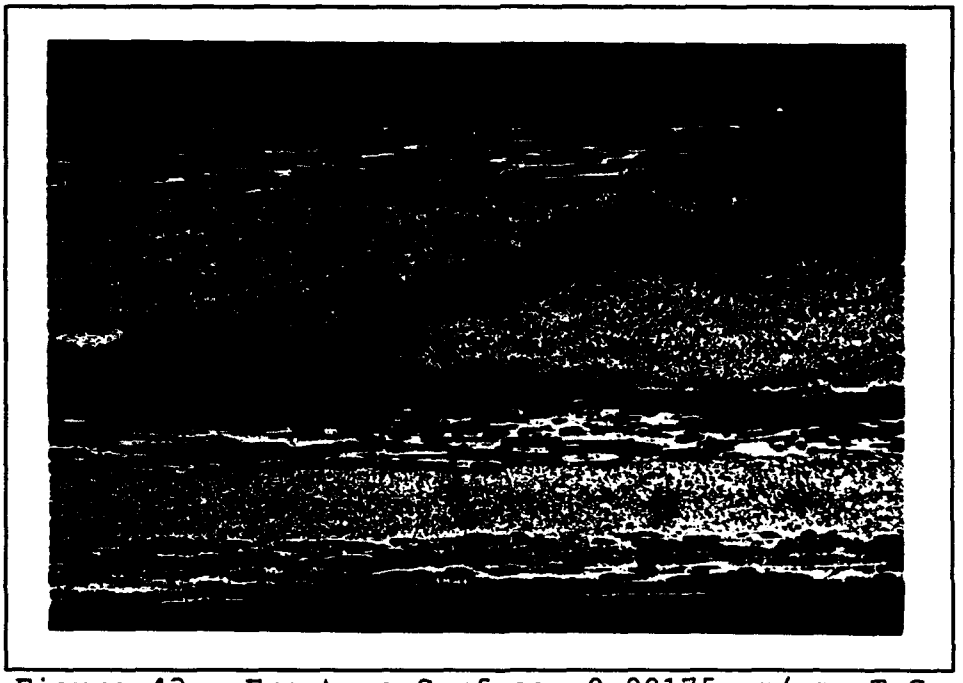

Figure 43. Fracture Surface, 0.00175 mm/mm, T-C, R=-1.0, 50X

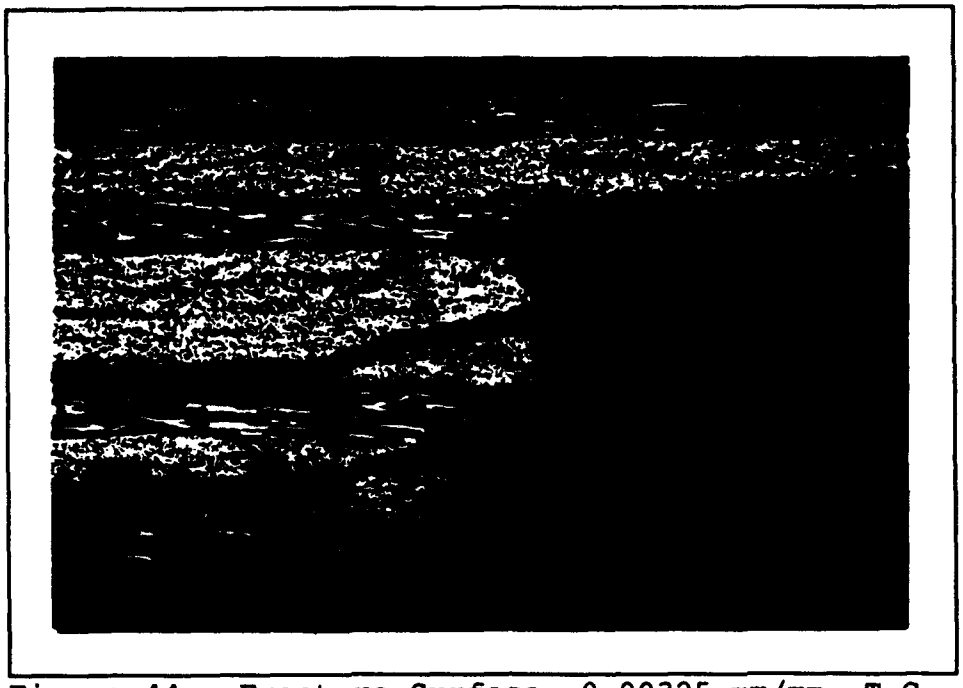

Figure 44. Fracture Surface, 0.00325 mm/mm, T-C, R=-1.0, 50X

These tension-compression failure modes were then compared with the failure modes that would be predicted by the Rotem Fatigue Failure Envelope [9] mentioned in Chapter II. As a reminder, this envelope was developed for a carbon reinforced epoxy, and there would be an attempt here to see if it could be applied to the Nicalon/CAS specimens used in this study.

The ultimate static tension stress of 285 MPa from this study and the ultimate static compression stress of -505 MPa from Opalski's study [1] were plotted on Figure 45, and then a line was drawn between these points. The mean stress of these two points was -110 MPa, and this point was plotted on

the abscissa of the graph. A vertical line was then drawn through this point (line A-B). According to Rotem, specimens tested at mean stresses that were to the left of this line would fail in compression, while those with mean stresses to the right of this line would fail in tension.

The mean stresses for the four specimens that failed during tension-compression testing were then found by taking the average of the maximum and minimum stresses over the fatigue life and then using these values to calculate a mean stress. These specimens had maximum strains of 0.00175 mm/mm (mean stress of -80 MPa), 0.00236 mm/mm (mean stress of -100 MPa), 0.00293 mm/mm (mean stress of -120 MPa), and 0.00325 mm/mm (mean stress of -135 MPa). The R ratio was -1.0 for all tests. These mean stresses were then plotted on Figure 45, along with the average maximum and minumum stresses from each test. This envelope would predict that the 0.00175 mm/mm and the 0.00236 mm/mm specimens would fail in tension (fall to the right of A-B), and the 0.00293 mm/mm and 0.00325 mm/mm specimens would fail in compression (fall to the left of A-B). These predictions are in agreement with the observed results for all four of the specimens.

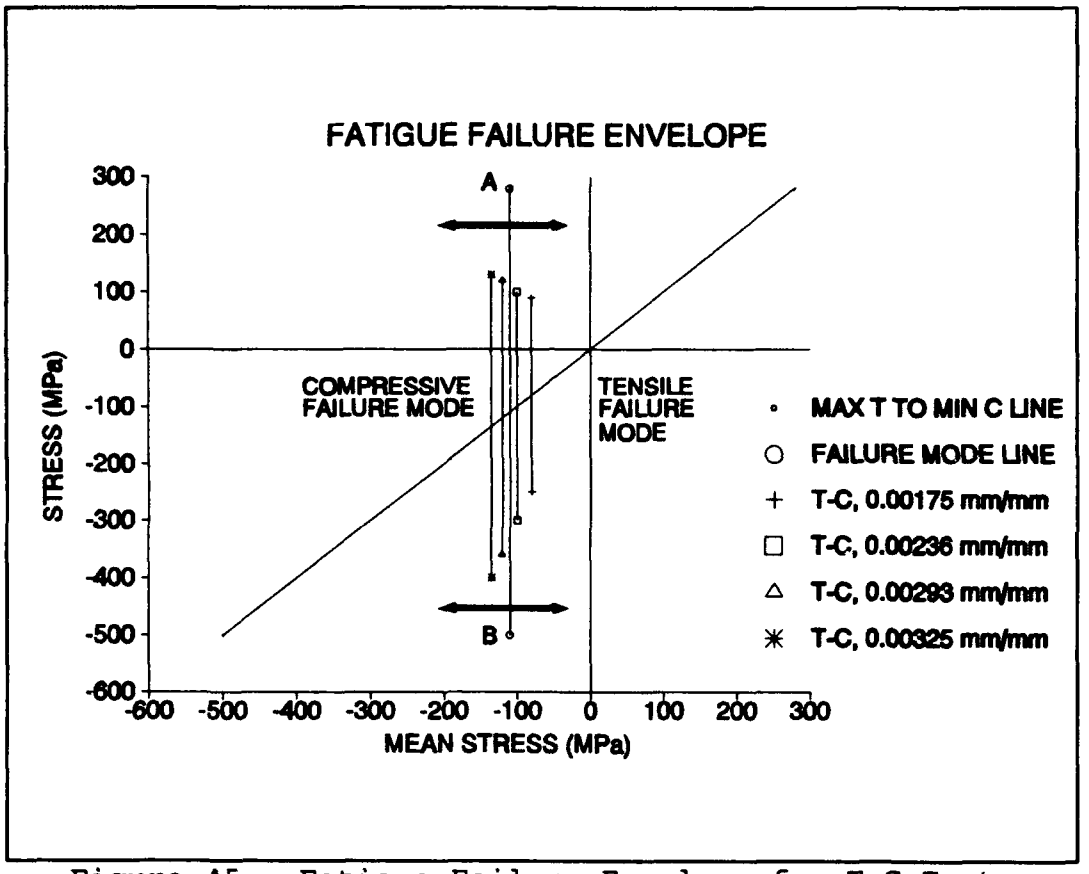

Figure 45. Fatigue Failure Envelope for T-C Tests

As mentioned in Chapter II, Talreja [10] introduced a fatigue life diagram of the form shown in Figure 2 to analyze fatigue life of polymeric matrix composites. He also proposed that this concept could possibly be applied to ceramic matrix composites. From the strain controlled data obtained from this study and from load controlled data from Opalski's study (supplemented by the two tension-compression tests done in this study), two separate fatigue life diagrams were developed. Figures 46 and 47 show the strain controlled and load controlled fatigue life data, respectively.

For the stain controlled data, $\Delta\varepsilon$ was plotted as a function of number of cycles so that both tension-tension and tension-compression data could be plotted together. Maximum stress was plotted as a function of number of cycles for the load controlled data for the same reason.

The tension-tension data under strain control does not seem to fall into the distinct failure regions that are depicted in Figure 2. The data seems to fall on a straight line (on a semi-logarithmic scale) inside a scatter band that extends from the 0.0027 mm/mm point at 1,000,000 cycles, to the ultimate static strain of 0.01 mm/mm at 1/2 cycle. This seems to show that there is no random fiber failure region, but only unstable fiber failure throughout the 1-1,000,000 cycle range. Evidence of this damage behavior was seen in replicas and scanning electron microscope (SEM) photographs from the tested specimens.

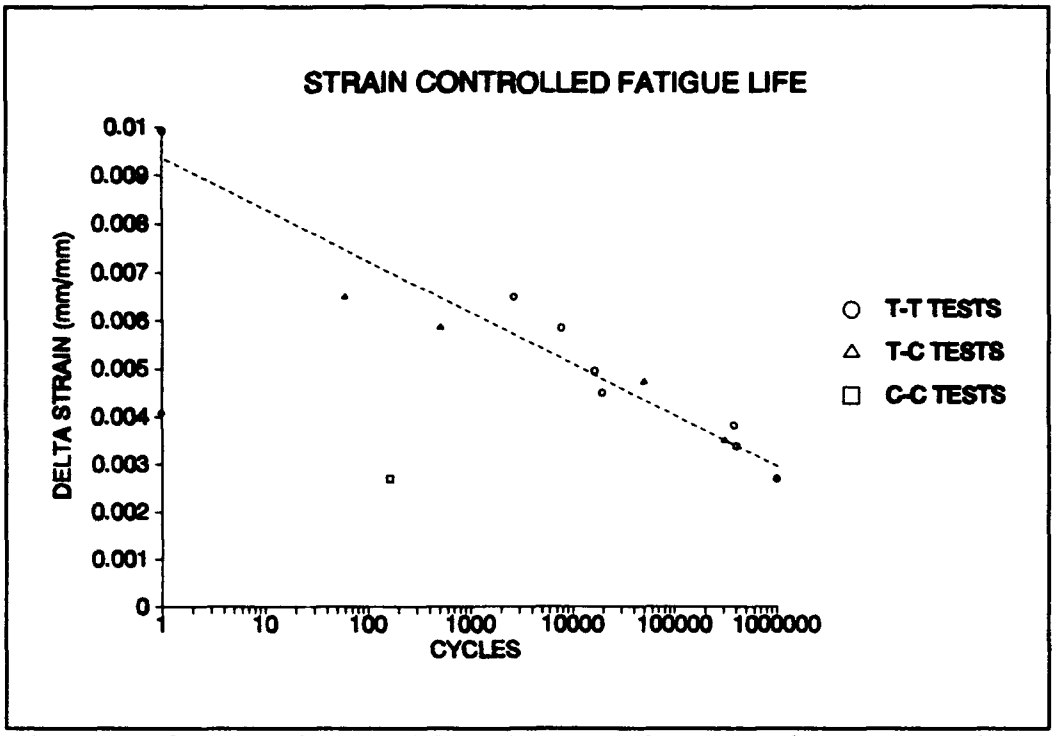

Figure 46. Fatigue Life Diagram for Strain Controlled Tests

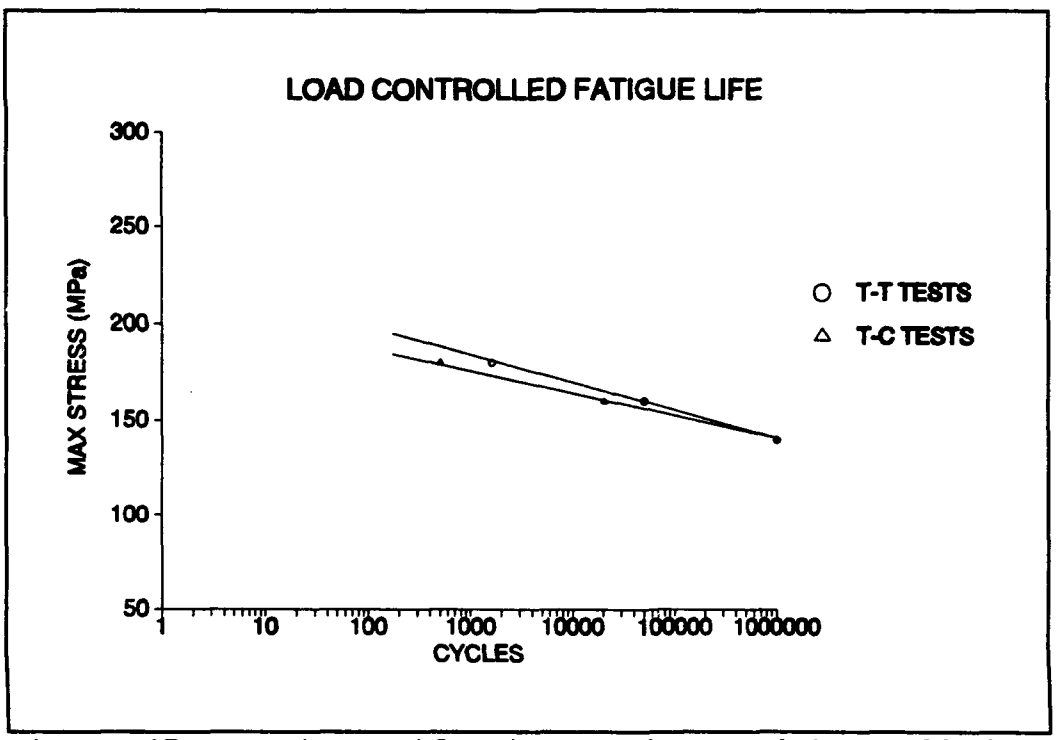

Figure 47. Fatigue Life Diagram for Load Controlled Tests

The divergence of the tension-tension data from the tension-compression data at the two highest $\Delta\varepsilon$ values can be attributed to the tension-compression specimens failing in the compressive mode at these strains. The rest of the specimens all failed in tension, and both sets of tension-tension and tension-compression data falls together within a scatter band.

Looking now at the load controlled data, it can be seen that both the tension-tension data and tension-compression data fall on straight lines (on a semi-logarithmic scale). Both of these lines would seem to fall in the same scatter band with the slight divergence being attributed to the extra damage to the tension-compression specimens being caused by the compressive part of the loading cycle. This data also does not seem to fall in a random fiber failure region.

A comparison of the failure mechanisms for six different strain controlled tests will now be made to get further insight of the fatigue response. The first two will be the tension-tension specimen with a $\Delta\varepsilon$ of 0.00270 mm/mm and the tension-compression specimen with a $\Delta\varepsilon$ of 0.00270 mm/mm. Both of these specimens lasted for 1,000,000 cycles without failure and the tests were stopped. These lives fall right on top of each other on the fatigue life diagram and within the same scatter band.

Figure 48 shows a crack density comparison for these two tests. The two sets of curves are just about parallel to each other. The gaps between them can be attributed to the

different maximum strains that were used for each test. The tension-tension test had a maximum stress of 140 MPa and the tension-compression test had a maximum stress of 93 MPa on the first cycle. Both of these stresses are high enough to cause considerable damage to the 90° plies and almost all of this damage is done during the first cycle (transverse cracking begins in the 90° plies at around 50 MPa). The difference between these stresses does produce a vastly different amount of cracks in the 0° plies due to the fact that matrix cracking in the 0° plies usually starts to appear at around 100 MPa and 93 MPa falls just below this value while the 140 MPa stress falls well above this value.

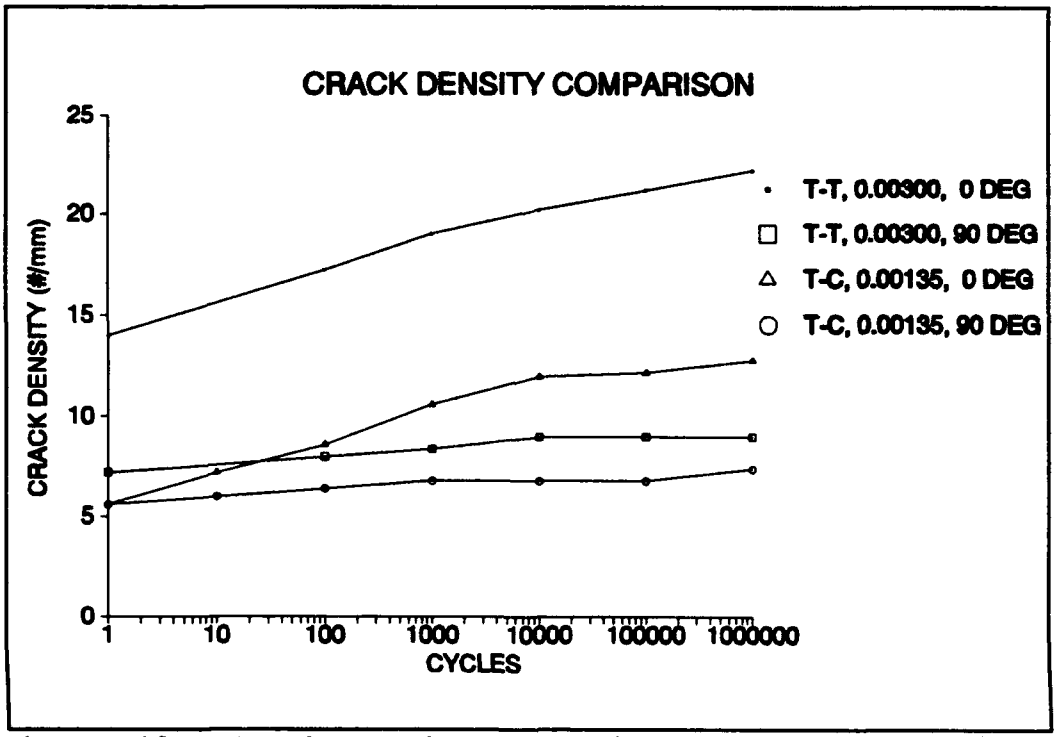

Figure 48. Crack Density Comparison for 0.00300 mm/mm T-T and 0.00135 mm/mm T-C

Figure 49 shows the modulus degradation comparison between these two tests. Both of the curves parallel each other very well, with the tension-compression curve being above the tension-tension curve. This difference again shows that more damage was done to the 0° plies in the tension-tension specimen as compared to the tension-compression specimen. Both curves slowly decrease until "bottoming out" around 10,000 cycles. Both curves then start to increase slightly as some of the cracks begin filling with debris [3].

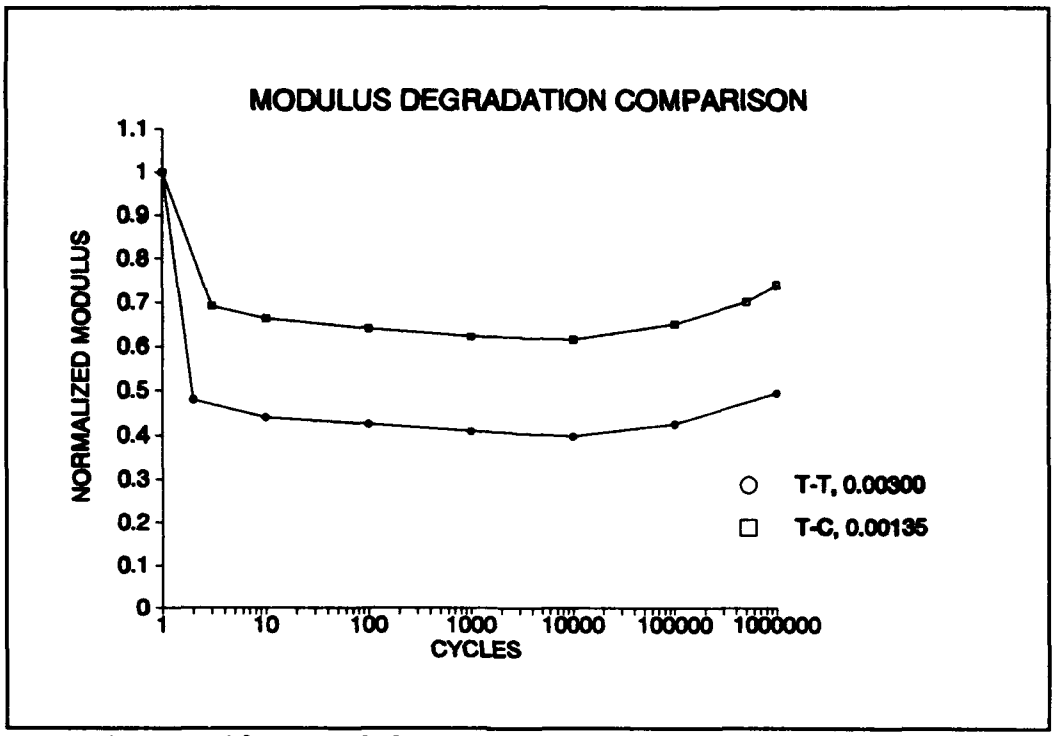

Figure 49. Modulus Degradation Comparison for 0.00300 mm/mm T-T and 0.00135mm/mm T-C

Before comparing the transverse strain data for these tests, a more detailed explanation will be given for how the transverse strain responds to both tension-tension and tension-compression loading. Figures 50 and 51 show stress-transverse strain curves for typical tension-tension and tension-compression tests, respectively.

The first cycle shown in Figure 50 shows the specimen's damage mechanisms as indicated by changes in transverse strain. As the specimen is initially tensile loaded, the transverse strain starts to become negative (as expected). After "bending" slightly due to the start of transverse cracks and then matrix cracks forming, the strain relaxes and drops off towards 0 as the matrix cracks steadily increase. On the unloading portion of the cycle, the specimen sustains a steady increasing positive strain. After the first few cycles, the transverse strain will no longer go "negative" due to the accumulation of damage. The typical cycle will then look like as shown for cycle 1000 in Figure 50.

The tension-compression transverse strain shown in Figure 51 has a fairly linear curve for the first cycle. This is due to the much smaller maximum stress that is used for these tests as compared to the tension tension tests. The first cycle is "negative" during the tension and "positive" during the compression. The cycles are then shifted to the right due to the permanent damage taking place. Cycle 310,000 is "bent" in the middle, with a decrease of strain on each end

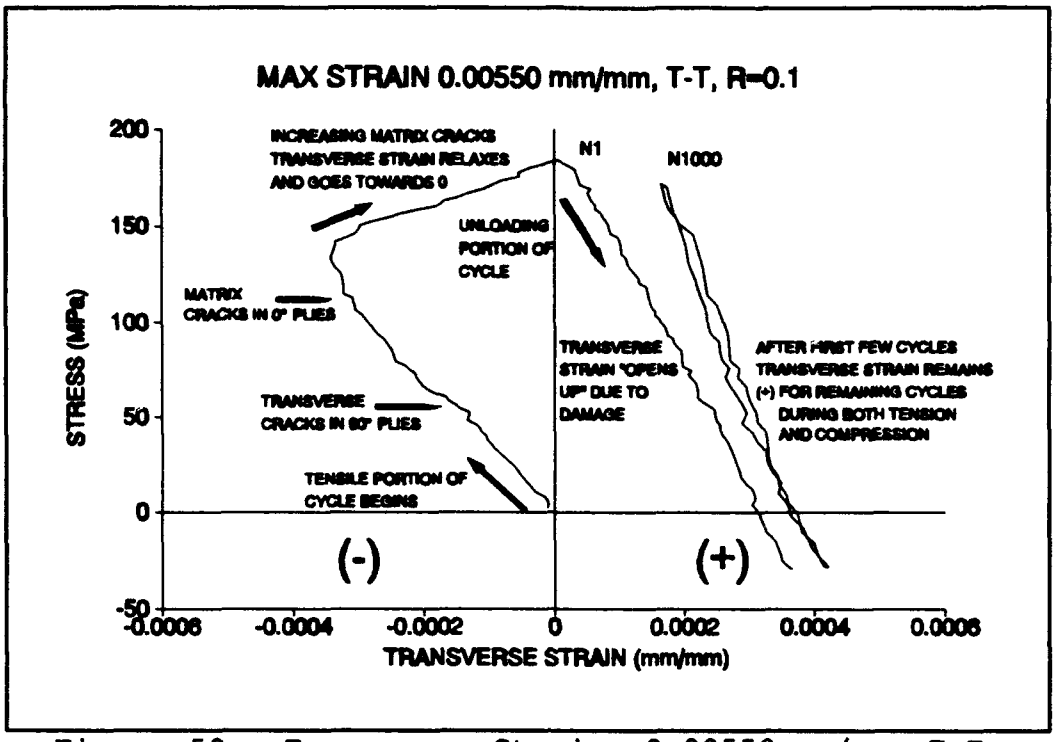

Figure 50. Transverse Strain, 0.00550 mm/mm, T-T, R=0.1

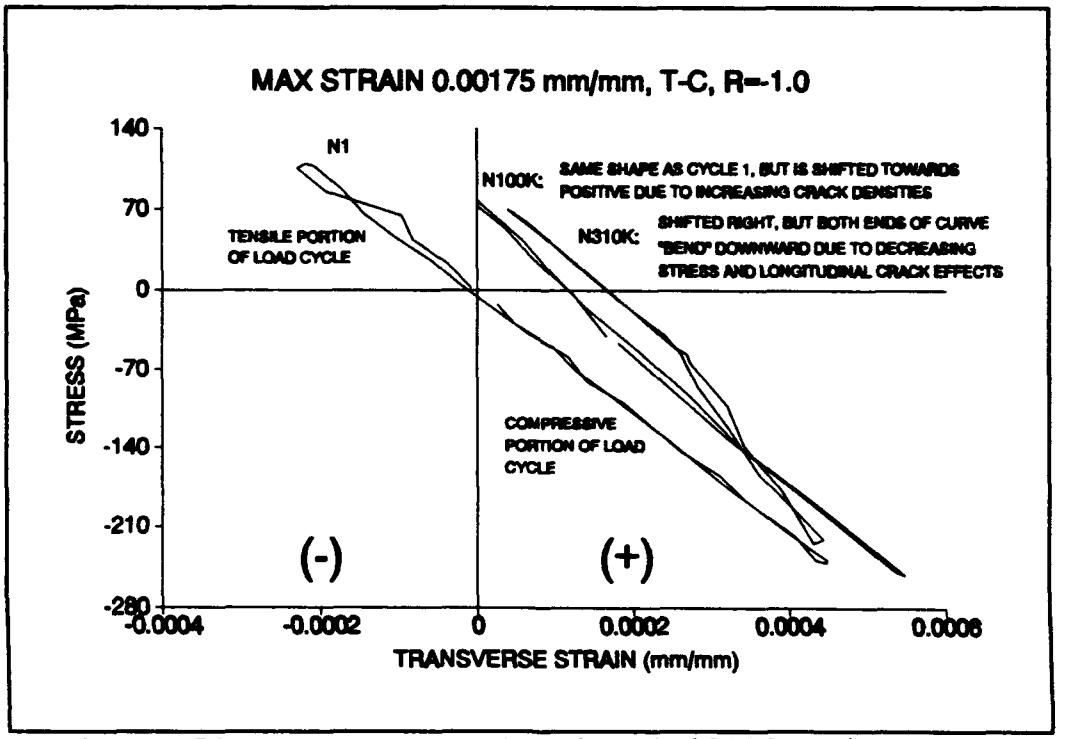

Figure 51. Transverse Strain, 0.00175 mm/mm, T-C, R=-1.0

of the curve. This is caused by the formation of longitudinal cracks and an associated drop in stress.

Figure 52 shows the transverse strain for the first set of tests. The tension-tension curves show the permanent damage the specimen experienced from the first cycle as the minimum strain goes from a negative value to around 0. After this cycle, both the minimum and and maximum strains are fairly constant through 1,000,000 cycles. This can be attributed to the slow rise in transverse and matrix crack densities and no longitudinal cracking during this test. No evidence of debonding or delamination was seen on any of the replicas taken during this test.

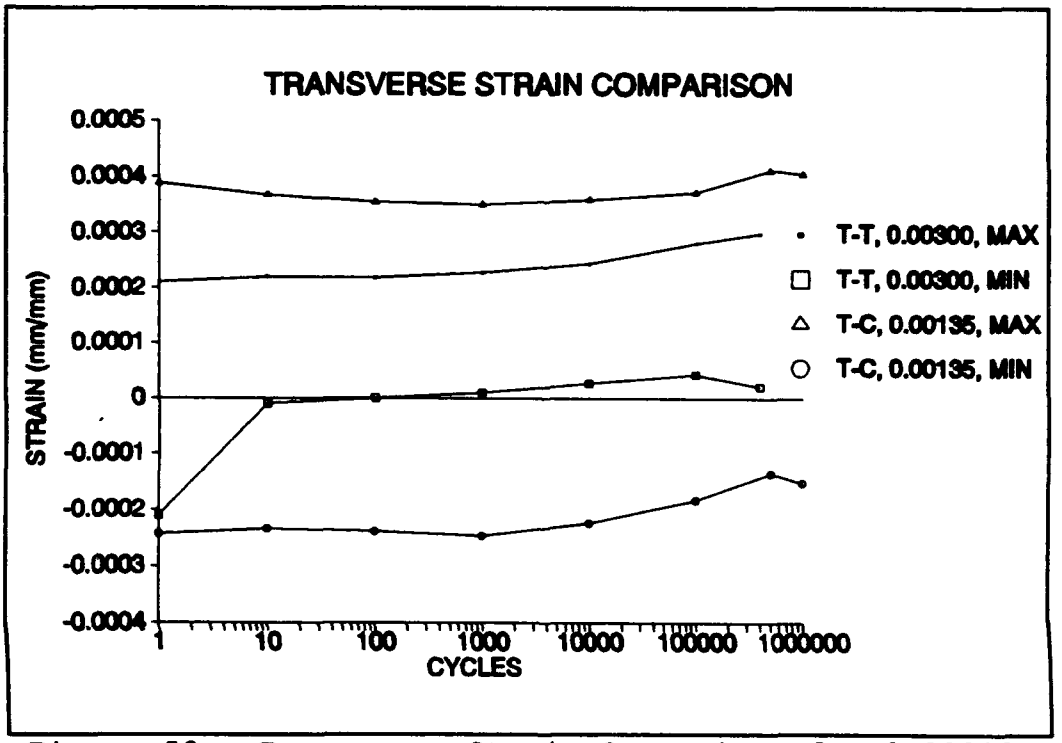

Figure 52. Transverse Strain Comparison for 0.00300 mm/mm T-T and 0.00135 mm/mm T-C

The tension-compression curves are also fairly steady until they reach around 500,000 cycles. Somewhere between 500,000 and 1,000,000 cycles, a few longitudinal cracks started to form and are reflected in the small drop-off of transverse strain in this area of the curve. One of these longitudinal cracks is shown in Figure 41. No signs of debonding or delamination were seen in this specimen.

The second set of two specimens to be compared are the tension-tension specimen tested with $\Delta\varepsilon$=0.00450 mm/mm and the tension-compression specimen tested with $\Delta\varepsilon$=0.00472 mm/mm. These specimens failed at 19,495 cycles and 50,531 cycles respectively. These specimens fall very close to each other on the fatigue life diagram and would be well within the same scatter band.

Figure 53 shows the crack densities for these two specimens. The densities in the 90° plies are about the same, and range from 5/mm to around 9/mm. These are similiar to the densities of the first two specimens compared, and show that even at these much higher strains, the damage in the 90° plies does not increase much at all since these plies are practically saturated with transverse matrix cracks. This shows that the 90° plies are effectively eliminated from supporting the loads at strains above 0.00100 mm/mm (100 MPa). The 0° ply curves show similiar increases in matrix cracking with each other but with the difference between the two being due to the higher maximum stress of 176 MPa in the tension-tension test versus 140 MPa in the tension-compression test.

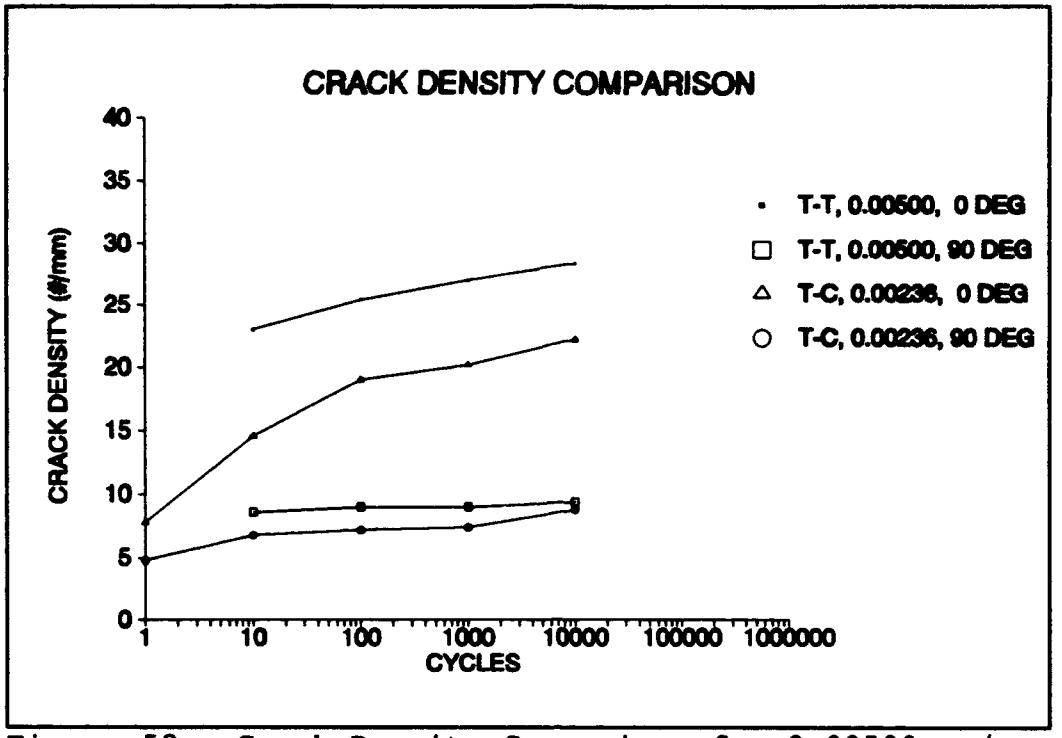

Figure 53. Crack Density Comparison for 0.00500 mm/mm T-T and 0.00236 mm/mm T-C

Figure 54 shows the modulus degradation curves for these two specimens. These curves are slightly lower than those from the previous specimens (Figure 49), due to the higher strains put on these two specimens. Like all the modulus curves, most of the damage occurs during the first cycle. Again, the tension-compression curve lies above the tension-tension curve due to the higher maximum strain (and more damage) that the tension-tension specimen was subjected to. The major difference between these two curves is seen on the tension-compression curve between 40,000 and 50,000 cycles. Small longitudinal cracks were seen on the replica from 10,000 cycles. These cracks grew rapidly between 10,000 and 50,000 cycles, and their effect can be seen on the sudden drop in the modulus in the tension-compression specimen prior to failure.

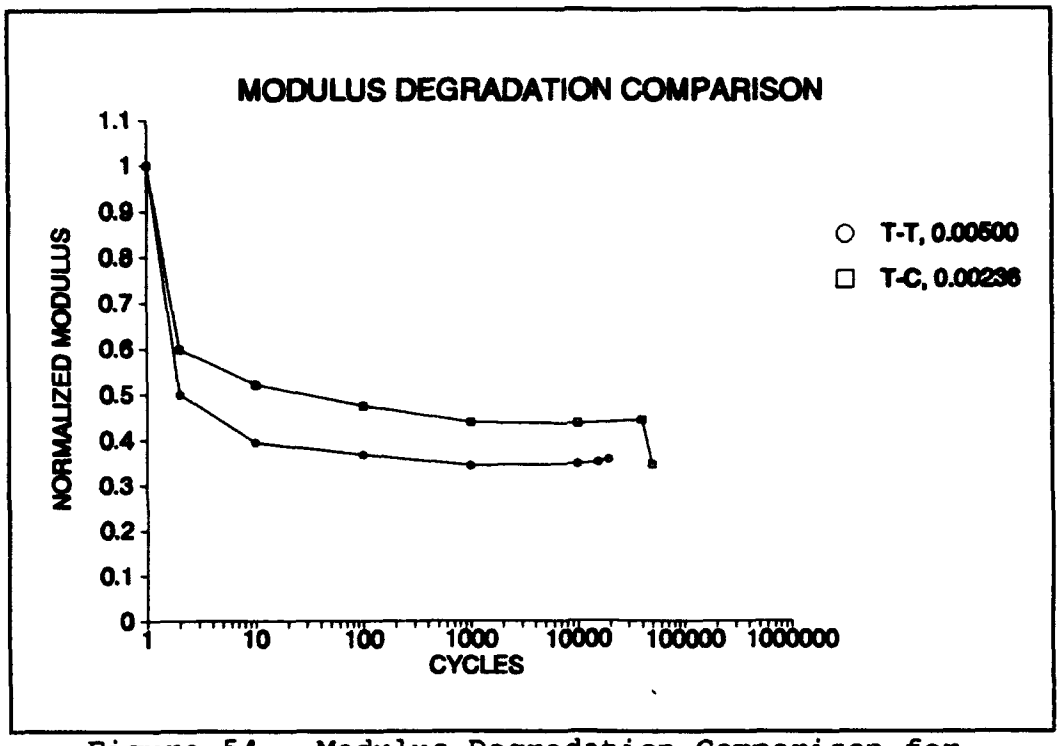

Figure 54. Modulus Degradation Comparison for 0.00500 mm/mm T-T and 0.00236 mm/mm T-C

Figure 55 shows the transverse strain curves for these two specimens. These curves are similiar to previous curves, but the tension-compression curve has a large decrease in maximum strain and an increase in minimum strain after 40,000 cycles due to the longitudinal cracks growing and spreading throughout the specimen. This decrease in compressive transverse strain would occur as the stress required to compress the specimen decreases due to these cracks.

Figure 56 shows a replica photograph for the $\Delta\varepsilon$=0.00450 mm/mm specimen, and Figure 57 shows a SEM photograph of the edge of a failed specimen tested at $\Delta\varepsilon$=0.00472 mm/mm under tension-compression fatigue. Figures 58 and 59 show SEM photographs of these same specimens after failure.

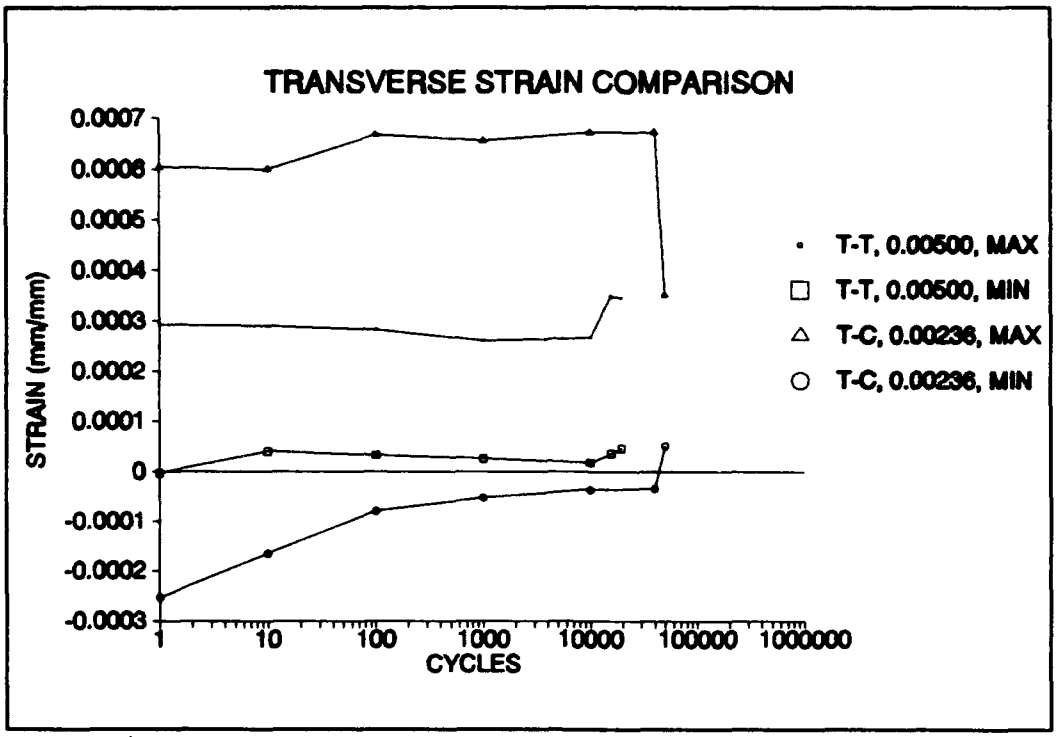

Figure 55. Transverse Strain Comparison for 0.00500 mm/mm T-T and 0.00236mm/mm T-C

The high crack densities in the 0° plies for the tension-tension specimen can be clearly seen in Figure 53. This specimen failed from fiber failure after the 0° matrix was saturated with cracks. No longitudinal cracks or evidence of ply delamination were seen in any of the replicas taken. It failed during the tensile portion of the cycle as can be seen in Figure 58. The longitudinal crack, from the tension-compression test, shown in Figure 57 started in a 0° ply and spread through the center 90° plies and caused fiber debonding and ply delamination. This crack and many other longitudinal cracks led to the failure of the tension-compression specimen. This specimen also failed during the tensile portion of the cycle (Figure 59).

Figure 56. Cycle 10,000, 0.00500 mm/mm, T-T, R=0.1, 125X

Figure 57. Specimen Edge, 0.00236 mm/mm, T-C, R=-1.0, 82X

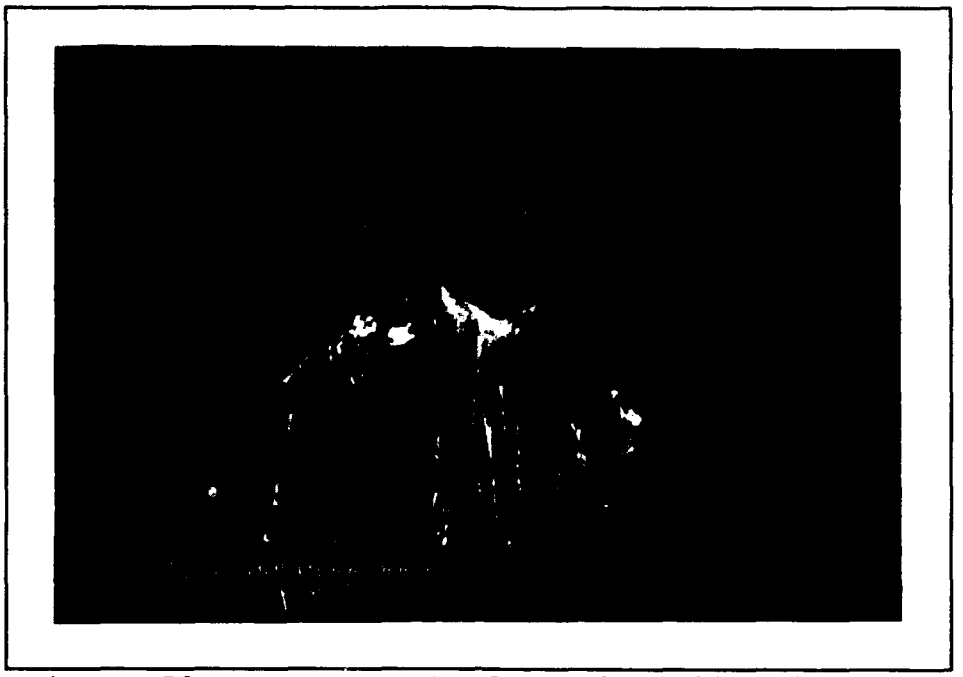

Figure 58. Fracture Surface, 0.00500 mm/mm, T-T, R=0.1, 13X

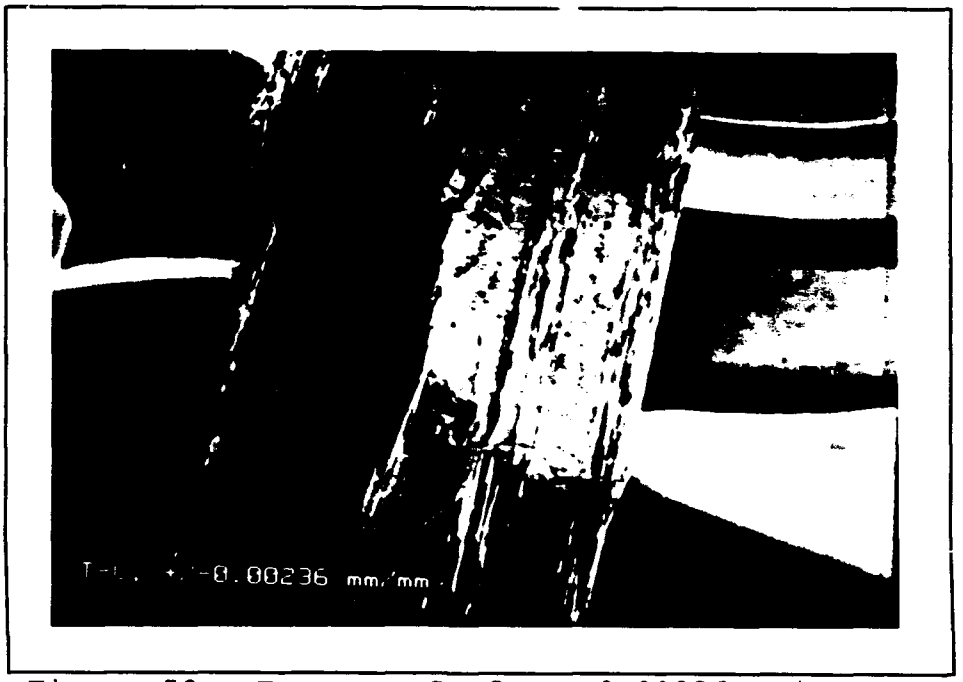

Figure 59. Fracture Surface, 0.00236 mm/mm, T-C, R=-1.0, 13X

Both of the fracture surface photographs, Figures 58 and 59, clearly show that both specimens failed during the tensile portion of the cycle. The 0° plies fibers are protruding out of the matix in both specimens. Aside from the longitudinal cracks seen on the tension-compression specimen, both of these fracture surfaces look like a typical tensile mode failure surface.

The third set of two specimens to be compared were the $\Delta\varepsilon$=0.00650 mm/mm tension-tension specimen and the $\Delta\varepsilon$=0.00650 mm/mm tension-compression specimen. These specimens failed after cycles 2,663 and 60 respectively. These specimens do not fall into the same scatter band on the fatigue life diagram (Figure 46). They have diverged due to the different failure modes involved, as elaborated in the following.

Figure 60 shows the crack densities for these two specimens. As with the previous comparisons, the densities in the 90° plies are about the same, and they are generally less than 10/mm. The density in the 0° plies for the tension-tension specimen is very high (above 35/mm) due to the very high strain to which the specimen was subjected. The density in the 0° plies for the tension-compression specimen was slightly above that for the 0.00300 mm/mm tension-tension specimen, as would be expected since the maximum strain was 0.00325 mm/mm.

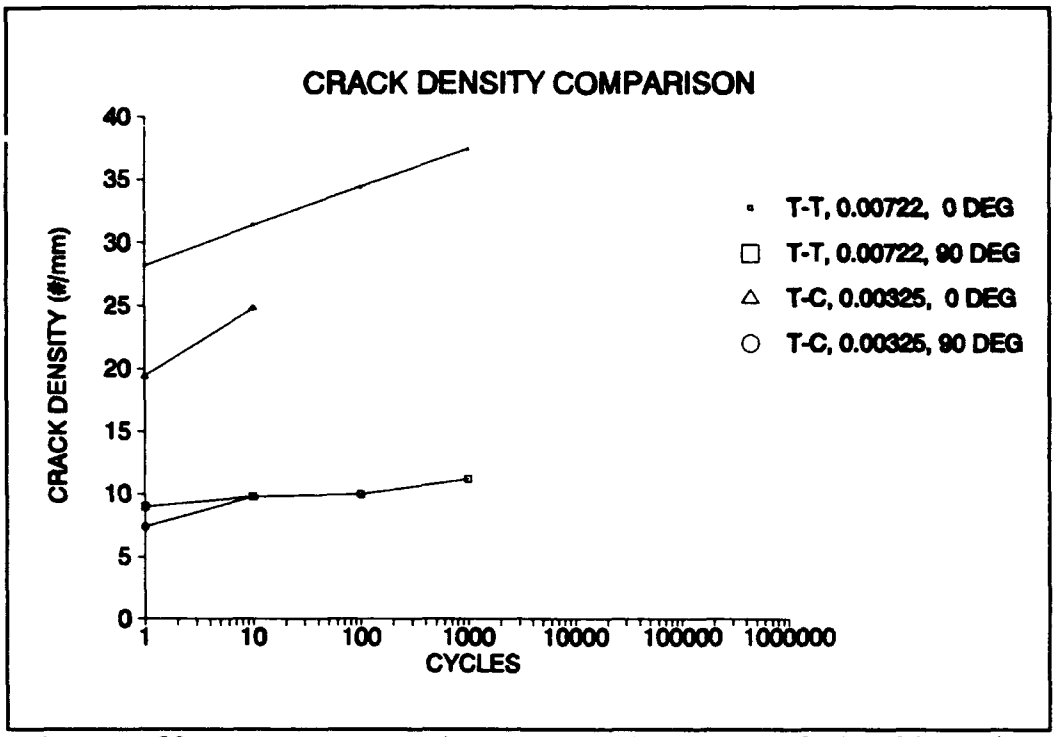

Figure 60. Crack Density Comparison for 0.00722 mm/mm T-T and 0.00325 mm/mm T-C

Figure 61 shows the modulus degradation for these two tests. These curves have the biggest first cycle modulus decrease out of the three pairs of specimens compared. Unlike the general trend of the others, these curves continued to decrease right up until failure. These trends can be attributed to the high crack densities in the 0° plies. These specimens both failed quickly, and although there were longitudinal cracks present on the tension-compression specimen at failure, there was no real indication of these on the modulus curve.

The transverse strain comparison for these specimens is shown in Figure 62. Here some evidence of longitudinal cracking can be seen from the large decreases in both the

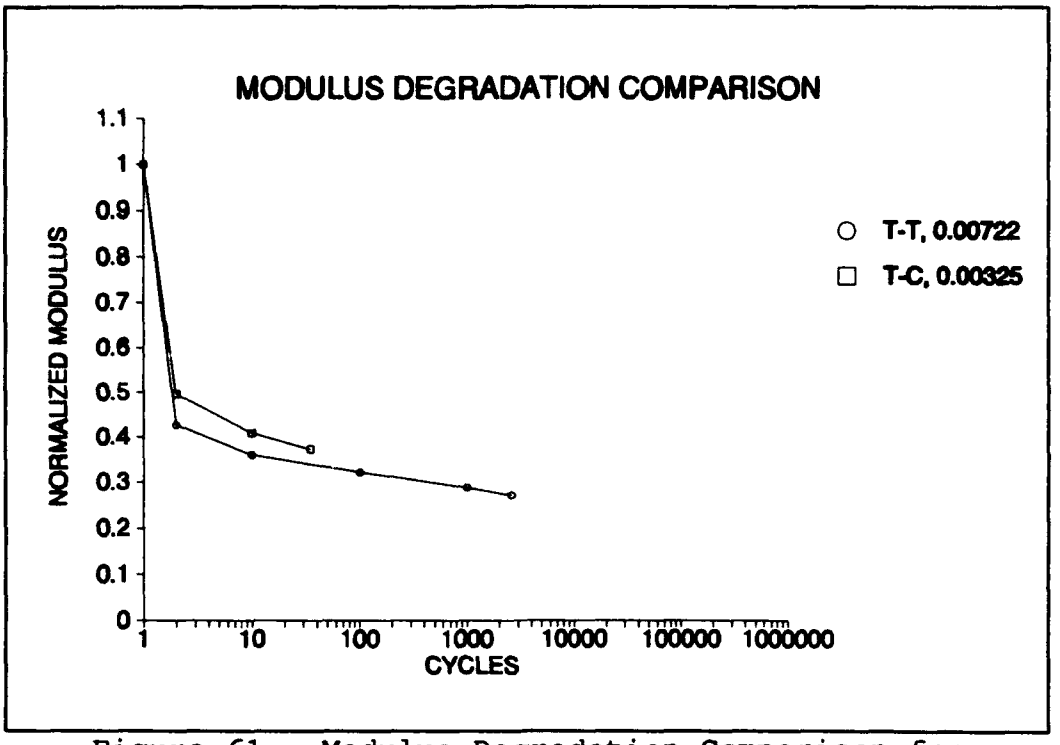

Figure 61. Modulus Degradation Comparison for 0.00722 mm/mm T-T and 0.00325mm/mm T-C

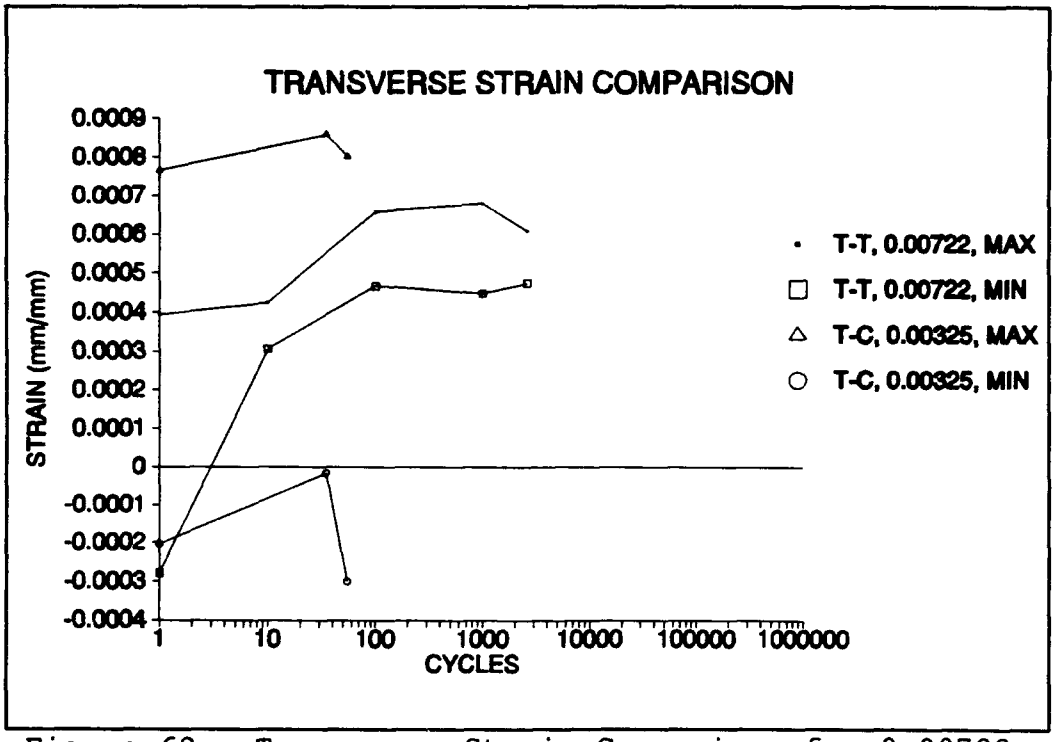

Figure 62. Transverse Strain Comparison for 0.00722 mm/mm T-T and 0.00325 mm/mm T-C

maximum and minimum transverse strain on the tension-compression specimen. Longitudinal cracks started to form quickly after around 35 cycles, and led to specimen failure after only 60 cycles.

Figures 63-66 show SEM edge photographs for both specimens (Figures 63-64 for T-T, Figures 65-66 for T-C). The SEM photographs for the tension-tension specimen show the matrix cracks in the 0° plies and the debonding that is occuring between fiber and matrix. Figure 64 shows how a matrix crack goes around a fiber instead of through it and causes part of the fiber to debond. This specimen was also cut in half lengthwise, polished, and scanned inside a SEM employing a special loading fixture. And even though this specimen was tested at the highest strain, there was no evidence of any fiber failure. This specimen failed in the tensile mode from massive fiber failure after coalesence of matrix cracks and debonding.

The photographs of the tension-compression specimen show a partially debonded fiber in a 0° ply (Figure 65) leading to a longitudinal crack over a good portion of the ply (Figure 66). This specimen failed in the compressive portion of the cycle due to individual ply buckling.

Figure 67 shows the edge view of the fracture surface of the tension-tension specimen and Figure 68 shows the fracture surface of the tension-compression specimen. Figure 69 shows the fracture surface of the compression-compression specimen tested at $\Delta\varepsilon$=-0.00270 for comparison purposes.

Figure 63. Specimen Edge, 0.00722 mm/mm, T-T, R=0.1, 130X

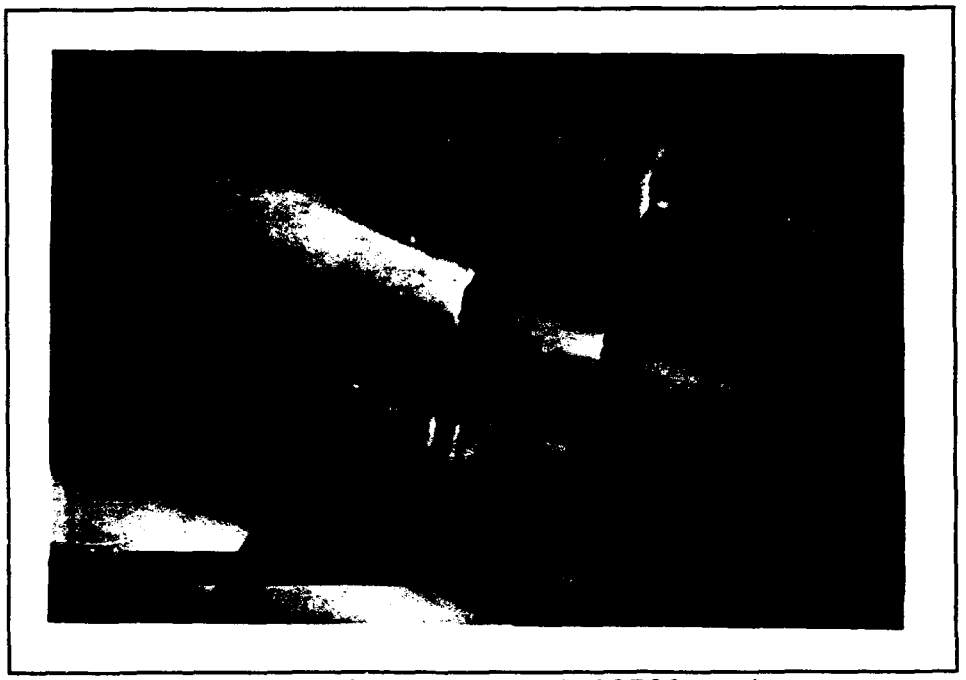

Figure 64. Specimen Edge, 0.00722 mm/mm, T-T, R=0.1, 474X

Figure 65. Specimen Edge, 0.00325 mm/mm, T-C, R=-1.0, 226X

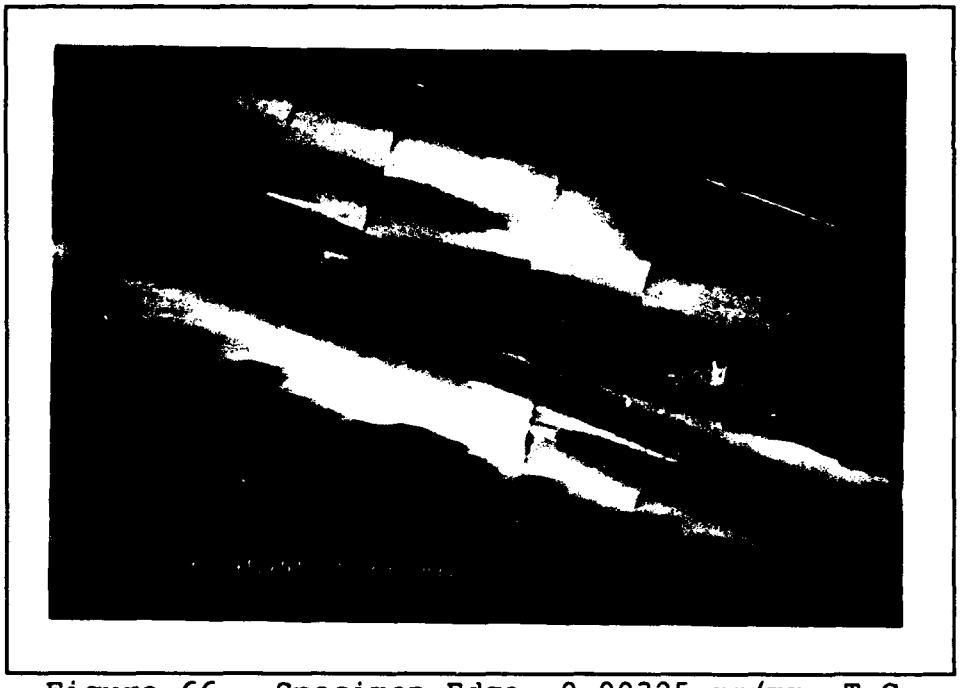

Figure 66. Specimen Edge, 0.00325 mm/mm, T-C, R=-1.0, 142X

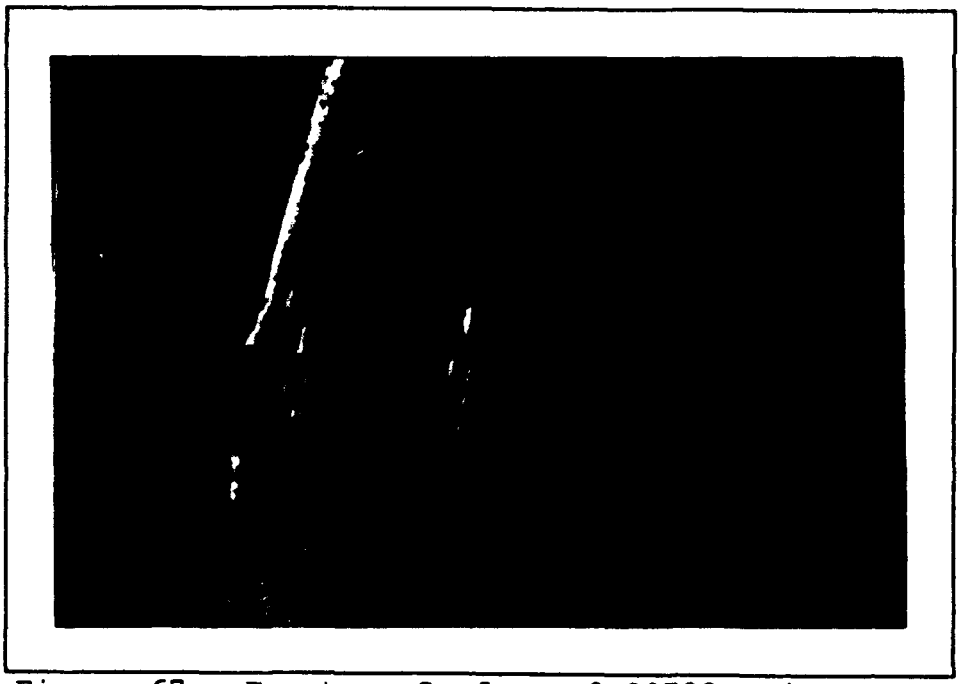

Figure 67. Fracture Surface, 0.00722 mm/mm, T-T, R=0.1, 15X

Figure 68. Fracture Surface, 0.00325 mm/mm, T-C, R=-1.0, 13X

Figure 69. Fracture Surface, -0.00030 mm/mm, C-C, R=10.0, 11X

The tensile failure mode surface is clearly resulting from tension-tension fatigue, Figure 67. It has protruding fibers and transverse cracks completely across the specimen. The fracture surface of the tension-compression specimen is much different, Figure 68 and 69. It failed in compression with delamination and longitudinal cracks. On both of these compressive failure fracture surfaces, it looks like the fibers in the 0° plies have been "sheared" off and all that remains of them at the surface is "stubble".

Using the data obtained from these six tests and all of the other strain controlled tests conducted during this study, the fatigue life diagram of Figure 46 can be redrawn with distinct failure regions and mechanisms. Figure 70 shows this

fatigue life diagram for the strain controlled tests with the regions noted.

The region at the far right of the diagram is the "no failure" region. At $\Delta\varepsilon$'s of less than 0.00270 mm/mm, neither tension-tension or tension-compression specimens will fail at less than 1,000,000 cycles. In this area the transverse cracks have just about saturated the 90° plies, but the amount of matrix cracks in the 0° plies is not enough to cause the fibers to carry the entire load. In the tension-compression specimens in this region, the compressive fatigue effects do not cause a significant amount of longitudinal cracks to develop by 1,000,000 cycles and thus the specimen does not fail.

For only the tension-tension tests, there is a failure region that extends from around $\Delta\varepsilon$=0.00300 to the maximum static strain of about 0.01000 mm/mm. This region is shown on the top part of the figure. The damage mechanisms, in this region, consist initially of 90° ply failure on the first cycle due to transverse crack saturation of these plies. This is followed by a continual increase in matrix cracks in the 0° plies until these plies are saturated and then the entire load is transferred to the 0° fibers. This transfer of load eventually leads to unstable fiber failue due to static overload. However, there was no fiber breakup seen due to fatigue. On some of the higher strain tests, there was some fiber debonding seen on the SEM, but it did not seem to contribute to the specimens failure.

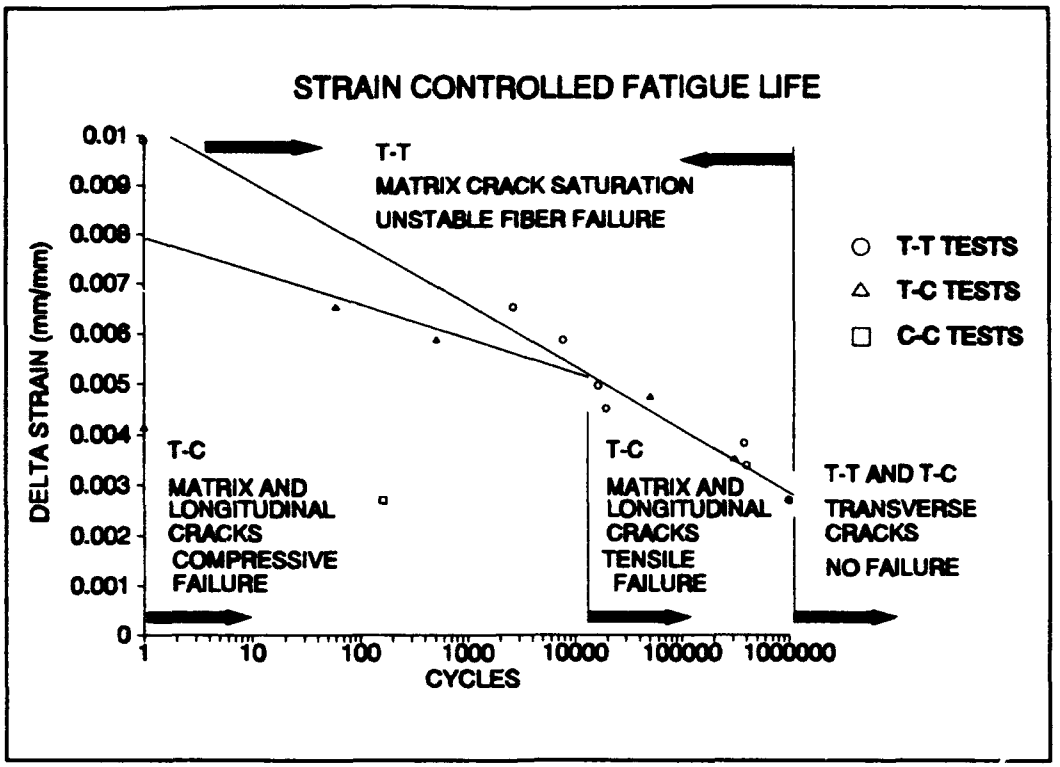

Figure 70. Fatigue Life Diagram for Strain Controlled Tests

The notable factor in the tension-compression fatigue tests was obviously the occurence of the longitudinal cracks. How soon these cracks formed and how fast they grew in comparison to the transverse matrix cracking would determine when the specimen would fail. The failure modes for these tension-compression specimens seemed to fall into two different regions. The specimens with a $\Delta\varepsilon$ between 0.00300 mm/mm and 0.00472 mm/mm had fatigue lives that were similiar to the tension-tension specimens that had almost the same $\Delta\varepsilon$'s, and these specimens failed during the tensile portion of the load cycle. Specimens which had a $\Delta\varepsilon$ greater than 0.00472

mm/mm had fatigue lives that diverged from the tension-tension fatigue lives by failing much sooner and by failing under the compressive portion of the loading cycle. This divergence which resulted from the different failure modes occuring, showed that different fatigue life diagram lines for tension-tension and tension-compression specimens were needed. These lines are indicated in Figure 70.

V. Conclusions

To summarize, the purpose of this study was to investigate the fatigue effects of both tension-tension and tension-compression strain controlled loading in a cross-ply, $[0/90]_{2s}$, Nicalon/CAS ceramic matrix composite at room temperature. A baseline static tension test was initially conducted, and then eight tension-tension tests, five tension-compression tests and one compression-compression test were completed. The fatigue limit for which 1,000,000 cycles would be reached was found for both tension-tension and tension-compression cycling. The $\Delta\varepsilon$-N curves for strain controlled cases were established. Two load controlled tests were also conducted, and an S-N curve was established from this data and from Opalski's data [1]. The damage mechanisms and failure modes for both types of loading were investigated.

The ultimate strain and strength in static tension was found to be 0.00988 mm/mm and 285.8 MPa, respectively. Two "bends" existed on the stress-strain curve in just about the same places under both load and strain controlled tests. The first bend appeared at around 0.0005 mm/mm (50 MPa) and corresponded to the matrix failure in the 90° plies. The second bend was at around 0.0025 mm/mm (135 MPa) and indicated a large increase in the matrix cracks of the 0° plies. The stress-strain curve under the strain controlled mode was slightly below the load controlled mode due to some relaxation.

In the tension-tension fatigue case, the maximum strain that achieved cycle runout of 1,000,000 cycles was 0.00300 mm/mm ($\Delta\varepsilon$=0.00270 mm/mm). The maximum first cycle stress for this test was 140 MPa. All tests conducted above this strain value failed before reaching 1,000,000 cycles. In these tests, the sequence of failure mechanisms began with the saturation of transverse matrix cracks in the 90° plies after the first cycle. Thereafter, upon further cycling the matrix in the 0° plies was saturated with cracks. And finally, failure occurred after unstable massive fiber failure.

In the tension-compression fatigue case, the maximum $\Delta\varepsilon$ that achieved cycle runout of 1,000,000 cycles was 0.00270 mm/mm. This was the same value of strain range that was found for the tension-tension case. Since most of the tension-compression tests were run at maximum strains that did not completely saturate the 0° plies with cracks, another failure mechanism was involved. All the specimens that failed showed significant evidence of longitudinal cracks. These cracks led to ply delamination, ply buckling and then to total failure of the specimen. The higher the strain applied, the quicker these cracks formed and the faster the specimen failed.

On the $\Delta\varepsilon$-N fatigue life diagram using both the tension-tension and tension-compression data, these sets of data fell together until the higher value of compressive strains caused longitudinal cracks to form very quickly on the tension-compression specimens which led to compressive failure.

The variation of modulus and energy during fatigue in all tests clearly showed that damage had occurred, but these methods were not very good predictors of when a specimen would fail. Two better indicators for predicting when failure would occur were transverse strain and crack density data. A significant decrease in transverse strain indicated that longitudinal cracks were forming, stresses were decreasing, and that failure would soon occur. Also, a steady increase of matrix cracks in the 0° plies above a saturation level of about 28/mm indicated that the tension-tension specimens would fail.

Overall, using a comparison based on strain range, the tension-tension and tension-compression cycling have relatively the same fatigue life when both types of fatigue lead to failure under tension. However, the fatigue lives start to diverge between tension-tension and tension-compression cycling when a compressive failure mode is present. All tension-tension specimens failed due to unstable fiber failure, while all tension-compression specimens failed due to longitudinal cracks.

VI. Recommendations

Now with the strain controlled fatigue response of $[0/90]_{2s}$ Nicalon/CAS at room-temperature known, the follow-on to this testing would logically be to investigate the fatigue response for a unidirectional lay-up of this material under strain control.

High temperature testing of this composite under strain control would also make a good follow-on study. This data could then be compared to the high temperature load controlled data available. There should be some interesting differences. Another type of temperature testing that might be beneficial would be thermal-mechanical fatigue (TMF).

Another area that deserves further attention would be that of varying the strain rate and looking more closely into the relaxation effects that will occur. The same maximum strains achieved under different strain rates can be compared to each other and then with load controlled data.

Finally, since tension-tension testing under strain control produces compressive loads on the minimum portion of the strain cycle, some tension-tension testing should be done that does not go into compression during the cycle. This would eliminate any possible effects that the compression is imparting to the specimen. This data could then be compared to the data of this study and these compression effects seen.

Bibliography

1. Opalski, F. A., Fatigue Behavior of a Cross-Ply Ceramic Matrix Composite Under Tension-Tension and Tension-Compression Loading, MS Thesis, AFIT/GAE/ENY/92D, School of Engineering, Air Force Institute of Technology (AU), Wright-Patterson AFB, Ohio, December 1992

2. Rousseau, C.Q., "Monotonic and Cyclic Behavior of SiC/Calcium-Aluminosilicate Ceramic Composite,"in Symposium on Thermal and Mechanical Behavior of Ceramic and Metal Matrix Composites ASTM STP 1080, Kennedy, J.M., Moeller, H.H., and Johnson, W.S., eds, American Society for Testing and Materials, Philadelphia, PA, 1990

3. Zawada, L.P., Butkus, L.M., and Hartman, G., "Tensile and Fatigue Behavior of Silicon Carbide Fiber-Reinforced Aluminosilicate Glass," Journal of the American Ceramic Society, Vol 74, No 11, November 1991, p 2851 - 2858

4. Mall, S., Fink, W.E., and Kim, R.Y., "Mechanical behavior of a fiber reinforced ceramic composite under off-axis loading," Advanced Composite Materials, Vol 2, No 2, 1992

5. Mall, S, and Kim, R.Y., "Failure Mechanisms in Laminates of Silicon Carbide/Calcium-Aluminosilicate Ceramic Composite," in Composites, Vol 23, No 4, July 1992

6. Highsmith, A.L., Stinchcomb, W.W., and Reifsnider, K.L., "Effect of Fatigue-Induced Defects on the Residual Response of Composite Laminates," Effects of Defects in Composite Materials, ASTM STP 836, American Society for Testing and Materials, 1984, p 194 - 216

7. Karandikar, P.G., and Chou, T.W., "Damage Development and Moduli Reductions in Nicalon-CAS Composites Under Static Fatigue and Cyclic Fatigue," to be published in the Journal of the American Ceramic Society

8. Rotem, A. & Nelson, H.G., "Failure of a Laminated Composite Under Tension-Compression Fatigue Loading," in Composites Science and Technology, 36 (1989) p 45-62

9. Rotem, A., "Tensile and Compressive Failure Modes of Laminated Composites Loaded by Fatigue with Different Mean Stress," Journal of Composites Technology and Research, JCTRER, Vol 12, No 4, Winter 1990, p 201-208

10. Talreja, R., "Fatigue of Fibre-Reinforced Ceramics," Proceedings of the 11th Riso International Symposium on Metallurgy and Materials Science: 'Structural Ceramics - Processing, Microstructure and Properties,', Denmark, 1990

11. Zawada, L.P. and Pernot, J.J., "Influence of Loading Rates on Tensile Behavior of Ceramic Matrix Composites," to be published in the Journal of the American Ceramic Society

12. Jones, R.M., Mechanics of Composite Materials, Hemisphere Publishing Company, New York, 1975

13. Agarwal, Bhagwan D. and Broutman, Lawrence J., Analysis and Performance of Fiber Composites, 2nd Ed., John Wiley & Sons, New York, 1990

14. Tracy, G.D., Failure Mechanisms in a Quasi-Isotropic Ceramic Composite Laminate Under Tensile Fatigue Loading, MS Thesis, AFIT/GAE/ENY/90D-30, School of Engineering, Air Force Institute of Technology (AU), Wright-Patterson AFB, Ohio, December 1990

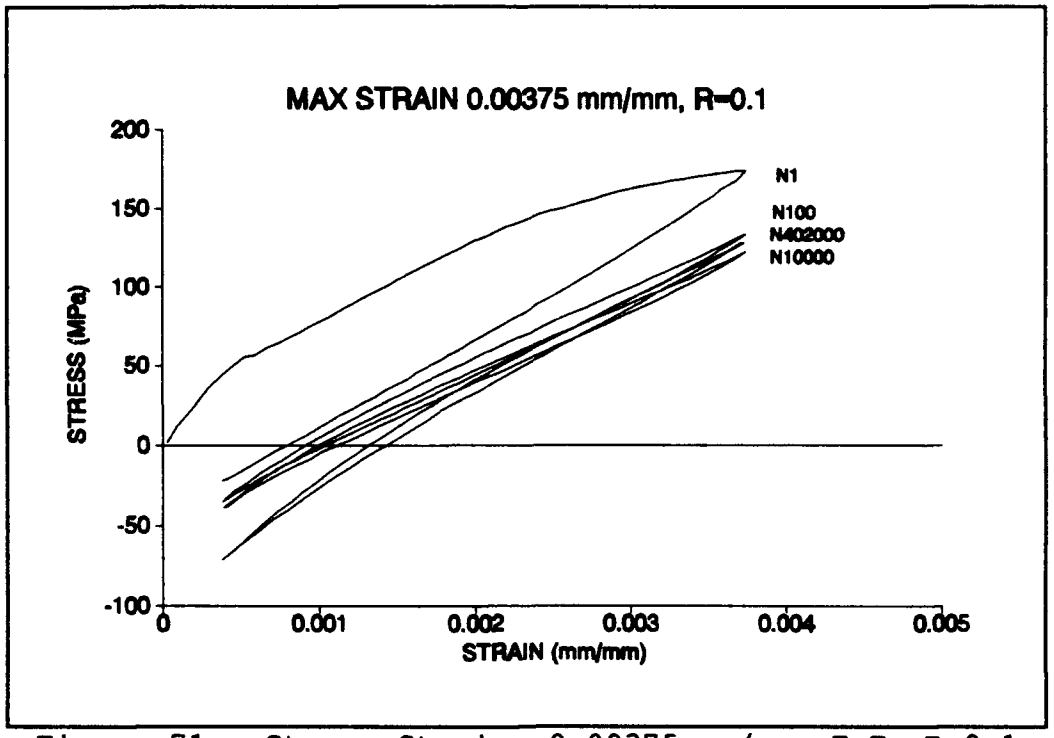

Figure 71. Stress-Strain, 0.00375 mm/mm, T-T, R=0.1

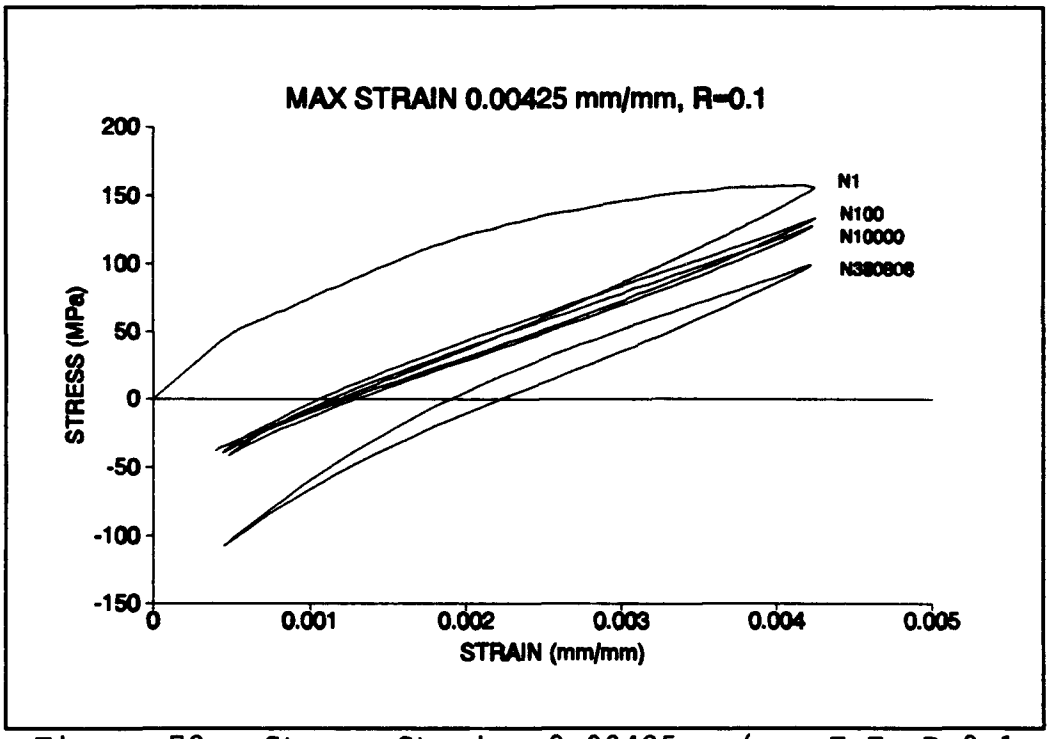

Figure 72. Stress-Strain, 0.00425 mm/mm, T-T, R=0.1

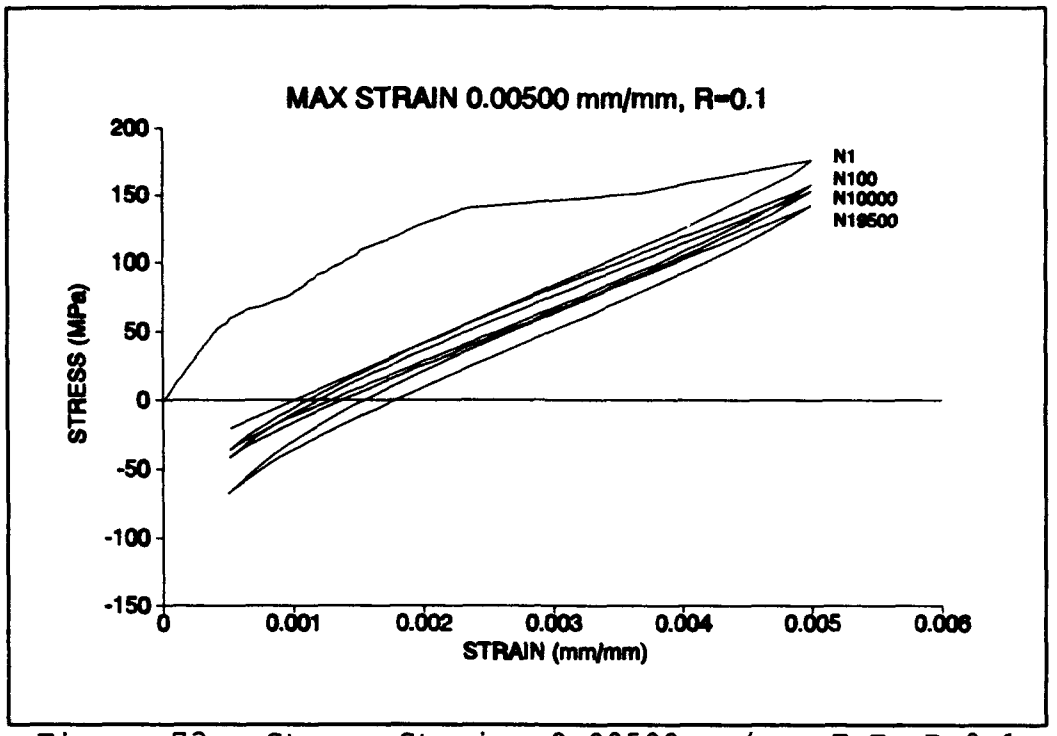

Figure 73. Stress-Strain, 0.00500 mm/mm, T-T, R=0.1

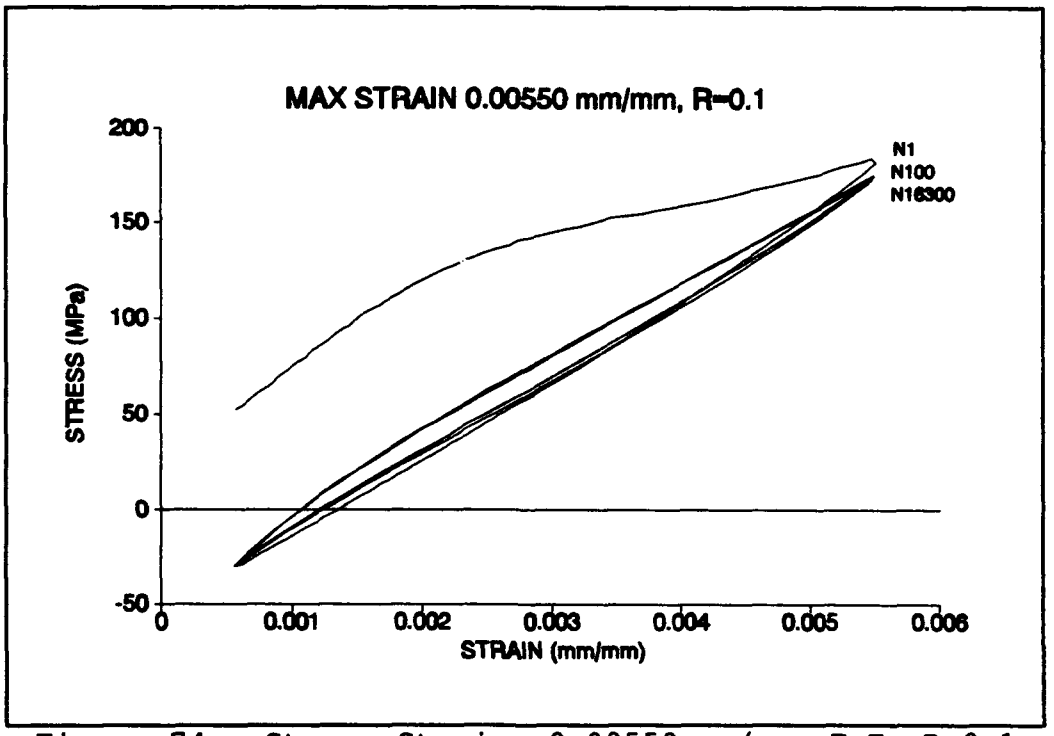

Figure 74. Stress-Strain, 0.00550 mm/mm, T-T, R=0.1

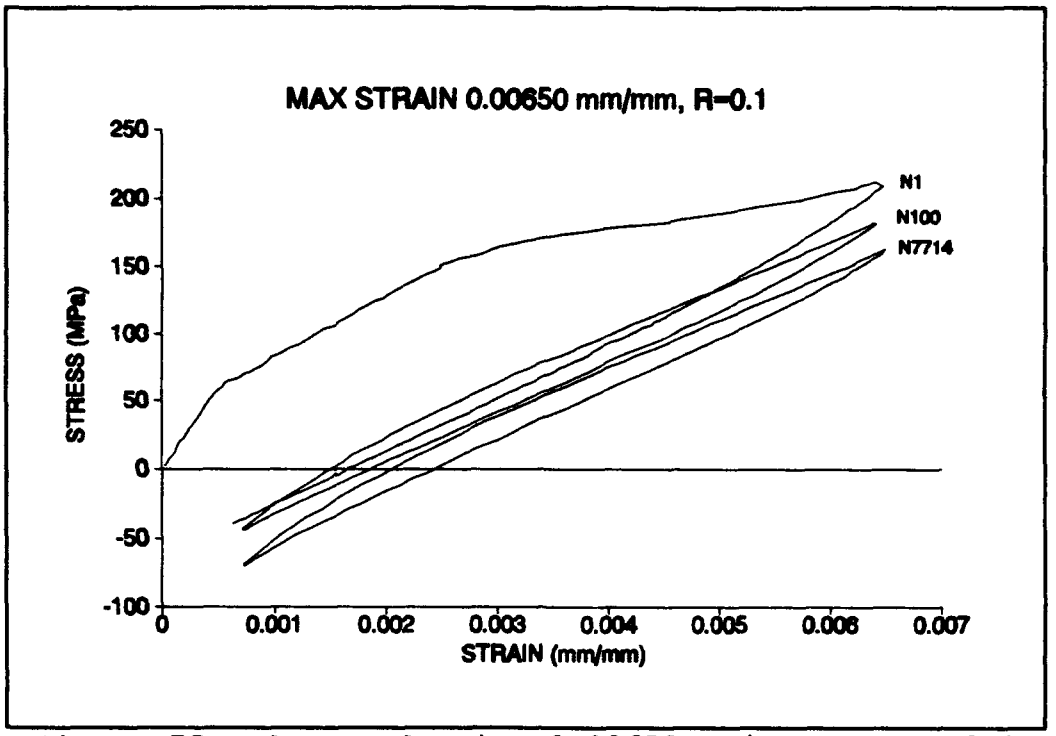

Figure 75. Stress-Strain, 0.00650 mm/mm, T-T, R=0.1

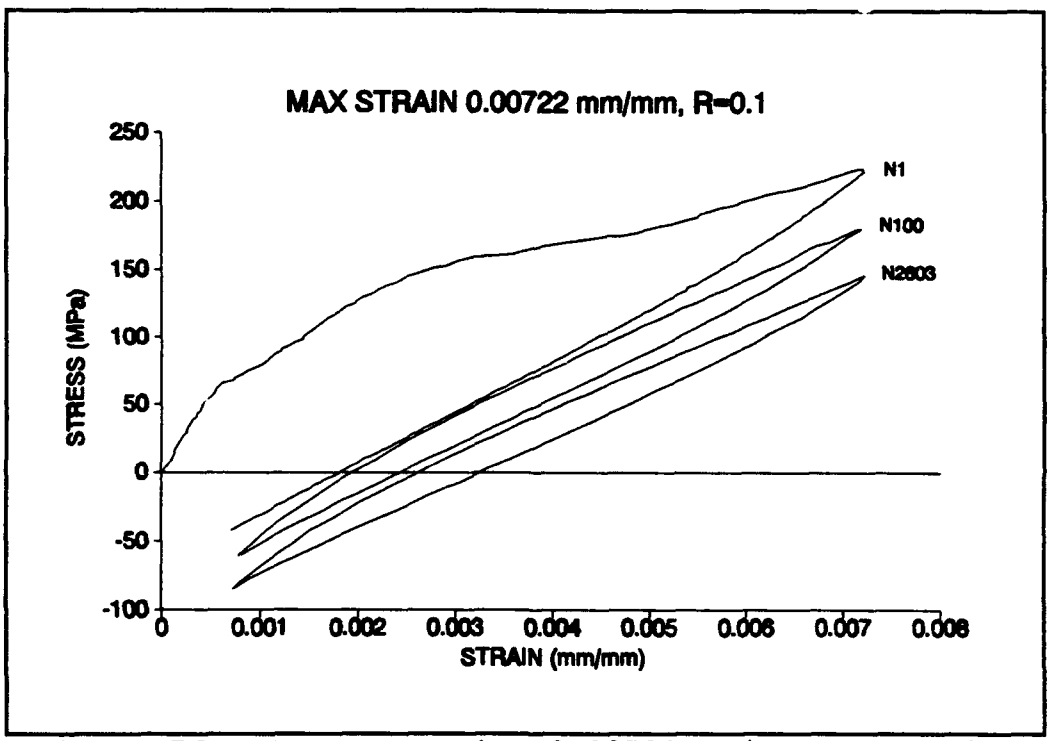

Figure 76. Stress-Strain, 0.00722 mm/mm, T-T, R=0.1

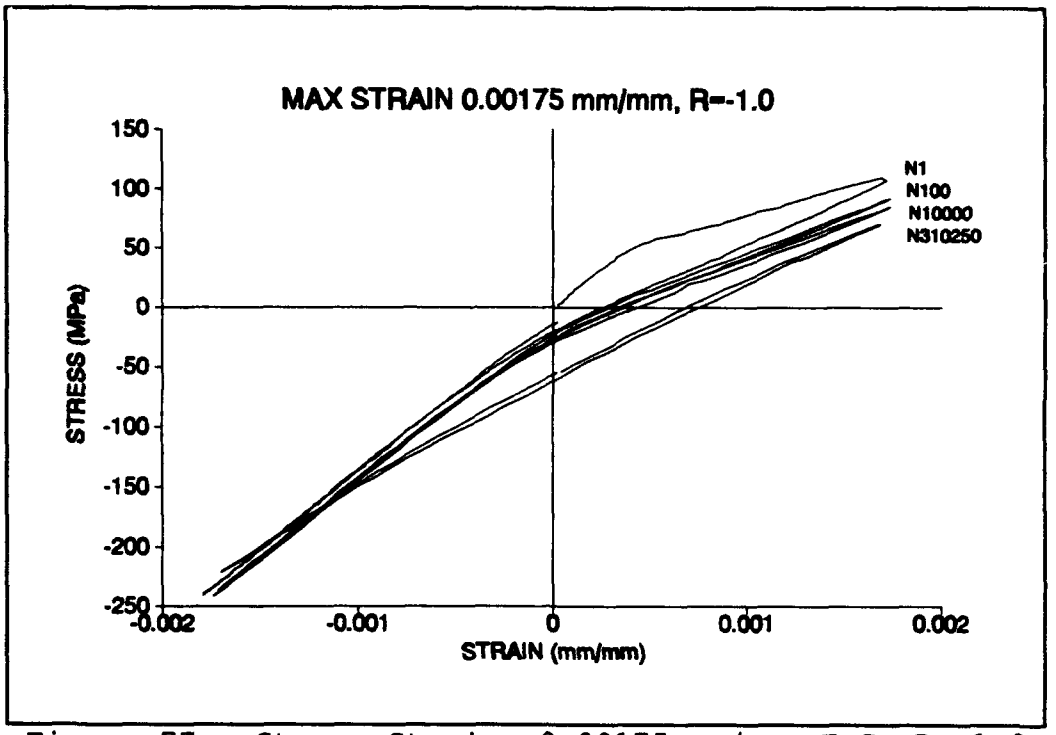

Figure 77. Stress-Strain, 0.00175 mm/mm, T-C, R=-1.0

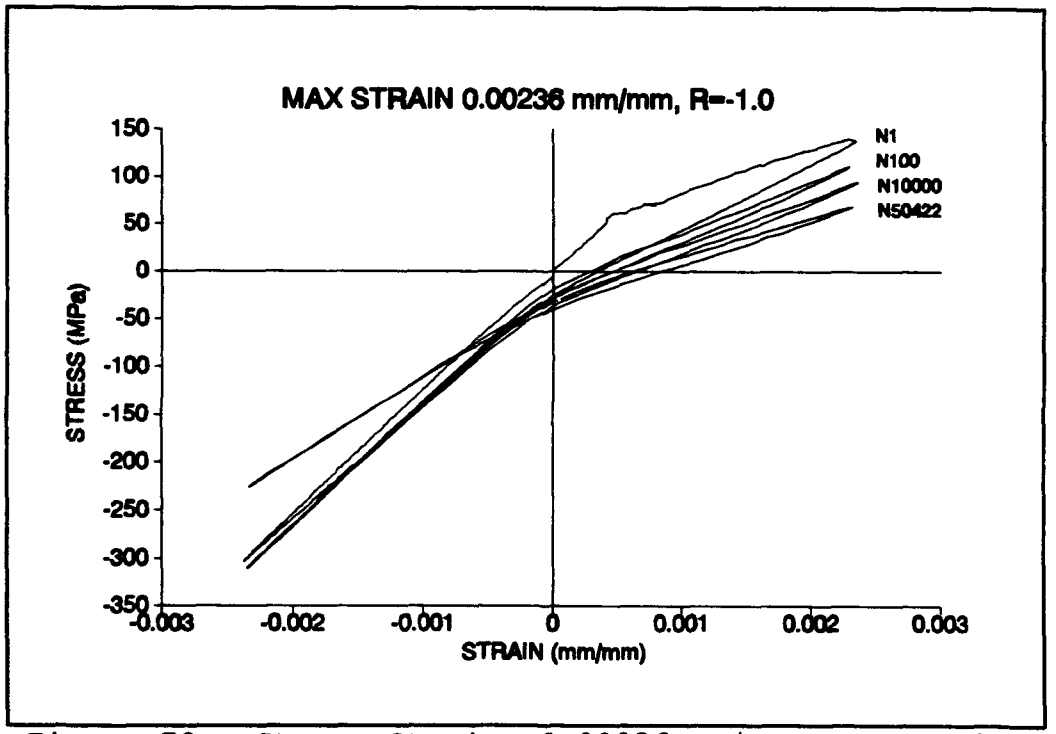

Figure 78. Stress-Strain, 0.00236 mm/mm, T-C, R=-1.0

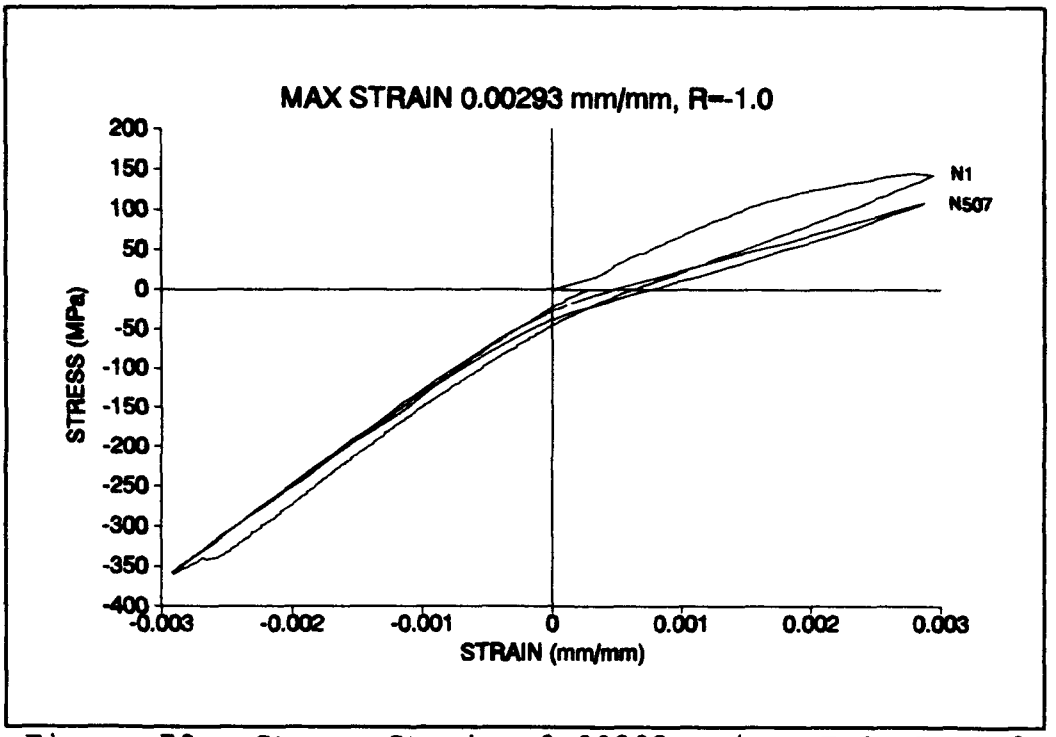

Figure 79. Stress-Strain, 0.00293 mm/mm, T-C, R=-1.0

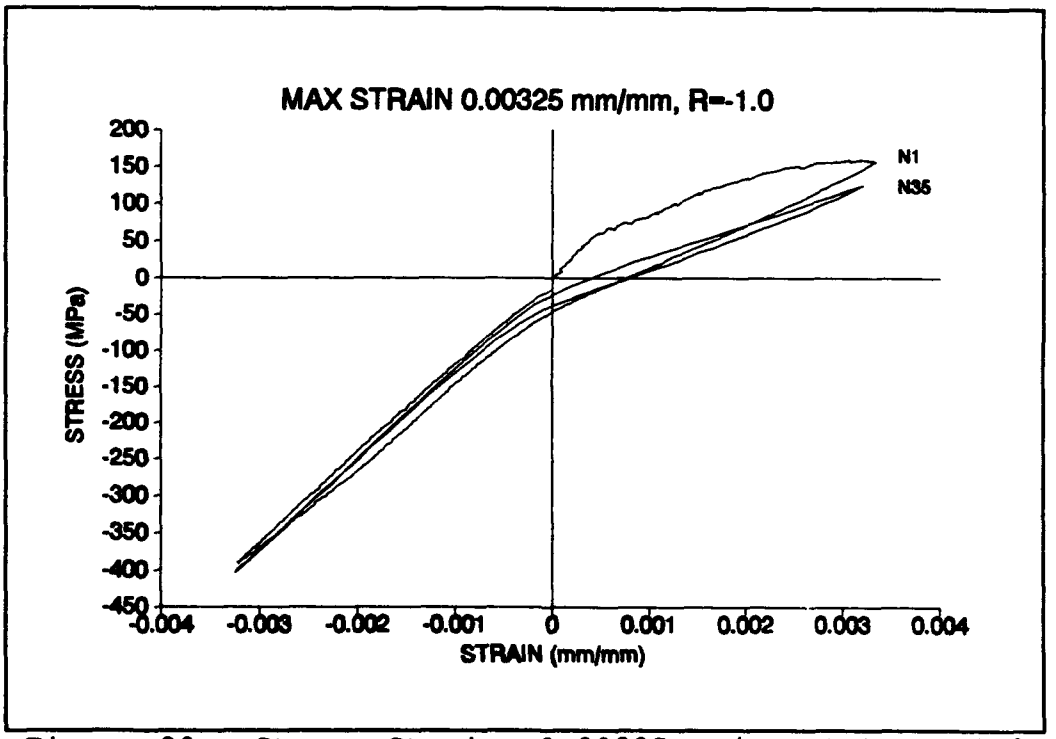

Figure 80. Stress-Strain, 0.00325 mm/mm, T-C, R=-1.0

Vita

Captain James J. Gudaitis was born on 1 December 1961 in Sandusky, Ohio. He graduated from Perry High School in Massillon, Ohio in 1980. He then attended the University of Akron from 1980 through 1984 and graduated with a Bachelor of Science Degree in Mechanical Engineering. He was commissioned through the Air Force Reserve Officer Training Corp (ROTC) program in May of 1984.

Captain Gudaitis' military assignments include three years at Eglin AFB, Florida working as a Test Engineer; successfully completing Specialized Undergraduate Navigator Training (SUNT) at Mather AFB, California; F-111A initial qualification training at Mountain Home AFB, Idaho; FB-111A Combat Crew Training School at Plattsburgh AFB, New York; Operational FB-111A navigator at Pease AFB, New Hampshire; F-111F initial qualification training and then as a weapons systems officer at RAF Lakenheath, England. He also spent six months in Saudi Arabia flying in support of Operations Desert Shield/Storm.

Captain Gudaitis entered the School of Engineering, Air Force Institute of Technology, in May of 1992.

REPORT DOCUMENTATION PAGE

Form Approved
OMB No. 0704-0188

1. AGENCY USE ONLY (Leave blank)	2. REPORT DATE	3. REPORT TYPE AND DATES COVERED
	December 1993	Master's Thesis

4. TITLE AND SUBTITLE
FATIGUE BEHAVIOR OF A CROSS-PLY CERAMIC MATRIX COMPOSITE UNDER STRAIN CONTROLLED TENSION-TENSION AND TENSION-COMPRESSION LOADING

5. FUNDING NUMBERS

6. AUTHOR(S)
Capt James J. Gudaitis

7. PERFORMING ORGANIZATION NAME(S) AND ADDRESS(ES)
Air Force Institute of Technology, WPAFB, OH 45433

8. PERFORMING ORGANIZATION REPORT NUMBER
AFIT/GAE/ENY/93D-17

9. SPONSORING/MONITORING AGENCY NAME(S) AND ADDRESS(ES)
AFOSR/NA, Bolling AFB, DC 20322-6448

10. SPONSORING/MONITORING AGENCY REPORT NUMBER

11. SUPPLEMENTARY NOTES

12a. DISTRIBUTION/AVAILABILITY STATEMENT
Approved for public release; distribution unlimited

12b. DISTRIBUTION CODE

13. ABSTRACT *(Maximum 200 words)* This study investigates the fatigue response of a cross-ply $[0/90]_{2s}$ Nicalon/Calcium Aluminosillicate (Nicalon/CAS) ceramic matrix composite at room temperature under strain controlled tension-tension and tension-compression fatigue loading. The primary objectives were to determine strain fatigue limits for both loading cases and to complete a fatigue life diagram (Δe-N) for all tests. Failure mechanisms were also studied. The average initial modulus value for this lay-up was 120 GPa. The ultimate tensile strain was 0.00988 mm/mm (285 MPa). Eight tests were conducted with maximum strains that ranged from 0.00300 mm/mm to 0.00722 mm/mm. The tension-tension fatigue limit was fround to be e=0.00270 mm/mm. There was no evidence of random fiber failure. Five tension-compression tests were performed at maximum strains that ranged from 0.00135 mm/mm to 0.00325 mm/mm. The fatigue limit for this set of tests was found to be the same as that fatigue limit for the tension-tension tests, Δe=0.00270 mm/mm. Longitudinal cracks formed in all the specimens, and were the major cause of failure. The fatigue life diagram for these tests coincided with the tension-tension tests until at the higher strains where the failure mode changed from tensile failure to compressive failure.

14. SUBJECT TERMS	15. NUMBER OF PAGES
Ceramic Matrix Composite, Tension-Tension Fatigue, Tension-Compression Fatigue, Strain Control, Crack Density, Transverse Strain	108
	16. PRICE CODE

17. SECURITY CLASSIFICATION OF REPORT	18. SECURITY CLASSIFICATION OF THIS PAGE	19. SECURITY CLASSIFICATION OF ABSTRACT	20. LIMITATION OF ABSTRACT
Unclassified	Unclassified	Unclassified	UL